Synthesis of Electron Deficient N-heterocyclic-carbenes and Activity of Imidazol-2-Imine Thioureate Ligand on Group 10 Transition Metals

Michael Byron Harkness

A THESIS SUBMITTED TO

THE FACULTY OF GRADUATE STUDIES

IN PARTIAL FULFILLMENT OF THE REQUIREMENTS

FOR THE DEGREE OF

MASTERS OF SCIENCE

December 2013

Abstract

Previous work in the Lavoie group has resulted in the synthesis of new imidazol-2-imine ligands that have low activity towards ethylene polymerization due to their electron rich nature. In an attempt to alleviate this an electron poor naphthalene-1,4-dione-IMes imidazol-2-imine ligand (L) was synthesized in 90% yield (**14a**) and coordinated to titanium ($LTiCpCl_2$, **15**). The resulting complex successfully polymerizes ethylene at a rate of 75 kg PE mol catalyst^{-1} h^{-1}.

A separate study focused on the coordination of functionalized imidazol-2-imine thioureate ligands (L') to late transition metal. Three complexes were synthesized. Ni(methylallyl)L' (**7**), Pd(allyl)L' (**8**), and NiL'_2 (**9**) were isolated in 85, 85, and 61% yields, respectively and all spectroscopically characterized. The X-ray crystallographic structure of **9** shows the unexpected N^S binding mode for the ligand. Complexes **7** and **8** have sparing activity towards ethylene polymerization, neither having productivity above 2 kg PE mol^{-1} h^{-1}.

Acknowledgements

I would like to thank the members of the Lavoie group, and especially Anna Badaj, Edwin Alvarado, and Tim Larocque for their constant support and guidance throughout my MSc degree. I owe most of my success to them. I would also like to thank Prof. Gino G. Lavoie for his supervision throughout my project. In addition I would like to thank Dr. Howard Hunter for his help with NMR experiments and Dr. Gusev for DFT calculations.

Some of the work discussed in my thesis has been reported in the peer reviewed journal Organometallics (**2013**, *32* (11), pp 3309–3321 **DOI:** 10.1021/om400220v).

I would like to thank my good friends Alex, James, and Vaczlav. I'd also like to thank Milton for his guidance. Most importantly I would like to thank my mother Themis. Her love and support throughout my degree was something I could always rely on.

Table of Contents

List of Figures

List of Schemes

List of Abbreviations

Cp – Cyclopentadienyl

NHC – N-heterocyclic carbene

MAO – Methylaluminoxane

CO – Carbon monoxide

THF – Tetrahydrofuran

FTIR – Fourier transform infrared spectroscopy

PPh_3 – Tri-phenylphosphine

NaHMDS – Sodium bis(trimethylsilyl)amide

DCM – Dichloromethane

HSAB – Hard Soft Acid Base

RT – Room temperature

NMR – Nuclear magnetic resonance

TOF – Turnover frequency

HSQC – Heteronuclear single-quantum correlation spectroscopy

HMBC – Heteronuclear multiple-bond correlation spectroscopy

COSY – Correlation spectroscopy

M+ – Molecular ion

ppm – part per million

DFT – Density functional theory

TEP – Tolman electronic parameter

ESI – Electrospray Ionization

COD – Cyclooctadiene

Chapter 1: Introduction

1.0 Introduction

1.1 General Introduction

Organometallic chemistry, more specifically transition metal organometallic chemistry, has had a large impact on the field of chemistry due to the unique properties observed when a metal and an organic fragment are combined. Transition metal organometallic complexes are often used in catalysis, which allows for enhanced activity as well as opening up novel synthetic pathways. The small amount of catalyst required for reaction also leads to green chemistry.[1] Due to their reactivity organometallic catalysts have played a large role in the advancement of synthetic chemistry over the past few decades, and the development of these catalysts has been an increasingly growing area of research. The effect of the metal, whether it is group 3, 12, or anywhere in-between, is often expressed in the reactivity of the corresponding metal complex. The success of a catalyst is therefore largely dependent on the ligand-metal combination. Therefore the targeted development of certain organometallic catalysts has led to the improvement of a multitude of synthetic reactions, which include but are not limited to hydroamination, olefin metathesis, and cross coupling.[2,3,4] The research in this field has been so prevalent that in the past decade a Nobel Prize was awarded for the work on olefin metathesis, and palladium-catalyzed cross coupling respectively.[5] These organometallic catalysts have been beneficial on a scope much larger than the laboratory, with many reactions being performed on industrial sized scales. However, perhaps one of

the most important uses for an organometallic complex is its ability to form polymers, a substance that is present in a large number of everyday items.

Polymers are found in a plethora of materials, including plastics and fabrics, making the polymerization of alkenes one of the most valuable catalytic reactions in commercial use.[6] Approximately 80 million metric tons of just polyethylene is produced yearly, making the polymer industry one of the biggest in the world.[7] The first ethylene polymerization catalyst, discovered by Ziegler and Natta, is a heterogeneous early transition metal catalyst that works in the presence of an organoaluminum co-catalyst, and has been a benchmark in the industry for several decades (Fig. 1).[8] The catalysts however act as a black box, since not much is known about the active site of the catalyst or the reaction mechanism. These catalysts also fail to produce functionalized polymer, which involve the incorporation of functional groups, oligomers or sometimes other polymers leading to new materials with improved capabilities. Furthermore they lack control over the polymer microstructure and they have poor functional group tolerance due to their high oxophilicity and Lewis acidic nature.[9]

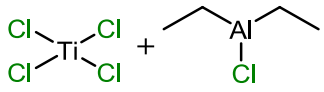

Figure 1. A Ziegler-Natta catalyst, the original polymerization catalyst

Access to new types of polymers can be very beneficial as they can provide materials with new properties and functionalities, such as that observed in mechanophore polymers that strengthen when exposed to an external force.[10] This is just one case that

shows the true value present in the advancement of polymerization chemistry. There has therefore been a widespread drive for the development of polymerization catalysts that not only have a known active site but can be tuned such that they show high activity under acceptable conditions with no decomposition.

1.2 Polymerization Catalysts

The next significant advancement in polymerization catalysts did not come until 1980, 27 years after the discovery of the Ziegler Natta catalyst, when Kaminsky reported on metallocene ethylene polymerization catalysts.[11] These metallocene catalysts, most notably zirconocene dichloride (Fig. 2), are not only highly active in ethylene polymerization but also have a well defined active single site. Metallocene catalysts make use of methylaluminoxane (MAO) as a co-catalyst. These catalysts are so active that they have become an industry benchmark. They have also helped in the elucidation of the mechanism for the polymerization of ethylene.

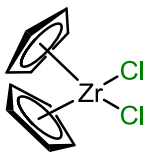

Figure 2. Zirconocene dichloride, a benchmark catalyst

The mechanism for ethylene polymerization shows that ligands play a crucial in whether or not the catalyst is active (Fig. 3). The ligand system in a catalyst can control much about the metal center such as its coordination number, coordination geometry, and formal oxidation state. The polymerization of ethylene begins with the activation of the

metal center. When MAO is the co-catalyst it first activates the catalyst through alkylation of the metal center, followed by the abstraction of one of the alkyl groups. Ethylene binds to the metal center, and then undergoes insertion to the metal carbon bond of the alkyl fragment that is oriented cis to it. The coordination and then insertion of ethylene is repeated, which grows the polymer chain, until chain growth termination is initiated through beta-hydride elimination. Three factors have therefore been important for the development of a highly active polymerization catalyst: the catalyst must be electron deficient, the active site must have a vacant site adjacent to the growing polymer chain, and the active catalyst should bear a positive metal center as this enhances electrophilicity and inhibits deactivation.[12] The alteration of a ligand system therefore is a very important feature.

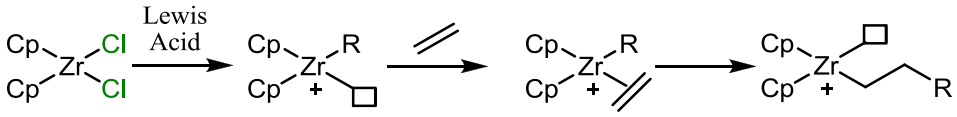

Figure 3. General mechanism for ethylene polymerization

Unfortunately, metallocenes are not easily tuned electronically, making necessary alterations to the catalyst difficult. The use of MAO as a co-catalyst means that these catalytic cycles can be quite expensive on an industrial scale due to a large excess of it being required for high activity.[13] The production of MAO is also quite expensive as it involves the hydrolysis of trimethylaluminum. The amount of MAO required for polymerization can be lowered by its partial replacement with aluminum alkyls, such as trimethylaluminum or trimethylaluminum, however these have shown deactivating

effects.[14] Another drawback is that catalyst residue can be found in the polymer. Furthermore it is very difficult for these catalysts to form hyper branched polyethylenes or functionalized polymers such as acrylates or α-olefin based block copolymers.[15]

Due to the shortcomings of the metallocene catalysts great effort has been put into the development of new single site catalysts that are highly active towards polymerizing functionalized monomers. Brookhart's discovery of α-diimine based complexes (Fig. 4) in 1995 was a big advancement in olefin polymerization catalysts. Upon coordination to nickel(II) or palladium(II) the corresponding complexes showed high activities in ethylene polymerization, comparable to those of metallocenes, and produced highly branched polymers from ethylene alone, with no need for α-olefins.[16] This ligand system makes use of bulky substituents that block the axial sites of the metal and prevent β-hydride elimination.[17] This prevents chain termination and allows for high molecular weight polymers to be formed.

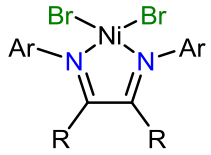

Figure 4. The general structure of Brookhart's α-diimine catalyst

Another ligand motif that proved to be quite active is the salicylaldiminate (also known as phenoxy-imine, FI) ligands which was independently reported by Fujita (Mitsui), Johnson (DuPont), and Grubbs (Caltech) in 1997.[18,19,20] The phenoxy-imine based ligand was coordinated to group 4 metals by Fujita and co-workers, and led to a distinct family of olefin polymerization complexes. These complexes have shown

substantially higher activity towards ethylene polymerization than metallocene catalysts.[21] When the phenox-imine ligand is coordinated to group 10 metals (Fig. 5) the resulting complexes, which contain a six-membered chelate, show a high tolerance for polar functional groups, higher than that of α-diimine nickel or palladium complexes, since they are uncharged in their active state. Phenoxy-imine nickel complexes have been used for the copolymerization of ethylene and polar functional comonomers, such as tertiary amine, ether, ester, ketone, and alcohol functional groups.[22]

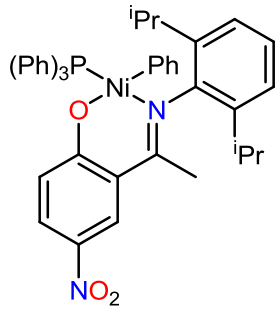

Figure 5. One example of an active group 10 phenoxy-imine catalyst

The phenoxy-imine and α-diimine are just two examples of the right ligand system leading to high activities not just for ethylene polymerization, but also the production of functionalized polymers. These catalysts however do have their limitations. Brookhart-type catalysts show turnover frequencies for copolymerization that are greatly reduced relative to ethylene homopolymerization making these catalysts commercially unfeasible for functionalized polymers. In addition to this, incorporation of certain functional groups (vinyl nitriles, vinyl halides, and vinyl acetate) as a copolymer has been shown to hinder polymerization activity.[23] Various FI catalysts have shown poor thermal

stability, with activities degrading at temperatures above 40 °C.[24,25] There is therefore always considerable effort being put forward in research for the rational design of new ligand systems that upon coordination to transition metals will result in the next highly active polymerization catalyst with enhanced performance.

1.3 N-Heterocyclic Carbenes

The synthesis and isolation of a stable N-heterocyclic carbene (NHC) in 1991 by Arduengo III was a crucial discovery that has led to extensive developments of this useful new class of ligands.[26,27] The past two decades has witnessed the development of experimental procedures for the synthesis of a variety of symmetrical and non-symmetrical imidazol-2-ylidene ligands, and the saturated imidazolin-2-ylidene analogue.[28,29] NHCs are strong σ-donors and weak π-acceptors, allowing for a normally very reactive carbene to form a strong metal carbon-bond leading to a stabilized metal center. They are a very versatile class of ligands since they are easily tuned, both sterically and electronically. Often compared to tertiary phosphines, NHCs are advantageous due to their stabilizing effects, high thermal stability of the resulting metal center, and resistance to dissociation from the metal center.[30] NHCs have therefore become widely used as ligands in; cross-coupling reaction, ring opening metathesis polymerization, transfer hydrogenation, and a variety of other catalytic organic transformations.[31,32,33]

NHC complexes however have not seen widespread use as polymerization catalysts, likely due to the tendency of carbene metal alkyl complexes to decompose.[34]

Despite this there are a few examples of NHC complexes being highly active towards both ethylene polymerization and oligomerization.[35] There is still much research to be done to determine the overall utility of NHCs as a ligand in polymerization catalysts, but the robust framework that NHCs provide makes them a desirable ligand scaffold for further ligand synthesis. The reactivity of NHCs towards varying functional groups has therefore been tested in recent years, and has led to the development of a wide range of ligand systems.[36,37]

1.4 Imidazol-2-Imine Based Ligand System

More recently the reactivity of NHCs towards azides has led to a new class of ligands, the imidazol-2-imine. A key feature of this fragment is the delocalization of electron density across the imidazol-2-imine leading to a zwitterionic resonance structure with an electron-rich exocyclic iminic nitrogen (Fig. 6).[38] This results in a ligand with enhanced basicity and nucleophilicity. An important feature of this ligand is its ability to act as a 2σ, 4π donor, making it isoelectronic with cyclopentadienyl (Cp^-) or more justifiably a phenoxide ligand, which was a key component of many catalysts including the aforementioned FI catalysts. However, unlike the Cp^- ligand the electronics of the imidazol-2-imine can be easily altered. Imidazol-2-imines are perhaps more electronically versatile than phenoxides as they are isoelectronic analogues of cyclopentadienyls, phosphidoimides and even imido ligands, depending on which resonance structure is considered.[39] Another important feature of the aforementioned FI catalysts is that there is a monoanionic chelating ligand bound to the metal center. This

gives further stability to the complex through chelation effects. The imidazol-2-imine can therefore be used as an appropriate ligand scaffold as it will allow for the development of a monanionic chelating ligand.

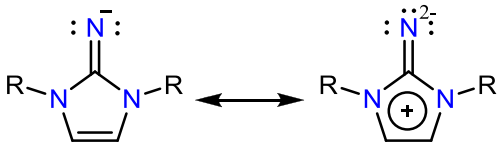

Figure 6. Mesomeric structures of the imidazol-2-imine

Previous work in the Lavoie group has focused on the methodical development of an imidazol-2-imine based ligand system. There are two very important properties to these ligands, being monoanionic it is analogous to salicylaldimine ligands which show high activity towards α-olefin and branched olefin polymers. In addition the bidentate binding mode adds extra stability through chelating effects.[40] These features allow for a ligand that is easily tuned, while minimizing bimolecular decomposition. By shifting the steric bulk to the second coordination sphere, the active site about the metal center is more open and will hopefully facilitate α-olefin polymerization, a feature that has been emulated from cyclopentadienyl, alkoxide, and phosphinimide ligand systems.[41]

One of the first ligands synthesized was **1a** (Fig. 7), which was a neutral species. Upon coordination to titanium the ligand was bound in a bidentate fashion, and indeed shows the shift of steric bulk to the second coordination sphere, as well as activity for ethylene polymerization, albeit lower than benchmark catalysts. Upon coordination to

late transition metals, **1a** binds in a monodentate fashion, and forms an unusual dimer. In an attempt to force a bidentate binding mode compound **1b** was synthesized, which upon deprotonation results in a monoanionic ligand that has been coordinated to early transition metals. Unfortunately an $N'_{p\text{-tolyl}}$^O binding mode is observed, leaving the imidazol-2-imine portion pendent, greatly limiting any effect it may have on the reactivity of the complex.[42] In contrast, coordination to late transition metals resulted in the desired $N_{\text{imidazol-2-ylidene}}$^$N'_{p\text{-tolyl}}$ binding mode.

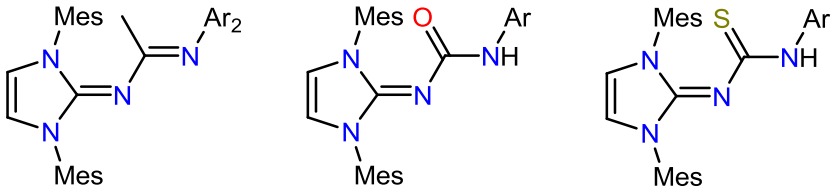

Ar = *p*-methylphenyl, 2,6-dimethylphenyl

Figure 7. Imidazol-2-imine based ligand class

Going from a ureate to thioureate ligand, could thus possibly give the desired $N_{\text{imidazol-2-ylidene}}$^$N'_{p\text{-tolyl}}$ binding mode, based on a previously reported scandium complex and the hard-soft acid-base theory.[43] Surprisingly upon coordination of deprotonated **1c** to group 4 transition metals an $N'_{p\text{-tolyl}}$^S binding mode was observed. It is therefore unclear which binding mode the thioureate ligand will adopt upon coordination to group 10 metals. The coordination of deprotonated **1c**, to Ni and Pd is still a desired avenue of research as it will result in complexes that structurally resemble FI catalysts, both of which incorporate monoanionic chelating ligands. Unlike the FI catalyst these complexes will result in a less stable 4 member metallacycle. The resulting Ni and Pd complexes

may be active polymerization catalysts, in addition to providing insight into structure property relationships between the corresponding early and late transition metal complexes of **1b** and **1c**. Herein the characterization and activity of group 10 transition metal complexes containing *N*-imidazol-2-ylidene-*N*-*p*-tolylthioureate ligands are discussed.

1.5 Electron Deficient Ligands

Research in the Lavoie group has lead to the development of a number of functionalized imidazol-2-imine ligands for their use in ethylene polymerization catalysts (Fig. 8). Upon coordination to a metal center, the resulting complexes have shown activity, albeit lower than those observed in benchmark catalysts.[44]

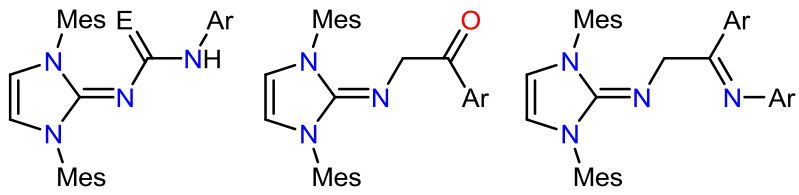

Figure 8. General representation of functionalized imidazole-2-imine proligands

It is hypothesized that the low activity of these complexes is due to the high electron density present on the metal center, which results in a less electrophilic metal center. The high electron density on the metal center is caused by the strongly donating functionalized imidazol-2-imine ligands. In order to mitigate this, the imidazol-2-imine scaffold can be altered with electron-withdrawing groups, ensuring that upon coordination the metal center is less electron rich. DFT calculations show that there are a

number of possible NHCs that can be used as ligand scaffold with the desired electron-withdrawing properties for the second-generation catalysts (Fig. 9).[45] Carbonyl stretching frequency for a $Ni(CO)_3(NHC)$ complex are a good indication of the electronic properties that the NHC possesses. Upon coordination to a metal, the NHC weakens the C-O bond of metal carbonyl complexes, leading to a decrease in $\nu_{C=O}$ stretching frequencies. This is because NHCs are strong σ-donors, which in turn leads to more electron density being present on the metal center for π-back-donation to the CO. This data is relevant to the corresponding imidazol-2-imine scaffold due to the characteristic delocalization of electron density that occurs across the imidazol fragment, which is directly affected by the electron withdrawing groups.

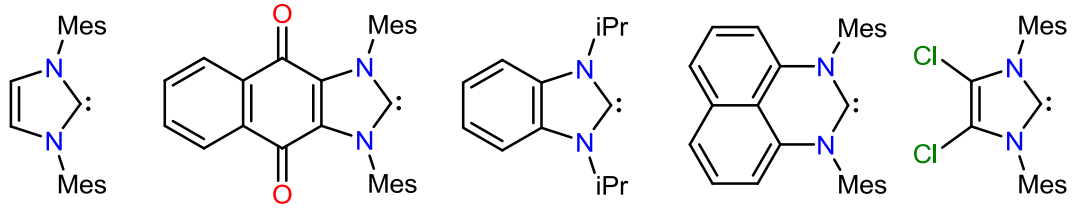

2 v(CO) = 2050.5 **3** v(CO) = 2055.7 **4** v(CO) = 2057.0 **5** v(CO) = 2058.5 **6** v(CO) = 2059.0

values in cm^{-1}

Figure 9. NHCs containing electron-withdrawing moieties in increasing order of electron withdrawing capabilities

There are a number of potential NHCs that are synthetically viable and are significantly less electron-donating than the imidazol-2-ylidene, the building block currently used for our first-generation ligands. With the substitution of the backbone protons, all the NHCs become more bulky in nature. However, these steric issues should

not affect reactivity as they are not blocking the carbenoid carbon itself. Herein, the attempted synthesis of theses NHCs and their functionalization are discussed.

Chapter 2: Results and Discussion

2.0 Results and Discussion

2.1 Coordination and Reactivity of *N*-Imidazol-2-ylidene-*N*′-p-tolylthioureate Ligand

The coordination studies of proligand **1b** showed that the binding mode of the ligand was dependent on the metal center used. The coordination of proligand **1b** to titanium(IV), which is a hard acid, resulted in the undesirable $N'_{p\text{-tolyl}}$^O binding mode. Coordination to nickel(II) however resulted in a $N_{\text{imidazol-2-ylidene}}$^$N'_{p\text{-tolyl}}$ binding mode, despite nickel being a harder acid. It was postulated that the use of sulfur as the heteroatom would force a $N_{\text{imidazol-2-ylidene}}$^$N'_{p\text{-tolyl}}$ binding mode to early transition metals because it is softer than oxygen. Ligand **1c** was therefore synthesized and upon deprotonation it was coordinated to titanium(IV). Surprisingly though a $N'_{p\text{-tolyl}}$^S binding mode was observed, resulting in a unfavourable hard-soft interaction between sulfur and titanium(IV). Therefore it became advantageous to determine the binding mode that proligand **1c** would adopt upon coordination to group 10 metals as the previous coordination studies had resulted in peculiar results. Stabilization through chelation effects would be observed through both binding modes however reactivity of the complex would benefit primarily from a $N_{\text{imidazol-2-ylidene}}$^$N'_{p\text{-tolyl}}$ binding mode.

Previous work in the Lavoie group had shown that coordination of proligand **1b** to nickel and palladium allyl complexes is simple and high yielding, resulting in the desired $N_{\text{imidazol-2-ylidene}}$^$N'_{p\text{-tolyl}}$ binding mode.[46] The coordination of the thioureate ligand to the corresponding nickel(II) and palladium(II) precursors was achieved in excellent

yields (Scheme 1). These complexes, despite the fact that they may be poor catalysts, provide an easy pathway for the determination of the binding mode of **1c**.

Scheme 1: Synthesis of Nickel(II) (**7**) and Palladium(II) (**8**) Thioureate Complexes

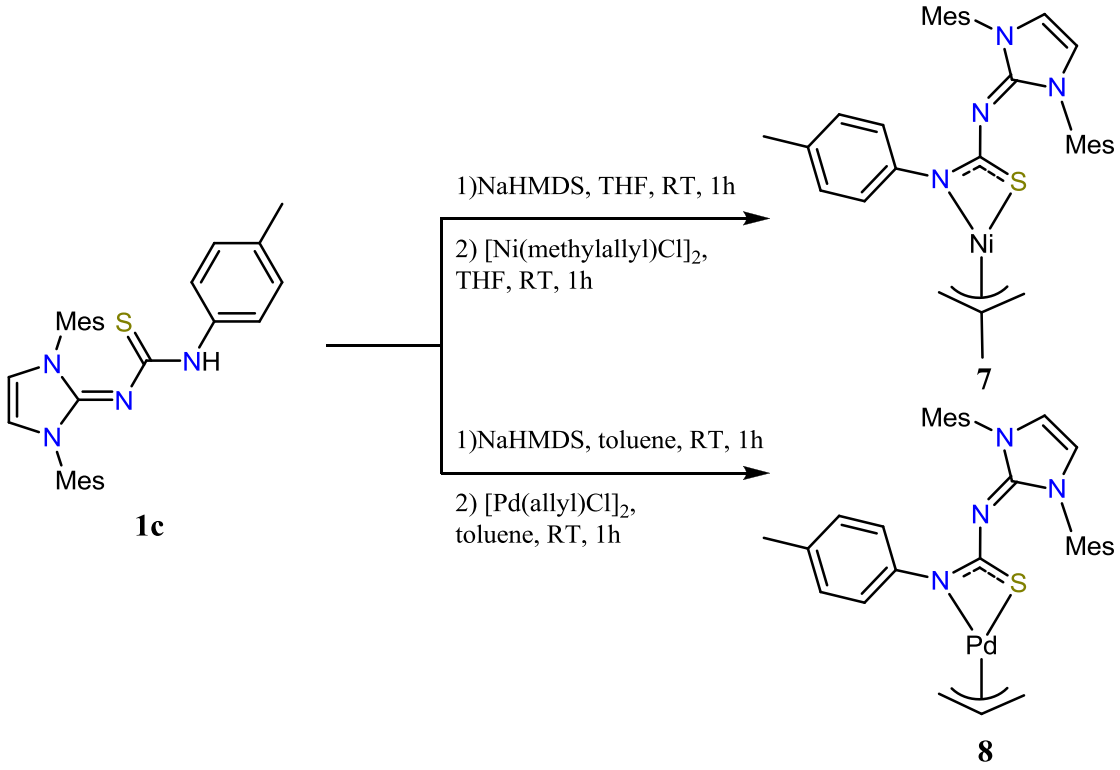

The proton NMR of the two complexes followed the same trend upon coordination, which was also observed in the coordination of **1c** to titanium(IV).[47] Upon coordination the ortho and meta protons of the *p*-tolyl group and the backbone protons of the azole ring resonated at higher frequencies than that of the proligand **1c**. The thioacyl carbon for **7** and **8** resonates at 175.7 and 176.8 ppm, respectively, which is upfield from what is observed in **1c** and consistent with sulfur coordination.[48] The resonances for the imine carbon were also quite similar appearing at 146.6 and 146.3 ppm in **7** and **8,** respectively. This spectroscopic data strongly suggests an $N'_{p\text{-tolyl}}$^S binding mode.

The FTIR spectrum of **1c** revealed strong absorption bands at 1400 – 1600 cm^{-1}. However, the identification of the vibration modes responsible for these absorptions is difficult due to mixing of bond deformation, rocking, bending, and stretching, characteristics of both organic thioureas and inorganic thioureate metal complexes.[49] Moreover absorption bands that are primarily due to stretching of C=S double bonds are expected at 700 cm^{-1} and are predicted to be weak, which was confirmed by DFT calculations of geometry optimized thioureate metal complexes.[50] The use of FTIR data for both complexes **7** and **8** therefore remains highly uncertain and questionable and will not be further discussed.

Crystals of **7** were grown via liquid diffusion of *n*-pentane into a saturated THF solution at – 35 °C. While satisfactory refinement was not possible (R = 20%), with prolate atoms, the diffraction data allowed for the determination of the atoms connectivity. The $N'_{p\text{-tolyl}}$^S binding mode is therefore unequivocally confirmed (Fig. 10).

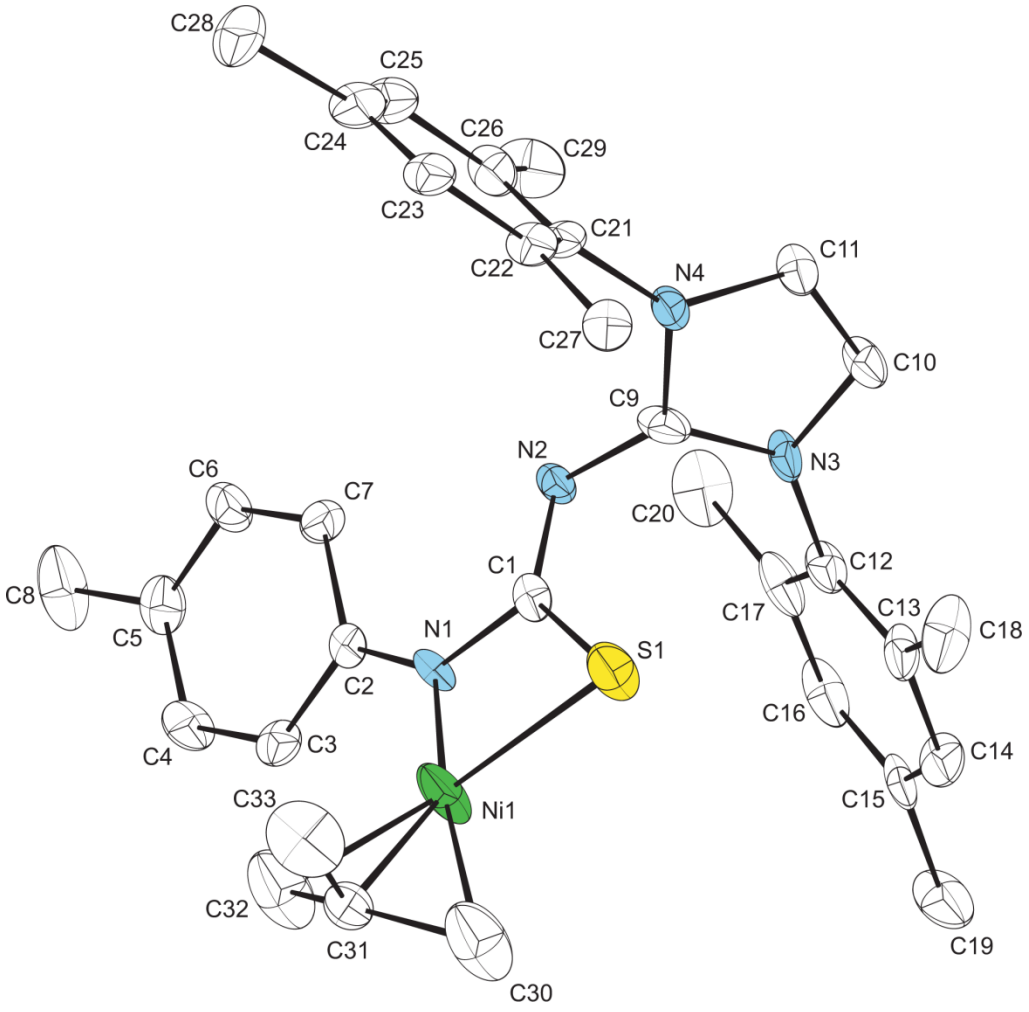

Figure 10. ORTEP diagram of complex **7** (40% probability level)

Despite the improper binding mode of both complexes, their catalytic activity was evaluated for ethylene polymerization (1 atm C_2H_4, room temperature) with 1000 equivalents of MAO as co-catalyst. Both catalysts gave no polymer over a 10 minute trial. It was postulated that the lack of activity is due to poor initiation kinetics that is often associated with allyl fragments. In order to alleviate this, the trials were repeated for 19 hours however over the course of this time both complexes decomposed, as observed

by a large amount of black particulates in solution. Trace amounts of polyethylene were recovered with neither catalyst showing productivity over 2 kg mol^{-1} catalyst.

Allyl complexes are known to be poor catalysts for polymerization compared to alkyl complexes, although there are reported cases of organometallic allyl complexes with high activity towards ethylene polymerization.[12,51] This is due to the inherent thermodynamic stability of η^3-allyl fragments, which leads to poor initiation kinetics. Nickel and palladium allyl complexes in fact all require elevated temperatures and pressures and long reaction times to produce polymer in moderate yields.[52,53] Complexes **7** and **8** were still useful as they allowed for the quick determination of the binding mode of proligand **1c** to late transition metals.

A few criteria are critical to achieve catalysts with desired performance. The mechanism for olefin polymerization shows labile or easily activated ligands, such as a solvent molecule or a chloride, is beneficial as it allows for a vacant site to be available on the metal center upon its dissociation (Fig. 3). This also results in a more electrophilic metal center. Furthermore an alkyl or aromatic fragment propagates the polymerization reaction through the insertion of the initially bound ethylene fragment. These two features therefore become very desirable in a catalyst.

Despite the poor activity of complexes **7** and **8**, it is still beneficial to determine if they would have any other utility. Therefore the reactivity of these complexes with CO was tested. In an atmosphere of CO, both complexes decomposed over the course of two hours, as determined by NMR spectroscopy. The decomposition was also supported by a

drastic colour change in solution, and the formation of a precipitate. The decomposition product could not be to be isolated and characterized. Nonetheless this experiment still proved to be beneficial as the complex was reactive with CO. It is postulated that this reactivity is possible due to the transformation of the allyl fragment from η^3 coordination to η^1 coordination, resulting in a η^1-allyl intermediate that may be capable of trapping ethylene. As reported in literature, complexes resembling these intermediates can be highly active for the co-polymerization of ethylene.[54,55] These complexes may therefore be activated in the presence of CO and then when exposed to ethylene lead to the co-polymerization of functionalized monomers (Scheme 2).

Scheme 2: Mechanism for the proposed synthesis of functionalized polymers via **8**

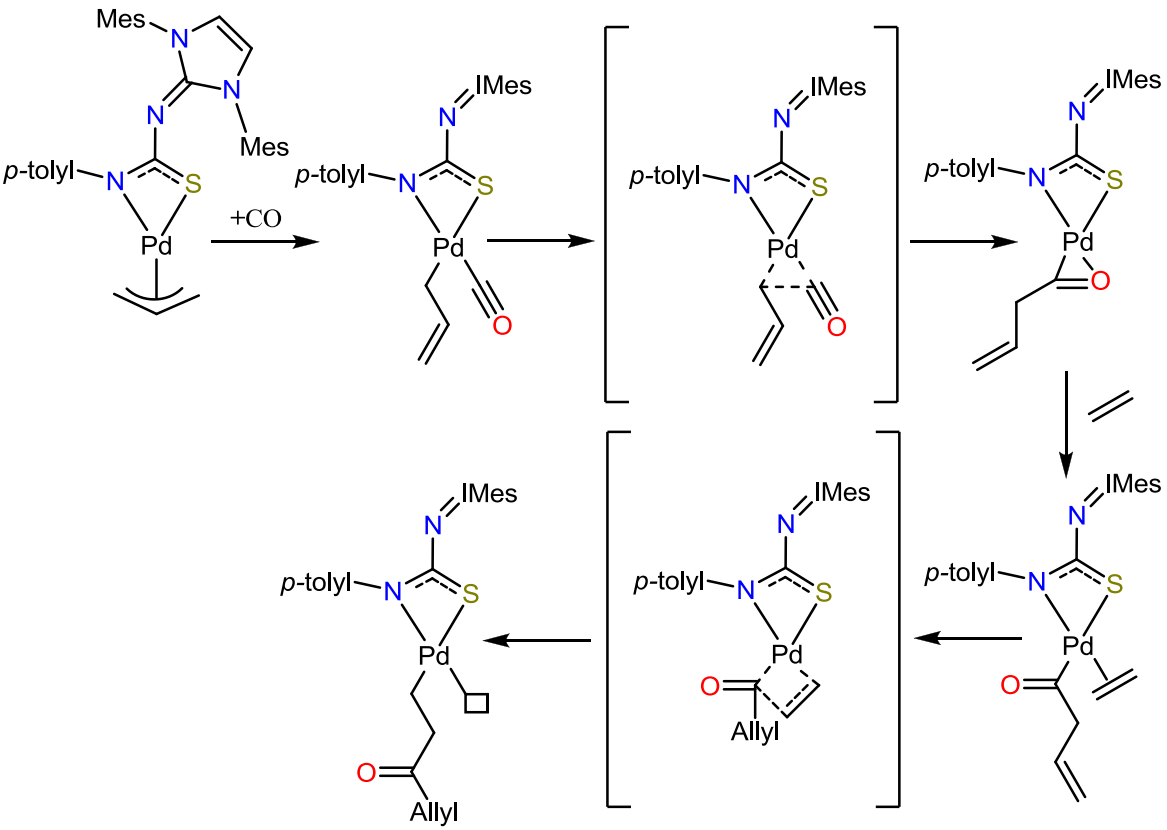

These polymerization experiments were performed in the presence of ethylene while under an atmosphere of CO. Over the course of 30 minutes no polymer formation was observed, and the appearance of black particulates in solution confirms that catalyst decomposition had occurred. These results show the generally poor nature of these allyl and methylallyl catalysts.

In an attempt to synthesize a more effective polymerization catalyst, reactions with more appropriate metal precursors were performed. With a similar experimental procedure used for **7** and **8**, coordination was attempted with $[PdCl_2(CH_3CN)_2]$, $[NiCl(PPh_3)_2Ph]$, $[Pd(TMEDA)Cl_2]$, and $[Pd(COD)CH_3Cl]$. To facilitate analysis by NMR spectroscopy, the thioureate salt of **1c** was isolated and fully characterized (Fig. 11).

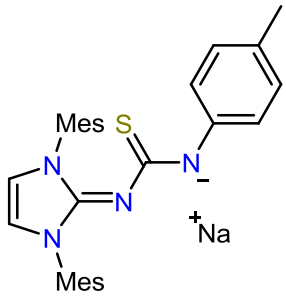

Figure 11. Ligand salt of **1c**

Reactions with all three palladium (II) precursors in THF and at room temperature were unsuccessful, and the ligand salt was recovered. Varying reaction conditions such as time, solvent (THF, toluene, DCM, pyridine) and temperature (-37 – 70 °C) for these reactions had no effect on the outcome.

The initial reaction of [NiCl(PPh_3)$_2$Ph] with deprotonated **1c** shows that coordination may have occurred. However, purification of the resulting mixture was quite difficult. The ^{1}H NMR spectrum shows that the aliphatic region has multiple peaks integrating to 21 protons in a 1:1:2:2:1 ratio. This is likely due to the inequivalence of the mesityl rings, as observed in **7** and **8**, and corresponds to the aliphatic protons on the mesityl and *p*-tolyl rings. The aromatic region is quite crowded with very broad signals present due to the triphenylphosphine ligand. Small black particulates, likely nickel black, were present in the NMR sample and causing line broadening.

In order to obtain a pure product, the reaction was repeated in toluene and performed overnight, according to the reported procedure for the coordination of a similar β-ketiminato monoanionic bidentate ligand to the same metal precursor.[56] The ^{1}H NMR spectra had slightly better resolution despite having the same peaks as the previous one. The aromatic region was still quite broad and in an effort to elucidate the structure, a ^{31}P NMR spectrum was taken with a capillary containing H_3PO_4 as an internal standard. Two peaks were observed, with one of them corresponding to the nickel precursor, which was roughly 3 times as intense as the other signal which resonated at 32 ppm. Similar monoanionic bidentate nickel complexes show the PPh_3 resonate around 28 ppm.[57] From just a ^{31}P NMR spectrum it is difficult to determine what the other resonance represents, although it very well may be the PPh_3 unit on the proposed nickel complex that has **1c** coordinated to it. In order to further support this idea, X-ray diffraction studies on single crystals and combustion analysis would need to be performed. Unfortunately, all attempts to purify this sample were unsuccessful, often resulting in decomposition.

Waymouth has done work with a monoanionc bidentate NHC enolate ligand that has been coordinated to nickel, similar to **1c**, and tested for ethylene polymerization.[58] Following this procedure, the reaction of **3b** with $Ni(COD)_2$ in the presence of pyridine and phenylchloride was performed to synthesize a metal complex similar to Waymouth's. However upon work up, it was evident that this was not observed, as complex **9** was synthesized in 20%. The reaction conditions were optimized, in the absence of pyridine from the reaction and **9** was isolated as a spectroscopically-pure green solid in 61% yield (Scheme 3).

Scheme 3: Synthesis of bis(thioureato) Nickel(II) Complex

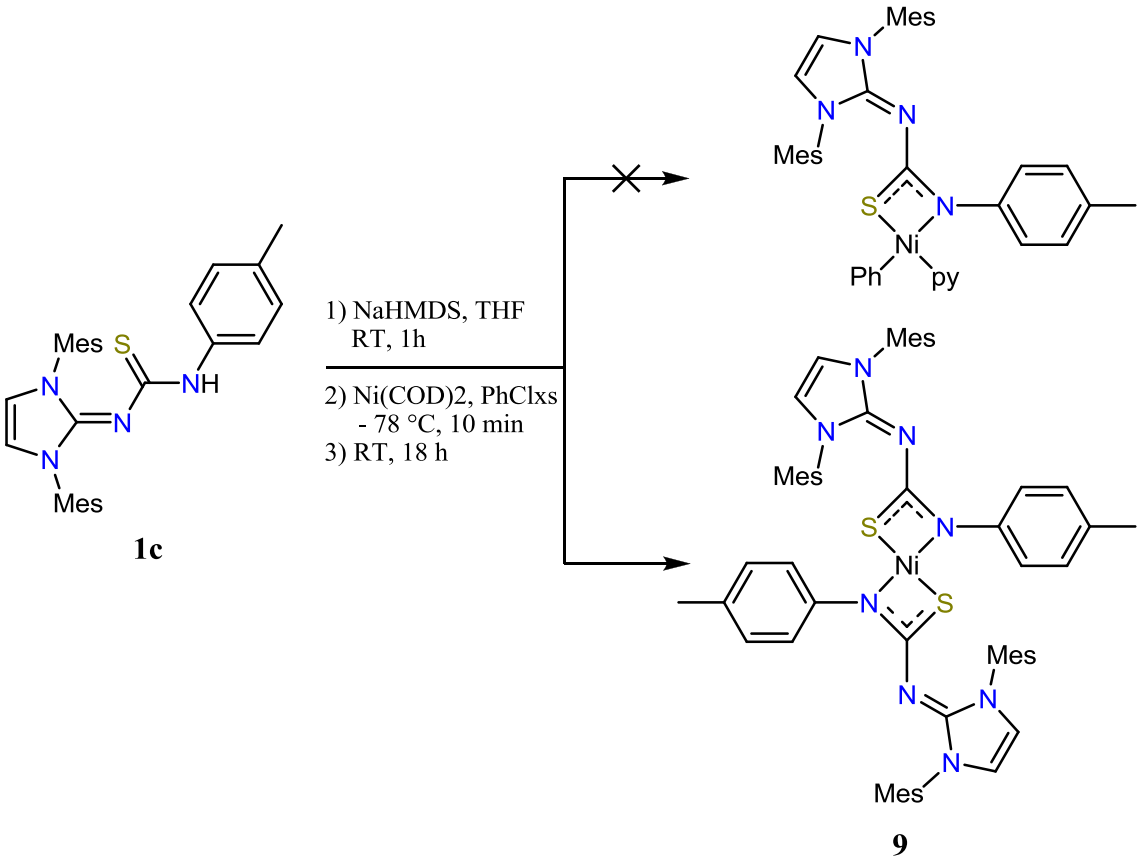

The generation of this complex is quite interesting as a postulated mechanism for the formation of **9** would first involve the dissociation of a single COD unit followed by the oxidative addition of phenyl chloride, forming a Ni (II) intermediate in which only one COD is bound (Scheme 4). A chloride is then displaced by the ligand salt, which produces NaCl, leaving the ligand singly bound to the metal center. The in situ deprotonation of ligand **1c** provides a proton source, allowing for the protonation of the phenyl unit and its dissociation as benzene. Displacement of the COD from the charged nickel intermediate then allows for the second ligand to bind, giving the structure **9**.

Scheme 4: The Proposed Mechanism for the Formation of **9**

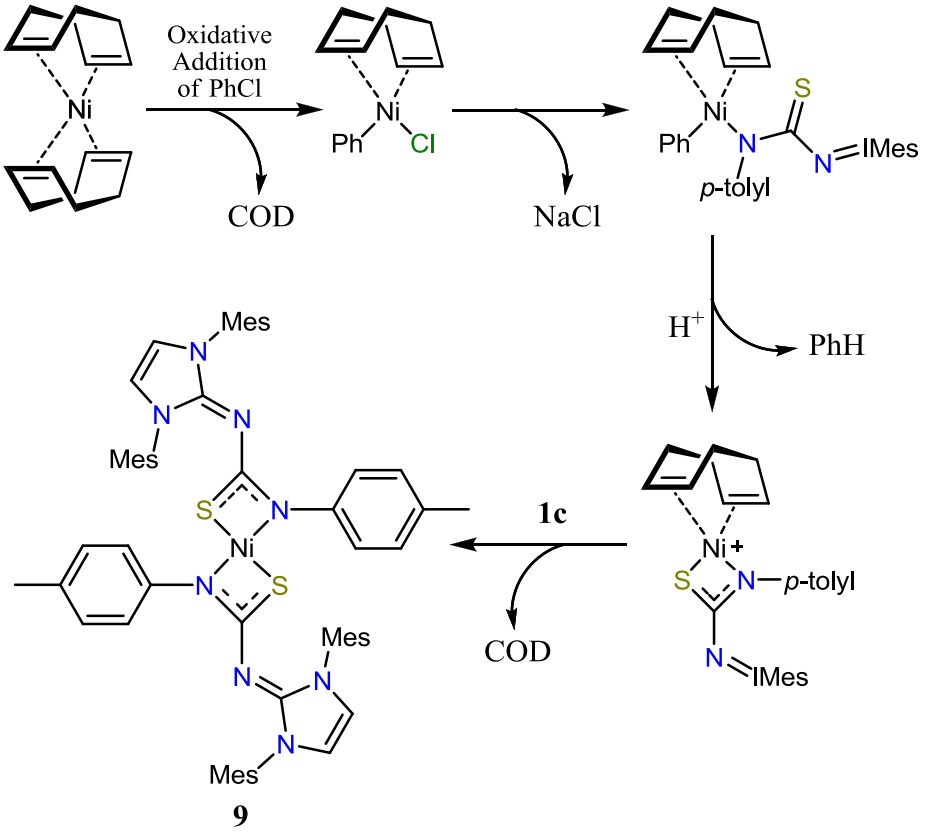

Upon its synthesis, the resulting bis(thioureato) nickel (II) complex was fully characterized. The ^{1}H NMR shows a shift in ppm for the imdazole backbone protons, from 5.84 ppm in **1c** to 5.64 ppm in **9**, which suggests an uncoordinated imidazol- 2-imine fragment. The benzylic protons for both the mesityl and *p*-tolyl rings show no significant change in chemical shift. Interestingly the protons of the methyl group on the ortho position of the mesityl ring had shifted upfield whereas the para position experienced a downfield shift. Finally the protons of the methyl group on the para position of the *p*-tolyl ring were shifted upfield. The ^{13}C{^{1}H} NMR spectra shows the ipso-carbon of the *p*-tolyl ring resonates at 145.0 ppm, an upfield shift from that of **1c**, suggesting coordination of the $N'_{p\text{-tolyl}}$ to the metal center. Coordination through the sulfur atom is substantiated by the thioacyl carbon resonance at 173.3 ppm, significantly lower than that observed for **1c** (181.0). This data is consistent with the generation of only one isomer where the ligand bound in an $N'_{\text{p-tolyl}}$^S binding mode. X-ray quality crystals of **9** were grown at room temperature by slow vapor diffusion of ether into a saturated THF solution. Complex **9** crystallized in a triclinic crystal system in the P-1 space group, with nickel located at an inversion center (Fig. 12).

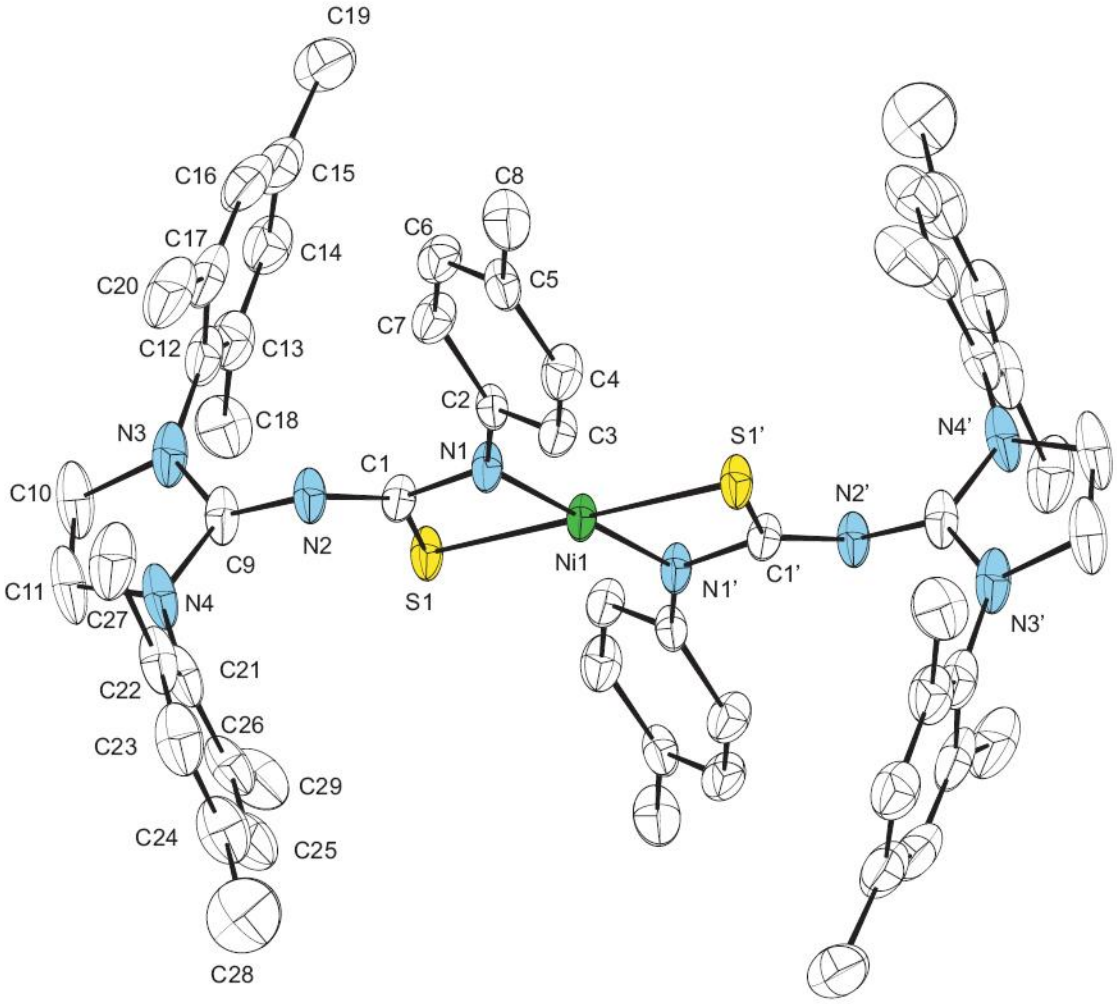

Figure 12. ORTEP diagram of complex **9** (40% probability level)

The solid-state structure of **9** confirmed the prediction based on spectroscopic data, with the thioureate ligand bound to the metal center through the sulfur atom. There is a significant amount of zwitterionic character displayed by the imidazole ring through the large and statistically equivalent N2-C9 and N2-C1 bond lengths (1.325 Å) and by the C1-N2-C9-N3 torsion angle (74.26°) which deviates greatly from expected values for a

square planar complex. The N2-C9 (1.326) bond length increased, showing less double bond character. Conversely, the N2-C1 and N1-C1 (1.325 Å) bond lengths decreased, showing more double bond character as compared to average bond lengths (1.28 Å for C=N and 1.35 Å for O=C-N).[59] This emphasizes the delocalization of electron density across the imidazol-2-imine fragment as they deviate from expected values

When tested for ethylene polymerization under previously mentioned conditions, complex **9** was completely inactive. This is because the complex is a stable four coordinate square planar complex, making for the formation of a metal alkyl that is required for polymerization quite difficult. In an attempt to synthesize a more active catalyst the reactivity of **9** towards HCl and MeOH was explored. This would result in a mono(thioureate)nickel complex, with either a chloro or methoxide substituent. Treatment of **9** with 1 or 2 equivalents of HCl in a solution of THF led to no reaction. In the presence of excess HCl, uncontrolled decomposition of the complex occurred, as noted by a large number of signals in the aliphatic region of the ^{1}H NMR. Reaction of **9** with both 1 and 2 equivalents of MeOH, as well as in a solution of just MeOH resulted in no reaction. These studies show the overall stability of this bis(thioureato) nickel complex towards protonolysis.

The change in coordination mode of the urea prolignad **1b** from $N'_{\text{p-tolyl}}$^O to $N_{\text{imidazol-2-ylidene}}$^$N'_{\text{p-tolyl}}$ when going from early to late transition metals was quite interesting. Therefore the determination of the binding mode that thiourea proligand **1c** would adopt upon coordination to group 10 metals was pursued. Unfortunately the

desired $N_{\text{imidazol-2-ylidene}}$^S binding mode was not observed upon coordination of **1c** to nickel and palladium. The study of these two ligands however became quite interesting from a coordination stand point. When **1b** had an $N'_{p\text{-tolyl}}$^O binding mode to titanium, it was postulated that by going from oxygen to the softer sulfur, the desired binding mode would be forced on the basis of the HSAB theory. However, **1c** coordinated to titanium through the sulfur atom. Interestingly, only two cases of a *N,N* coordinated mode for thioureate transition metal complexes have been registered with the Cambridge Structural Database.[60] Furthermore, despite oxygen and group 10 metals being closer to one another in the hard soft spectrum, coordination to nickel and palladium was through sulfur but not through oxygen. This system clearly illustrates the short comings of the HSAB theory, which has also recently been documented by Mayr.[61] Even though the ureate and thioureate systems described herein showed low activity in ethylene polymerization, the coordination studies that resulted from their synthesis were quite valuable.

2.2.1 Attempted Synthesis of Electron Deficient NHCs

Although there is a multitude of possible electron deficient NHCs with a wide variety of functional groups and steric properties, efforts were put towards isolating whichever were most synthetically viable. The synthesis of the electron deficient NHCs would be followed by their functionalization to the imidazol-2-imine by adopting literature procedures for the synthesis of IMes imidazol-2-imine (Scheme 5).[62] There are currently no reports for the synthesis of the corresponding electron deficient imidazol-2-imines.

Scheme 5: General Synthesis of the Imidazol-2-imine

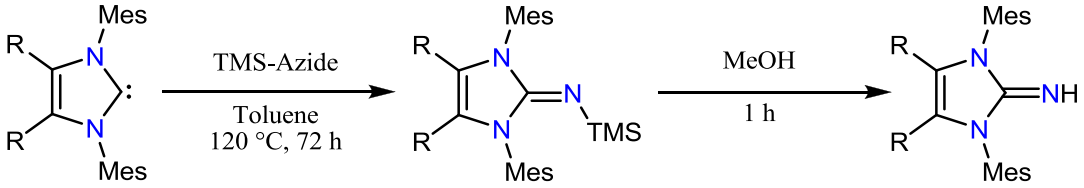

Following literature procedures, a solution of **2** in THF was added to CCl_4 in THF at room temperature and allowed to stir for 20 minutes.[63] The $IMesCl_2$ carbene **6** (Fig. 9) was isolated in high yields. Reaction of CCl_4 with IMes results in the chlorination of the 2-position of the imidazole-2-ylidene, and the production of Cl_3C^-, followed by the deprotonation of the backbone and production of chloroform (Scheme 6). Finally dechlorination of the 2-position results in the formation of **6**. The reaction of the chlorinated imdazol-2-ylidene with TMS-azide was performed, following the general procedure in Scheme 5. However, no product could be isolated. Over the course of 72 hours new minor resonances slowly appeared in both the aliphatic and aromatic regions

of the ^{1}H NMR spectrum. The resonances from **6** however remained dominant throughout the experiment.

Scheme 6: Reaction Scheme for the Synthesis of $IMesCl_2$

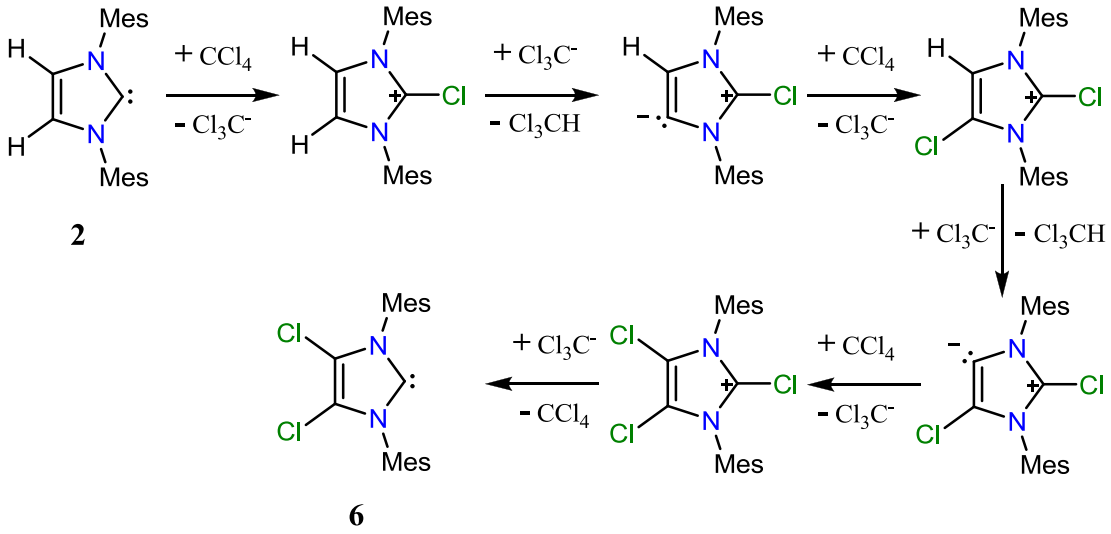

The synthesis of the imidazol-2-imine directly from the $IMesCl_2$ carbene was attempted by modifying a second literature procedure, which involved dissolving **3** in THF, adding it to a solution of TMS-azide and stirring for 14 hours, instead of under reflux conditions in toluene for 72 hours.[64] Much like the previous reaction, there was an appearance of multiple minor resonances, which would account for approximately 5% conversion of starting material, in both the aromatic and aliphatic regions. Purification through recrystallization was attempted through slow diffusion with DCM and *n*-pentane. However no crystals were formed.

Arduengo III has shown that **6** is quite stable as a NHC, which may explain the difficulty in synthesis of the corresponding imidazol-2-imine.[65] Normally NHCs are very basic and cannot handle prolonged exposure to acidic solvents, such as chloroform, without reacting. However in the case of **6,** it is still easily isolated despite being in the presence of an excess of chloroform, which is a by-product of the chlorination reaction, which exemplifies its lack of reactivity. This could also be accounted for by the poor nucleophilicity of **6**, preventing any reaction with TMS-azide from occurring. The use of **6** as an NHC was therefore deemed unfruitful.

Considering the synthetic challenges that came with the functionalization of **6**, the synthesis of another electron deficient NHC and its reactivity to TMS-azide was explored. The benzimidazole carbene **4** (BiPr), was another electron-poor NHC which was synthetically viable. However it would be more desirable to work with aromatic substituents than isopropyl, this is because aromatic groups such as mesityls provide considerably more steric protection. The synthesis of **4'** (BIMes) could be achieved in three steps, the first of which is the synthesis of *N*,*N*'-dimesitylbenzene-1,2-diamine. This can be via a simple cross-coupling reaction between 1,2-dibromobenzene and 2,4,6-trimethylaniline with the use of $Pd(OAc)_2$ as a catalyst, and was achieved in moderate yields.[66] The next step is the formation of the benzimidazolium salt by reaction of the resulting diamine with triethyl orthoformate in the presence of HCl (Scheme 7). The reaction did not however proceed even at elevated temperatures for prolonged periods of time.

Scheme 7: Attempted Synthesis of Benzimidazole Salt of NHC **4'**

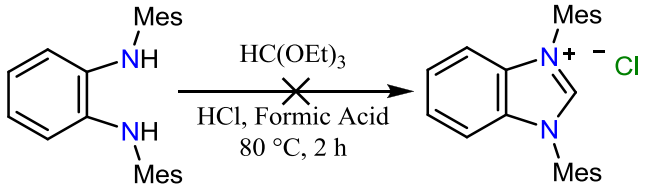

While the synthesis of the benzimidazolium salt in Scheme 7 had not been reported in the literature, the analogous derivative where the mesityl rings are replaced by phenyl rings can be prepared in high yield.[67] One reason for the difference of reactivity between the phenyl and mesityl substituted diamines is likely due to the steric bulk present on the mesityl rings themselves. The ability to install substituted phenyl rings on the benzimidazole nitrogen atoms is desirable as the substituents provide means to control the coordination sphere about the metal center, in addition to preventing bimolecular decomposition. The "bulky" mesityl groups thus seemingly increase the activation energy required for the formation of the corresponding benzimidazolium salt. This is supported by a recent report in the literature where the isolation of this salt required harsh conditions, prolonged reaction times, and more synthetic steps, resulting in poor yields (Scheme 8).[68] This synthetic pathway was however only reported very recently and could not be used at the time this compound was being pursued.

Scheme 8: Synthesis of Benzimidazole Salt of NHC **4'**

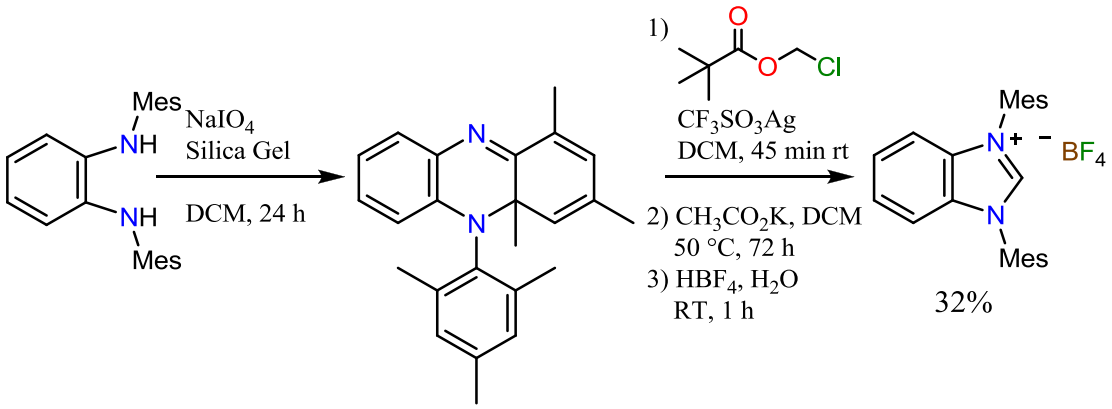

Preliminary experiments for the formation of the *N,N'*-diphenyl-benzimidazole-2-ylidene NHC seemed promising. A small-scale NMR reaction of the salt with 1.2 equivalents of NaHMDS showed the complete disappearance of the imidazolium proton from the NMR spectrum as well as an upfield shift in aromatic signals, suggesting the formation of the free carbene. The aromatic region was quite crowded due to the abundance of signals from the phenyl rings and benzimidazole backbone, as well as the C_6D_6 signal overlapping with characteristic peaks, making the analysis of the NMR data quite difficult. Furthermore, there was the inexplicable appearance of a singlet at 6.5 ppm. In hopes of acquiring a clearer NMR spectrum, the reaction was performed again in a glove-box. This also resulted in the disappearance of the imidazole proton peak. However the unidentifiable resonance at 6.5 ppm was still present and residual peaks of impurities made the NMR data less comprehensible than the previous test, even after several purification processes. Efforts to isolate and identify the components of the reaction mixture were unsuccessful. The difficulty in synthesizing the benzimidazole-based NHC forced attention to be shifted towards the synthesis of other carbenes.

The perimidine-based NHC **5**, consisting of a naphthalene backbone, has the second highest electron withdrawing capabilities of the originally targeted carbenes (Fig. 8). Reports of the synthesis of **5** show it is a high yielding two step synthetic pathway.[69] This NHC in particular has some unique properties, one of which is the electron-rich six membered heterocyclic ring. This attunes the donor properties on the carbon center and imposes geometric constraints on the mesityl rings. In particular the mesityl rings are closer to the carbon atom than they normally would be, increasing the steric effects on the NHC and the metal it is coordinated to, leading to a more stable metal center.[70] The synthesis of the perimidinium salt requires a perimidinone intermediate, **10**, which proved to be a significant synthetic challenge despite multiple reported procedures for its synthesis.[71] Following literature procedures, upon work-up the desired product was not recovered. Instead the intermediate **11** was isolated as a brown solid in 73% yield (Scheme 9). In an effort to drive the reaction to completion pyridine was added to a solution of **11** and allowed to stir for 24 h at 60 °C as the mechanism is believed to be base catalyzed. Upon work-up **10** was isolated in 9% yield. These results were however irreproducible.

Scheme 9: Attempted Synthesis of Perimidinone Intermediate **10**

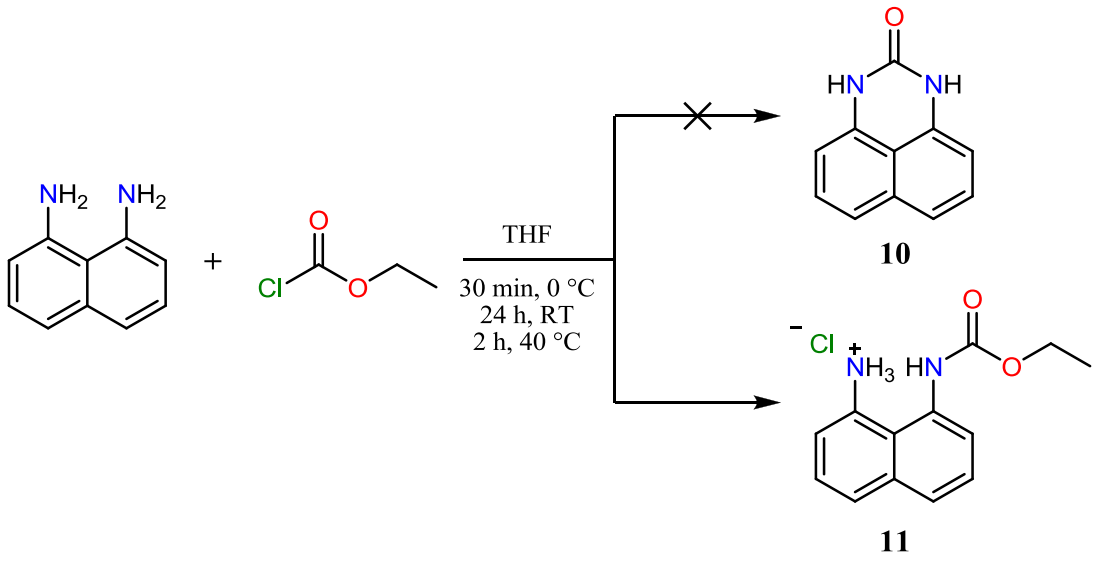

Other literature procedures report the reaction of 1,8-diaminonaphthalene with NaOCN in a solution of hot HCl to give **10**.[72] Unfortunately when this reaction was performed no product was recovered. Although the NHC **5** had several advantageous properties, the difficulty in synthesis made the pursuit of a more synthetically viable NHC the focus of research.

2.2.2 Synthesis and Coordination of *N*-1,3-Dimesityl-4,5-naphthoquino-imidazol-2-ylidene-*N*′-p-tolylureate

Due to its electron withdrawing properties, its known ease of synthesis, and because of its reactivity towards azides, which is crucial in the formation of the imidazol-2-imine, **3** is a desirable ligand scaffold.[73] According to literature reports, the iminium proton of the salt of **3** resonates at 12.8 ppm, which is one of the largest downfield shifts reported for any known imidazolium compound and emphasizing the highly electron-withdrawing capabilities of the quinone moiety as a whole.[74] The synthesis of **3** (QIMes) is performed on a large scale giving a spectroscopically pure light green solid with a yield of up to 65% following literature procedures. Upon reaction of **3** with TMS-azide and the subsequent work-up, **13** is isolated as a spectroscopically pure dark purple solid in a yield of 62% (Scheme 10). The TMS-protected QIMes imidazol-2-imine was also isolated in moderate yields. However its use in further reactions was not required.

Scheme 10: The synthesis of the novel QIMes imidazol-2-imine **13**

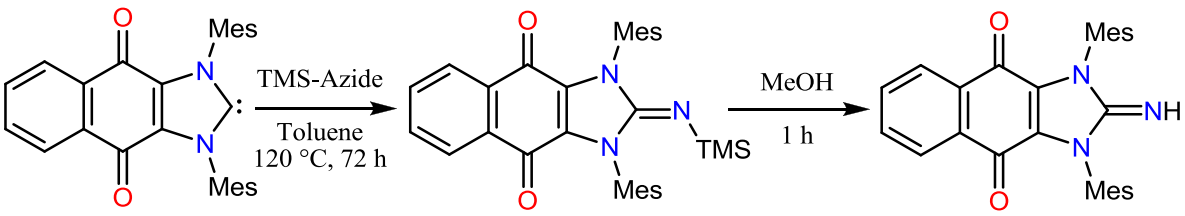

3 **12** **13**

The characteristic imine proton resonates as a broad singlet at 6.71 ppm in the proton NMR, which is a significant downfield shift compared to the IMes imidazol-2-

imine at 4.28 ppm.[75] This again emphasizes the strong electron-withdrawing properties of the quinone moiety present in **13**. There was also an upfield shift of both protons on the naphthalene-1,4-dione backbone. These backbone peaks correspond to two very diagnostic complex multiplets at 7.84 and 6.92 ppm. Furthermore, the $^{13}C\{^{1}H\}$ NMR shows characteristic peaks for the carbonyl and imine carbon at 173.8 and 151.4 ppm, respectively. There is also a strong carbonyl stretch observed at 1653 cm^{-1} in the FTIR.

Following previously established procedures, the synthesis of the corresponding *p*-tolyl ureate and thioureate ligands of **13** was performed.[50] The synthesis of **14a** was performed to yields as high as 90%, leading to a spectroscopically-pure red solid (Scheme 11). The ^{1}H NMR spectrum shows the diagnostic backbone peaks have a slight shift upfield from 7.84 and 6.92 to 7.82 and 6.90 ppm. As well, there is a shift in the aliphatic protons with the mesityl ortho-methyl protons shifted downfield from 2.15 to 2.30 ppm, and the mesityl para-methyl protons shifted upfield from 2.11 to 2.09 ppm, with a new resolved resonance for the *p*-tolyl para-methyl protons at 1.97 ppm. The presence of a broad singlet at 6.23 ppm integrating to one proton represents the ureate NH proton. The $^{13}C\{^{1}H\}$ NMR shows two carbonyl peaks one at 173.7 for the dione, and 156.1 ppm for the ureate as well as the imine carbon being shifted upfield to 147.9 ppm. The FTIR shows that there are two carbonyl stretches observed at 1663 and 1591 cm^{-1}.

Scheme 11: Synthesis of QIMes Imidazol-2-imine *p*-tolylureate Ligand **14a**

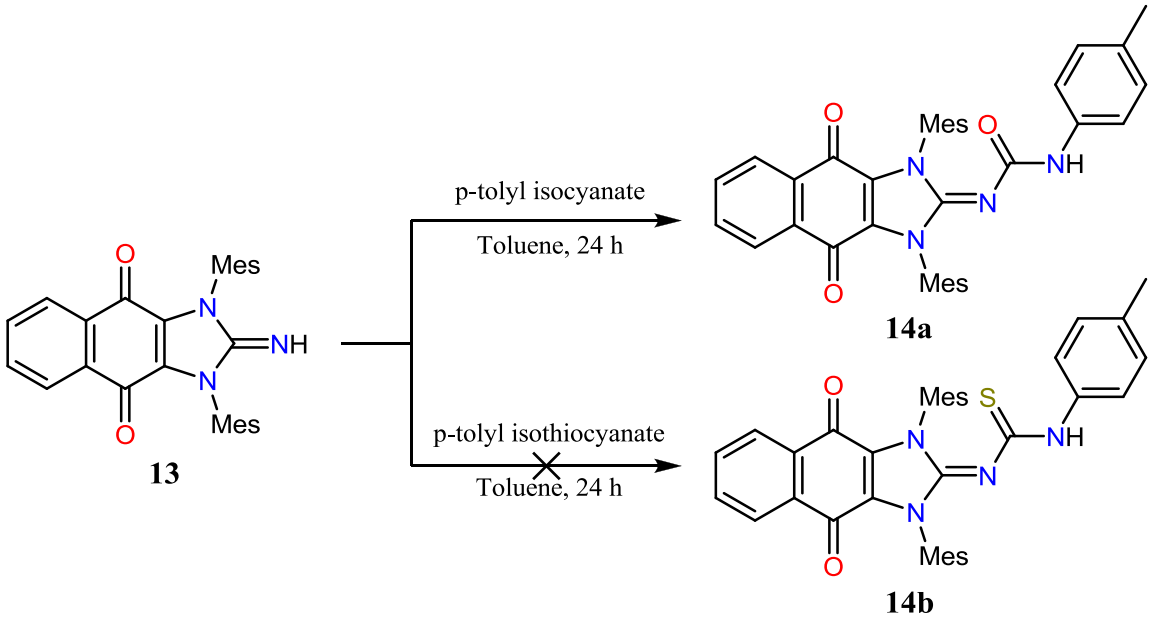

Unlike with the *p*-tolyl isocyanate, the reaction of **13** with *p*-tolyl isothiocyanate led to no reaction. Even under varying conditions such as solvent (THF, toluene, DCM), reaction time, and temperature (-37 – 70 °C), no reaction occurs and **13** is fully recovered. Even the reaction of the TMS-protected imidazol-2-imine, **12**, with *p*-tolyl isothiocyanate leads to no product formation. This can be explained by the electron-withdrawing capabilities of the quinone moiety making the overall molecule less nucleophilic upon deprotonation and therefore less prone to reaction with *p*-tolyl isothiocyanate. Furthermore, *p*-tolyl isothiocyanate is less electrophilic than *p*-tolyl isocyanate which explains the formation of **14a** and not **14b.** The binding mode of **14a** to group 4 and 10 transition metals was thus of interest, along with the activity of the resulting complexes in ethylene polymerization.

$CpTiCl_3$ acted as a desirable metal precursor due to its previous use in complex synthesis in the Lavoie group, allowing for comparative studies of both ligand coordination and catalyst activity. Deprotonation of ligand **14a** using NaHMDS, followed with subsequent addition to a solution of the titanium precursor had varying results depending on both reaction time and solvent used. The coordination reaction was carried out multiple times under varying conditions. In the presence of THF and a reaction time of 2 hours, there is a mixture of products, in roughly a 2:1 ratio, as observed by the diagnostic quinone backbone multiplets that resonate between 7.9 and 7.6 ppm in the proton NMR. The mixture of products is believed to be at least two geometric isomers present in solution, as observed in previous coordination studies in the Lavoie group.[42] Furthermore the lack of a singlet at 5.90 ppm, which represents the Cp ring in $CpTiCl_3$, and the appearance of singlets at 6.08 and 6.13 ppm, in an approximate 2:1 ratio, provides evidence of the coordination of **14a** to titanium(IV). By repeating the reaction in toluene instead of THF, the ratio of the two species present in solution changes to 2:3 with the previously minor geometric isomer being present in a larger quantity. The reaction was repeated a third time, with toluene as the solvent and the addition of the deprotonated ligand to precursor was performed at -37 °C, leading to one species being present in a 10:1 excess in the NMR solution. **15** was recovered in a 83% yield, and was a pure brown solid (Scheme 12).

Scheme 12: Coordination of *p*-tolylureate ligand to $CpTiCl_3$

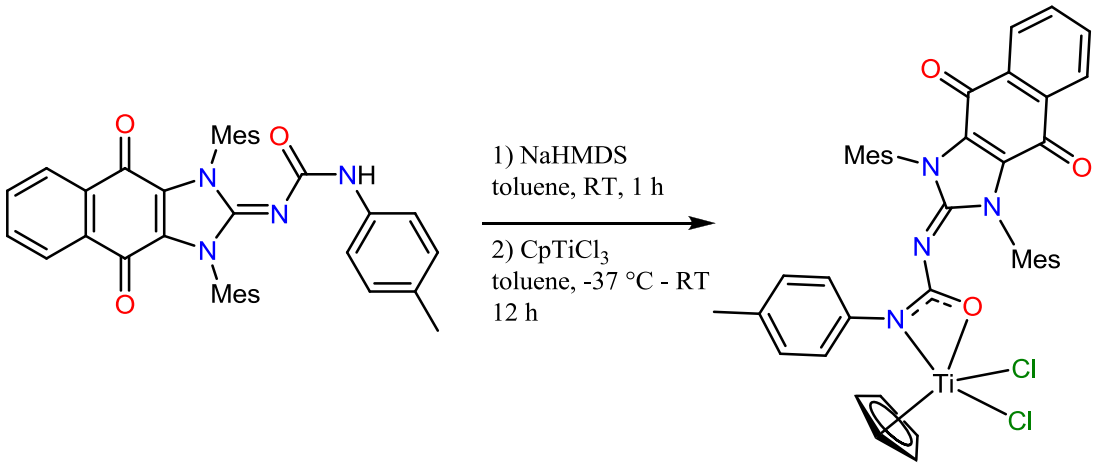

14a **15**

The newly synthesized titanium complex **15** was full characterized using 1D and 2D NMR experiments as well as IR spectroscopy and combustion analysis. In the ^{1}H NMR spectrum the two diagnostic quinone backbone quartets have chemical shifts of 7.75 and 6.88 ppm. The *p*-tolyl protons are now inequivalent, and two doublets integrating to two protons each at 7.31 and 7.11 ppm are present. The FTIR of **15** has two carbonyl stretches at 1604 and 1495 cm^{-1}, which is considerably lower than that observed the ligand. This trend is observed in the previous *N*-imidazol-2-ylidene-*N'*-*p*-tolylureate ligand system and supports the ligand being bound in an $N'_{p\text{-tolyl}}$^O fashion.[48] As expected, despite the electronics being significantly altered, ligand **14a** does not show the initially targeted binding mode.

In an effort to form X-ray quality crystals, a toluene solution of **15** was set up for vapor diffusion of *n*-pentane. Upon work-up the resulting ^{1}H NMR spectrum showed the

appearance of a previously unobserved species that was now in a 1:1 ratio **15**. Variable-temperature NMR studies were performed with no appreciable change in the ratio of the two species observed in the range of 0 to 50 °C. X-ray quality crystals formed from the NMR sample standing at room temperature for a week. The X-ray structure revealed that the product had decomposed to di-*p*-tolylurea and the protonated form of **13** (Fig 13).

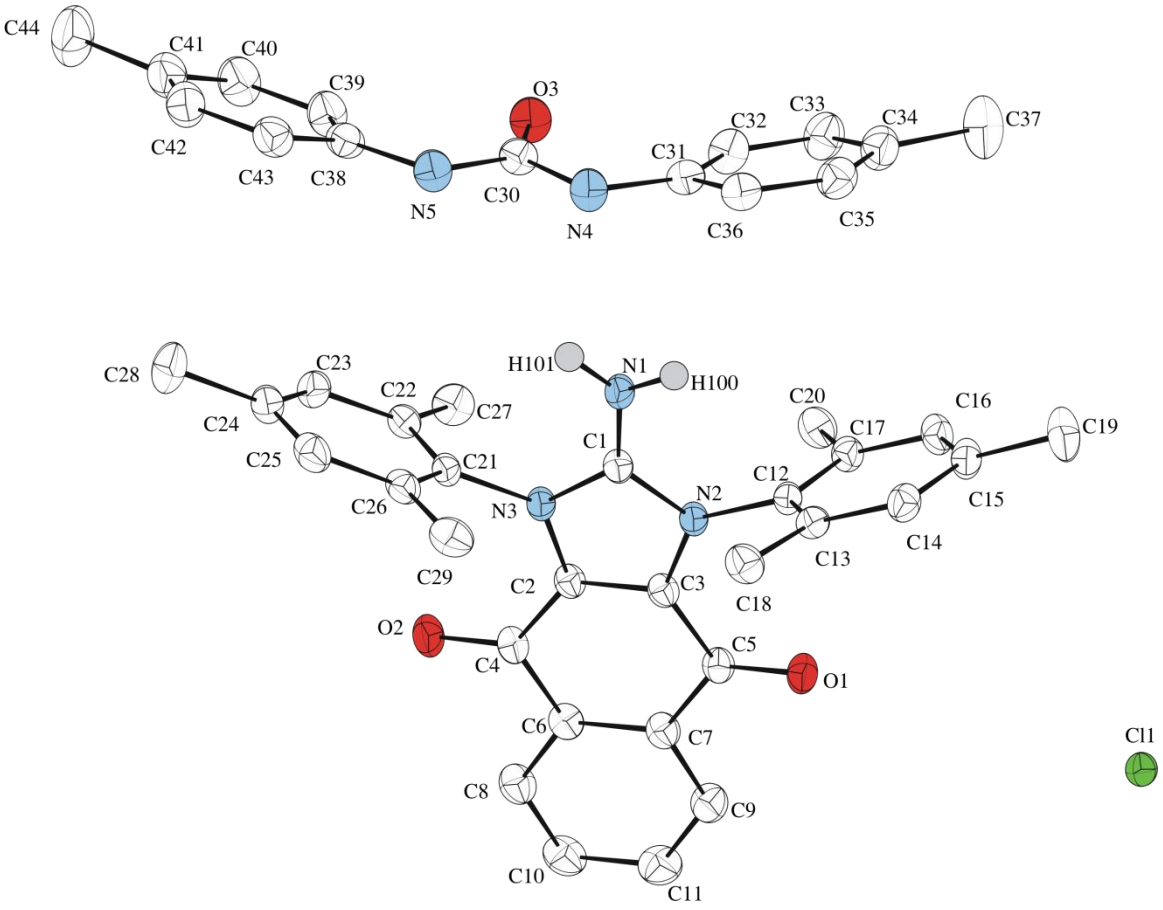

Figure 13. ORTEP diagram of the decomposition product of complex **15** (40% probability level)

A postulated mechanism for the decomposition pathway to these products is facilitated by the presence of adventitious water in the solution of **15** (Scheme 13). Similar decomposition pathways, which involve nucleophilic attack of adventitious water on the iminic carbon of the ligand due to the enhanced electrophilicity of the carbonyl carbon, have been reported in the literature.[76] The electron-withdrawing naphthalene-1,4-dione backbone may therefore account for the decomposition of the metal complex. While these were the only decomposition products that were structurally characterized, there is likely other decomposition species present in solution. This shows the overall sensitivity of the ligand system due to its electron-deficient nature.

Scheme 13: The proposed mechanism for the decomposition of **15**

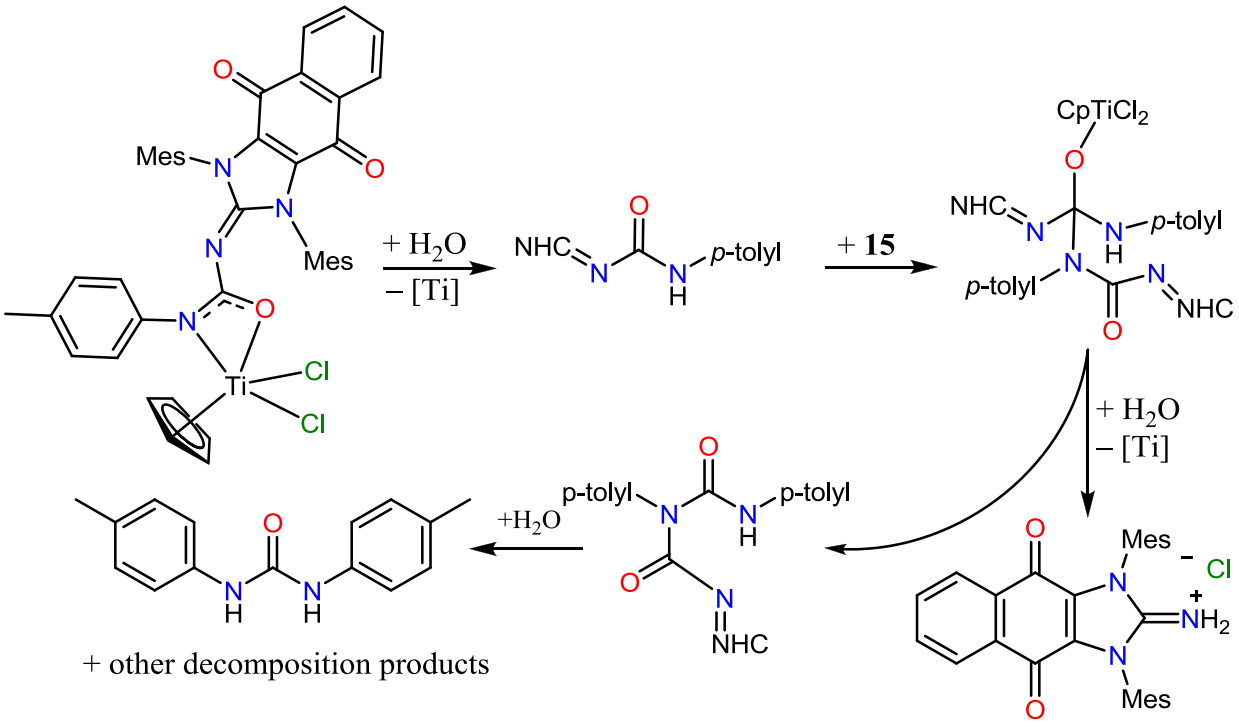

Despite the *N'*$_{p\text{-tolyl}}$^O coordination mode of the ligand in **15** and the observed decomposition of the complex, the performance of **15** as an ethylene polymerization catalyst was still investigated as it could still be compared to previous generations. Under standard conditions and a trial time of 10 minutes **15** had a turnover frequency of 75 kg PE mol Ti^{-1} h^{-1}, slightly higher than the second generation *N*-imidazol-2-ylidene-*N'*-*p*-tolylureate catalysts, specifically the titanium complexes which had activities as high as 60 kg PE mol Ti^{-1} h^{-1}.[50] This result supports the initial hypothesis that an electron-deficient NHC would lead to a less electron rich metal center and subsequently a more active ethylene polymerization catalyst. The activity of **15** compared to that of other highly active catalysts, such as zirconocene dichloride, was three orders of magnitude lower, and in an effort to synthesize more active catalysts coordination with a variety of other metal precursors was employed.[77]

Initial reactions of **14a** with $CpZrCl_3$ and $TiCl_4(THF)_2$ showed promising results for its coordination and the formation of the corresponding metal complexes. However, the *N'*$_{p\text{-tolyl}}$^O binding mode of the ligand in **15**, as well as the tendency for **15** to decompose, made the isolation and characterization of these complexes undesirable. Coordination of the ligand to other metal precursors was therefore evaluated to synthesize more active titanium ethylene polymerization catalysts. Following procedures in the literature for similar ureate ligands with a *N*^O binding mode, the coordination of **14a** to group 4 metals busing a multitude of tetrakis(dimethylamido) precursors was explored due to their ease of synthesis.[78,79,80] Unlike previously used procedures, these reactions require no base and require mild heating (50 – 60 °C). Reaction of $Ti(NMe_2)_4$ and

$Zr(NMe_2)_4$ precursors in hexanes at 1.0 and 0.5 equivalents of **14a** should yield the mono(ureato) and bis(ureato) complexes respectively. However, upon work-up ligand **14a** was recovered and no reaction had occurred. Further attempts at coordination with group 10 metals, such as $[Ni(methylallyl)Cl]_2$ and $[Pd(allyl)Cl]_2$ following previous established methods were also unsuccessful. In both cases no reaction had occurred as starting material was recovered. This shows the ligands general lack of reactivity towards coordination.

Recently, ^{31}P and ^{77}Se NMR spectroscopy has been utilized to better describe the electronics of carbenes.[81,82] Carbenes have been known and highly regarded as purely σ-donors for quite some time, but recent computational and experimental work has shown that π-back donation may contribute significantly to the metal carbon bond.[83,84] There are several techniques used for the determination of the donor properties of carbenes, with the most frequent technique being the measurement of the carbonyl stretching frequency of CO ligands in nickel complexes ($Ni(CO)_3(L)$), also known as the Tolman electronic parameter (TEP).[85] This technique relies on the fact that electron density from a ligand is passed onto the metal and the π* orbital of CO. Unfortunately this technique does not differentiate the σ-donation and π-back donation of the ligand in question, leaving the overall contribution of these two factors unknown.

NHC-phosphinidene adducts can be represented by two major canonical structures (Fig. 14). These adducts are known for having very characteristic and high-field ^{31}P NMR resonances compared to that of normal phosphoalkenes.[86] These high-field

resonances signify an electron rich phosphorous atom, represented by structure **B** as confirmed by single-crystal diffraction studies.[87] Increases in the π-accepting capabilities of the carbene on the phosphinidene adduct favors π-back donation of the lone pair on the phosphorous into the vacant p orbital of the carbene, increasing the contribution of resonance form **A**. Consequently a downfield shift will be observed in the ^{31}P NMR spectrum of the carbene-phosphinidene adduct, making this a straight forward technique for the evaluation of a carbenes π-accepting properties.

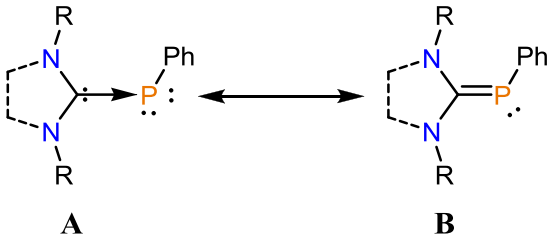

A **B**

Figure 14. Limiting canonical structures of carbene-phosphinidene adducts

In order to get a more accurate understanding of the electronics of **3**, the synthesis of its phosphinidene adduct was pursued. If **3** is a larger π-acceptor than the TEP shows then the initial electronic properties that made this a desirable NHC to work with would have been inaccurate. Furthermore the functionalization and coordination of the QIMes to a metal could lead to a metal center that is much more electron deficient than initially thought. There are several examples of π-acidic NHCs leading to less active metal catalysts in the literature, one of which involved Fürstner et al. showing that the accepting NHC ligands detrimentally impacted the outcome of gold-catalyzed reactions.[88] The synthesis of the phosphinidene adduct of **3** was therefore explored.

Following literature procedures, a reaction mixture of **3**, $PPhCl_2$, and magnesium turnings in THF was set up.[65] Within the span of several minutes, the reaction mixture had changed colour to a deep red solution. After 24 hours the solution was decanted, dried, and washed with *n*-pentane. In attempting to record a ^1H NMR spectrum of the sample, it became evident that the species in solution was paramagnetic, as observed by a large shim line and very broad resonances.

These observations are analogous to the reduction of benzophenone, which is a common indicator when distilling toluene over sodium. When there is no more water present in toluene, sodium can begin reduction of benzophenone, which leads to a deeply purple coloured diphenylketyl radical anion.[89] Mg could thus possibly react with the naphthalene-1,4-dione backbone, which resembles benzophenone, and leads to the formation of a deeply red coloured radical anion and a dianionic species (Scheme 14). There is also precedent in the literature for the reduction of the quinone backbone.[90] These two species could possibly form an aggregate, which would result in line broadening as observed in the NMR spectrum.[91]

Scheme 14: The Free Radical Reduction of **3** to a Paramagnetic Species

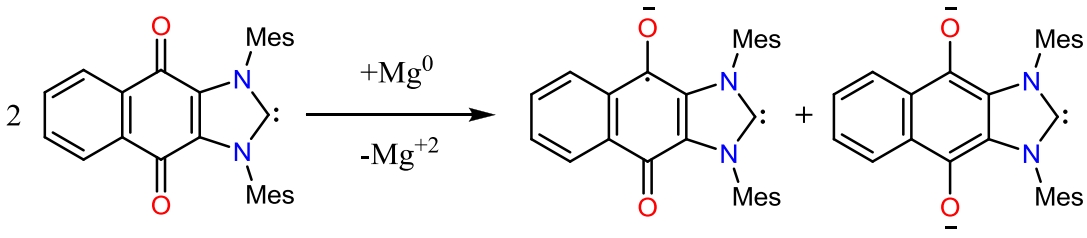

Due to the unwanted reduction of NHC **3**, an alternative synthesis for the phosphinidene adduct was employed. Following literature procedures the reaction of NHC with $P_5(Ph)_5$ in THF over 24 hours results in the formation of **17** in 70% yield.[92.93] A ^{31}P NMR spectrum of **17** was taken with a capillary containing H_3PO_4 as an internal standard had a resonance at - 3.6 ppm. This is considerably higher field than both the SImes and IMes which resonate at -10.4 and -23.0 respectively, indicating that QIMes is a much better π-acceptor. This is not accounted for in the TEP calculations for **17**, as both TEP and ^{31}P NMR data are required for an accurate understanding of a carbenes σ-donation and π-donation.

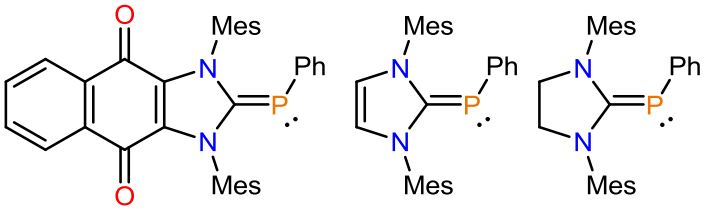

17 -3.6 ppm **IMes** -23.0 ppm **SIMes** -10.4 ppm

Figure 15. QIMes phosphinidene adduct compared to IMes and SIMes

The π-accepting nature of the QIMes NHC can be one explanation for the shortcomings observed in this ligand system. For example the decomposition of the titanium complex **15** is analogous to the difficulty of formation of stable titanium (IV) CO complexes. This is because titanium(IV) is a d^0 metal and has no d electrons to back bond to CO, which is a strong π-acid. This also leads to a less nucleophilic ligand framework as observed by the difficulty in synthesis of **14b**, as well as the difficulty in coordination of ligand **14a**. Regardless, the use of the quinone-based ligand still afforded

complex **15** which is more active that the second generation *N*-Imidazol-2-ylidene-*N*′-*p*-tolylureate complexes that were synthesized in the Lavoie group. To see what effect this NHC would have on other ligand systems, synthesis of a QIMes imidazol-2-imine ethenolate ligand, which has only one likely binding mode, was attempted.

2.2.3 Attempted Synthesis of 1,3-Dimesityl-4,5-naphthoquino-imidazol-2-imine Ethenolate Ligand

In an effort to better understand the utility of imidazol-2-imine **13**, its incorporation as a fragment into a more active class of ligands was attempted. The imidazol-2-imine ethenolate ligand system is the most active systems synthesized in the Lavoie group. With activities as high as 170 kg PE mol^{-1} h^{-1}, it is an excellent system not just for its activity but because it is a monoanionic bidentate ligand with a forced binding mode.[94] It also resembles successful ligand systems such as the salicylaldiminate, by having a neutral nitrogen and anionic oxygen that it can bind through.

Experimental procedures were adopted for the synthesis of naphthalene-1,4-dione backbone version of these ligands. In an attempt to isolate a pure halide salt, reaction with three different *para*-substituted phenylethanones was evaluated (Scheme 15). Unfortunately, despite promising ^{1}H NMR spectra, the isolation of a spectroscopically pure ligand salt could not be achieved.

Scheme 15: The Attempted Synthesis of QIMes Imidazol-2-imine Arylethanone Salt

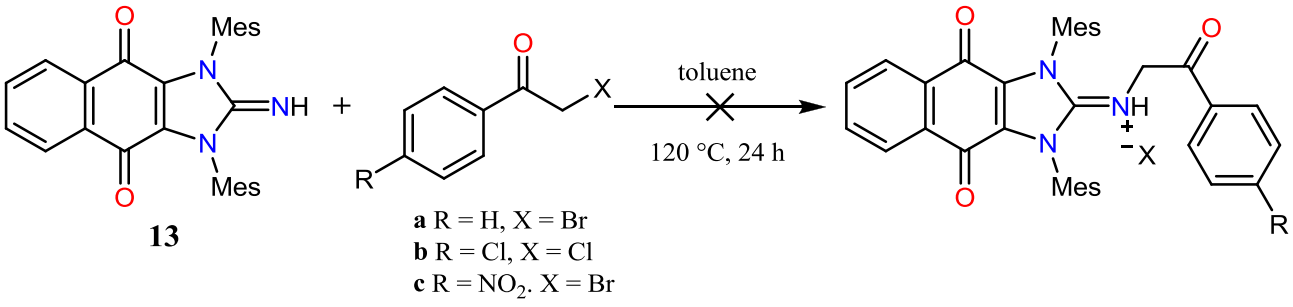

a R = H, X = Br
b R = Cl, X = Cl
c R = NO_2. X = Br

Only the attempted synthesis of the *para*-chlorophenyl ethanone hydrochloride salt will be discussed, although these observations apply to all three derivatives. Much like for the synthesis of the first generation of imdazol-2-imine ethenolate ligand, refluxing a reaction mixture of **13** and 2-chloro-1-(4-chlorophenyl)ethanone in toluene resulted in the appearance of a coloured precipitate. After filtration and a pentane wash a yellow solid was isolated. Diagnostic multiplet resonances for the quinone backbone in the ^{1}H NMR spectrum showed a downfield shift with respect to the corresponding resonances in **13**. However, the NMR spectrum had a multitude of resonances making analysis quite difficult. The first generation of imidazol-2-imine arylethanone salts had a few isomers in solution, which might explain the multitude of resonances in spite of several purification processes. The diagnostic iminic proton represented as a triplet, typically between 8.0 – 10.0 ppm, was not observed. Furthermore the CH_2 resonance was not accounted for in the NMR spectrum.

To make analysis of this spectrum easier, 1D ^{1}H NMR and 2D ^{1}H-^{1}H COSY NMR spectra of the unknown yellow solid was run on a 600 MHz NMR spectrometer. The increased resolution in the ^{1}H NMR spectrum along with the COSY spectrum allowed for the identification of the naphthalene-1,4-dione backbone peaks as well as the phenyl peaks. There was however still no characteristic triplet resonance that accounted for the iminic proton, and there was no resonance for the CH_2 linker. Multiple purifications to isolate one species consistently led to no significant change in the NMR spectra. The NMR spectroscopy could not therefore provide evidence to confirm whether or not the QIMes imidazol-2-imine *p*-chlorophenylethanone salt had been synthesized.

To assist in determining the structure of the product, mass spectrometry of the reaction product was performed using the ESI method.

If the QIMes imidazol-2-imine *p*-chlorophenylethanone salt were successfully synthesized then it would be expected that the M+ peak to be at *m/z* 603. This however is not observed as there are multiple higher *m/z* peaks, with the M+ peak being at *m/z* 961 (Fig. 17). The peaks at *m/z* 603 and 450 represent the desired ethanone salt and the imidazol-2-imine **13**, respectively. However, there are multiple unexplained peaks, which may represent hypothesized side-products due to reactivity at the iminic nitrogen and the carbonyls in the quinone backbone. One such product is a diazene consisting of two QIMes units, which would be represented by the *m/z* 899 peak, with literature examples of similar triazene structures (Fig. 16).[95]

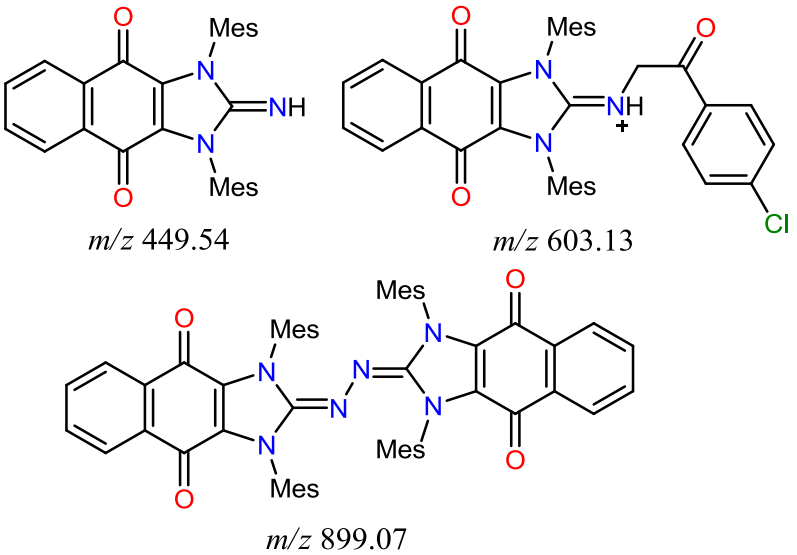

Figure 16. A few structures present in the mass spectrum

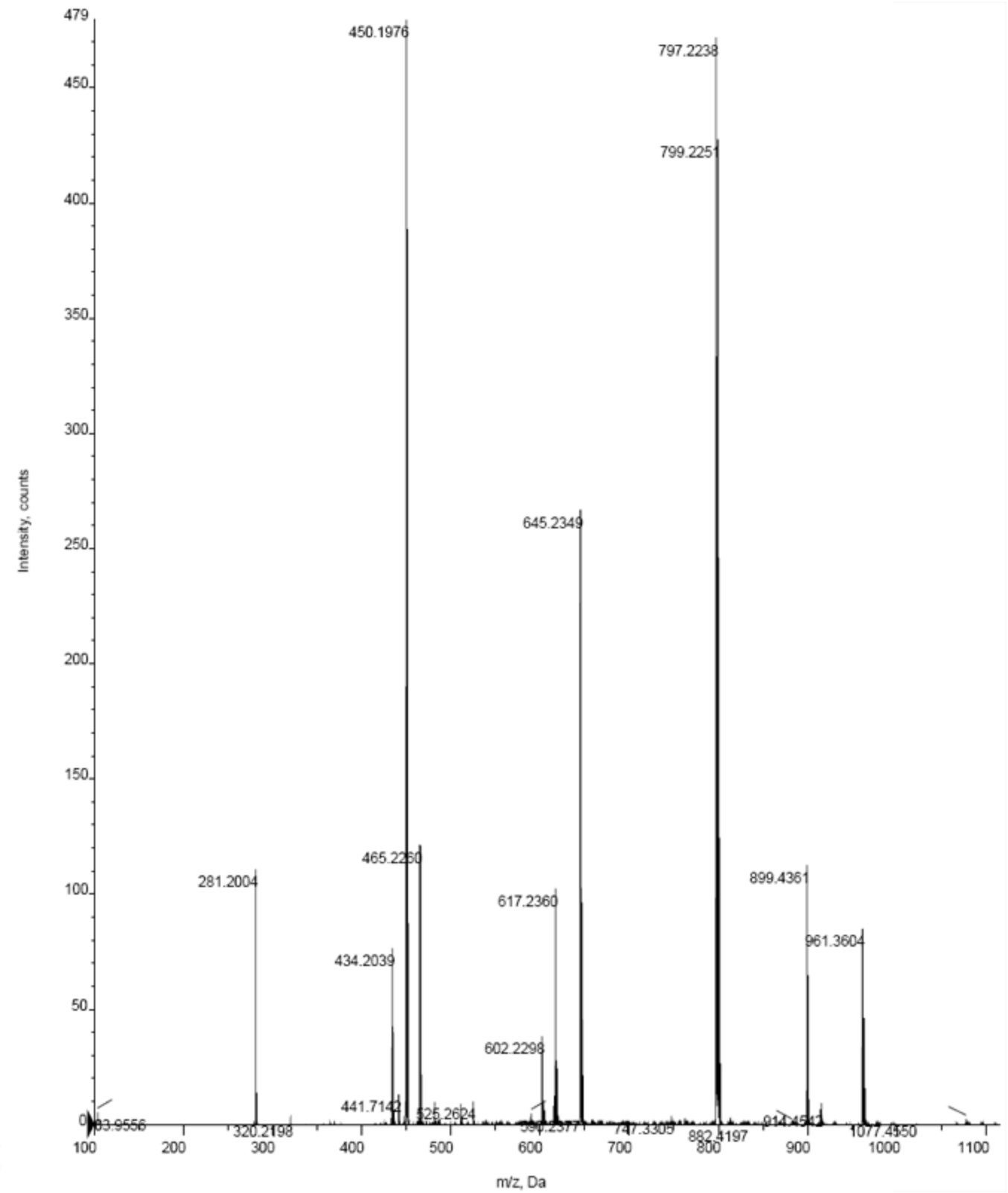

Figure 17. Mass spectrum of the unknown yellow solid

Due to several inexplicable peaks in the mass spectrum, the reaction was repeated in hopes of isolating a pure sample. A pale yellow precipitate was isolated. However, 1D and 2D NMR experiments did not provide enough information to support the synthesis of the QIMes imidazol-2-imine *p*-chlorophenylethanone salt. The sample was analyzed by mass spectrometry and interestingly a slightly different spectrum resulted. The *m/z* peaks that were present in both spectrums were: 899, 797, 645, 617, 603, 465, and 450 m/z, three of which are accounted for (Fig. 16). The identity of these fragments remains unknown. However, based on previous observations with the QIMes *N*-imidazol-2-yilidene,*N'*p-tolylureate ligand (**14a**), undesired reactivity with the naphthalene-1,4-dione backbone carbonyl groups might explain these observations.

In an effort to synthesize the desired ligands, the sodium salt of the QIMes imidazol-2-imine was synthesized by reaction of **13** with NaHMDS (Fig. 18). With the strong electron withdrawing group on the back of the imidazol-2-imine, a lack of nucleophilic character could be the reason that a pure clean product could not be isolated in high yields. Interestingly the ^{1}H NMR spectrum of **18** revealed that the mesityl rings had become inequivalent on the NMR time scale, as the protons had become magnetically inequivalent. There were therefore two resonances observed for each proton present on the mesityl ring. This isn't observed in the proton spectra of other QIMes units such as **13** or **14a**, due to the symmetry in the molecule as well as rigidity of the naphthalene-1,4-dione backbone leading to equivalent mesityl rings on the NMR timescale. The reaction of **18** and 4-chloroacetophenone in toluene under reflux for 24 h led to a pale yellow precipitate. Unfortunately the ^{1}H NMR spectrum was no different

than spectra from other attempted reactions. In the interest of time, work with this ligand system was not pursued any further.

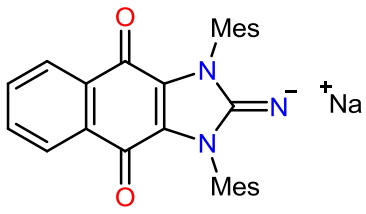

18

Figure 18. QIMes imidazol-2-imine sodium salt

Chapter 3: Conclusions

3.0 Conclusions

The new *N*-Imidazol-2-ylidene-*N*′-*p*-tolylthioureate ligand coordinates to nickel and palladium in a bidentate fashion, through a $N'_{p\text{-tolyl}}$^S binding mode. The nature of the chelate was determined by a combination of NMR and FTIR spectroscopy as well as solid-state structures. The isolated palladium and nickel complexes (**7**, **8**, **9**) showed negligible activity in ethylene polymerization, but provided an interesting coordination study. In the interest of improving the performance of these catalysts, synthesis of electron-poor imidazol-2-ylidene fragments was pursued.

The attempted synthesis of electron deficient NHCs had resulted in the isolation of QIMes *N*-imidazol-2-yilidene,*N'p*-tolylureate ligand (**14a**) in yields as high as 90%. The coordination of **14a** to titanium was the first example of coordination for electron deficient NHC based ligands in the Lavoie group. The titanium (IV) complex **15** showed activities as high as 75 kg PE mol^{-1} h^{-1}, higher than observed in the second generation *N*-imidazol-2-ylidene-*N*′-*p*-tolylureate catalysts, specifically the titanium complexes. Unfortunately the naphthalene-1,4-dione backbone led to the uncontrolled decomposition of **15**, as well as the difficulty of synthesis in the QIMes imidazol-2-imine ethenolate ligand. More work must be put towards the isolation of QIMes imidazol-2-imine ethenolate ligands, and subsequent coordination to early transition metals. This work may result in highly active catalysts as the ligand will resemble the highly active salicylaldiminate ligands as well as having a forced binding mode. However, they may be prone to decomposition, as previously observed with QIMes ligands. Therefore future

work with electron deficient NHCs would benefit from a backbone that is nonreactive such as the benzimidazole NHC **4'**. As discussed herein the recent isolation of the salt of **4'**, as well as its electron withdrawing capabilities and poor π-accepting properties make it a desirable NHC framework.

Chapter 4: Experimental

4.0 Experimental

4.1 General Experimental

All reactions were performed in a N_2 atmosphere in a MB150BG-II Glove Box or on a standard Schlenk line using proper techniques in oven-dried glassware and were at room temperature unless otherwise reported. Solvents were obtained from commercial sources (Sigma Aldrich, Alfa Aesar). When appropriate solvents were dried using an MBraun SPS fitted with alumina columns and stored over molecular sieves under a positive pressure of N_2. All reagents were purchased from Sigma Aldrich, Strem Chemicals, or Alfa Aesar and were used as received, without further purification. MAO was graciously donated by Albermarle Corp. FTIR spectra were recorded on a Nicolet 6700 FT-IR spectrometer with data reported in wave numbers (cm^{-1}). Elemental composition was determined by Guelph Chemical Laboratories Incorporated. ^{1}H, ^{2}H, ^{13}C, and ^{31}P NMR spectra were recorded on a Burker 400 AV or 300 AV spectrometer at room temperature. Deuterated solvents were degassed using three freeze-pump-thaw cycles. C_6D_6 was vacuum distilled over sodium and stored under N_2. $CDCl_3$ was vacuum distilled over calcium hydride and stored under N_2. The spectra were referenced internally relative to the residual protio-solvent (^{1}H) and solvent (^{13}C) resonances as well as internal standards (^{31}P), and chemical shifts were reported with respect to $\delta = 0$ ppm for tetramethylsilane. *J*-coupling constants are reported in hertz (Hz). The multiplicities of signals is reported as s (singlet), d (doublet), t (triplet), and m (multiplet). Where ^{13}C spectra are reported, the ^{1}H and ^{13}C assignments were confirmed by two-dimensional ^{1}H - ^{1}H , and ^{13}C - ^{1}H correlation NMR experiments.

4.2 Experimental Procedures

(1-(1,3-Dimesityl-1H-imidazol-2(3H)-ylidene)-3-*p*-tolylthioureato) Nickel (II) 2-methylallyl (7)

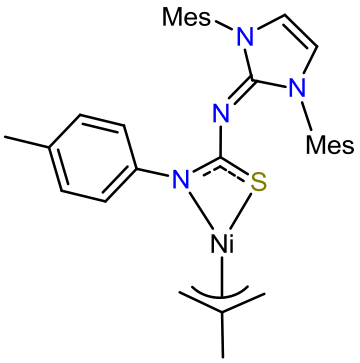

1c (75.0 mg, 0.200 mmol) dissolved in 2 mL of THF was added to a solution of NaHMDS (32.3 mg, 0.200 mmol) in 2 mL of THF. The reaction mixture was stirred for 1 h at room temperature and subsequently added to a THF solution of $[Ni(methylallyl)Cl]_2$ (23.9 mg, 0.100 mmol). The resulting solution was stirred for 1.5 h, filtered and dried under reduced pressure. The recovered brown solid was dissolved in THF and recrystallized by slow diffusion of *n*-pentane, giving a spectroscopically-pure orange solid (79 mg, 0.10 mmol, 85%). **^{1}H NMR (400 MHz, C_6D_6, 25 °C):** δ 7.28 (d, $^{3}J_{HH}$ = 8.32 Hz, 2H, *o*-$CH_{(p\text{-tolyl})}$), 7.00 (d, $^{3}J_{HH}$ = 8.08 Hz, 2H, *m*-$CH_{(p\text{-tolyl})}$), 6.70 (s, 2H, *m*-$CH_{(mesityl)}$), 6.63 (s, 2H, *m*-$CH_{(mesityl)}$), 5.74 (s, 2H, NCHCHN), 2.73 (d, $^{3}J_{HH}$ = 2.76, 1H, methyl*allyl*), 2.41 (d, $^{3}J_{HH}$ = 2.56 Hz, 1H, methyl*allyl*), 2.29 (s, 6H, *o*-$CH_{3(mesityl)}$), 2.20 (s, 6H, *o*-$CH_{3(mesityl)}$), 2.18 (s, 3H, *p*-$CH_{3(p\text{-tolyl})}$), 1.99 (s, 6H, *p*-$CH_{3(mesityl)}$), 1.70 (s, 1H, methyl*allyl*), 1.69 (s, 3H, *methyl*allyl), 1.51 (s, 1H, methyl*allyl*) ppm. **^{13}C{^{1}H} NMR (100 MHz, C_6D_6, 25 °C):** δ 175.7 (*C*=*S*), 147.6 ($C_{ipso(p\text{-tolyl})}$), 146.6 (N*C*N), 139.1 (*p*-*C*$CH_{3(mesityl)}$), 136.0 (*o*-*C*$CH_{3(mesityl)}$), 135.9 (*o*-*C*$CH_{3(mesityl)}$), 132.6 ($C_{ipso(mesityl)}$), 130.2 (*p*-*C*$CH_{3(p\text{-tolyl})}$), 129.7 (*m*-*C*$H_{(mesityl)}$), 129.6 (*m*-*C*$H_{(mesityl)}$), 123.6 (*o*-*C*$H_{(p\text{-tolyl})}$), 117.2 (*2*-methylallyl), 116.5 (N*CC*N), 53.1 (*1*-methylallyl), 44.9 (*3*-methylallyl), 23.5 (*methyl*allyl), 21.1 (*p*-C*C*$H_{3(mesityl)}$), 21.3 (*p*-C*C*$H_{3(mesityl)}$ + *p*-C*C*$H_{3(p\text{-tolyl})}$), 18.7 (*o*-C*C*$H_{3(mesityl)}$), 18.6 (*o*-C*C*$H_{3(mesityl)}$) ppm. **Anal.**

Calcd. for $C_{33}H_{38}N_4SNi$ (%): C, 68.17; H, 6.59; N, 9.64; **Found (%):** C, 67.89; H, 6.32; N, 9.78.

(1-(1,3-Dimesityl-1H-imidazol-2(3H)-ylidene)-3-*p*-tolylthioureato) Palladium (II) allyl (8)

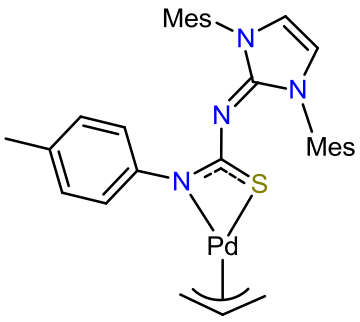

1c (50.0 mg, 0.100 mmol) dissolved in 2 mL of toluene was added to a solution of NaHMDS (21.0 mg, 0.100 mmol) in 2 mL of toluene. The reaction mixture was stirred for 1 h at room temperature, and subsequently added to a 2-mL toluene solution of $[Pd(allyl)Cl]_2$ (19.4 mg, 0.050 mmol). The resulting solution was stirred for 1.5 h, filtered and the volatiles removed under reduced pressure. The recovered dark red solid was purified by crystallization using toluene and pentane to afford a spectroscopically-pure red solid (52 mg, 0.070 mmol, 85%). **^{1}H NMR (400 MHz, C_6D_6, 25 °C):** δ 7.52 (d, $^3J_{HH}$ = 8.08 Hz, 2H, *o*-$CH_{(p\text{-tolyl})}$), 7.01 (d, $^3J_{HH}$ = 8.08 Hz, 2H, *m*-$CH_{(p\text{-tolyl})}$), 6.67 (s, 2H, *m*-$CH_{(mesityl)}$), 6.63 (s, 2H, *m*-$CH_{(mesityl)}$), 5.78 (s, 2H, NCHCHN), 4.24 (m, 1H, *allyl*), 3.50 (d, $^3J_{HH}$ = 6.80 Hz, 1H, *allyl*), 3.24 (d, $^3J_{HH}$ = 7.76 Hz, 1H, *allyl*), 2.31 (s, 6H, *o*-$CH_{3(mesityl)}$), 2.26 (s, 6H, *o*-$CH_{3(mesityl)}$), 2.20 (s, 3H, *p*-$CH_{3(p\text{-tolyl})}$), 2.08 (d, $^3J_{HH}$ = 4.52 Hz, 1H, *allyl*), 1.93 (s, 6H, *p*-$CH_{3(mesityl)}$) ppm**. ^{13}C{^{1}H} NMR (100 MHz, C_6D_6, 25 °C):** δ 176.8 (*C*=*S*), 146.4 ($C_{ipso(p\text{-tolyl})}$), 146.3 (N*C*N), 138.8 (*p*-*C*$CH_{3(mesityl)}$), 135.7 (*o*-*C*$CH_{3(mesityl)}$), 135.2 (*o*-*C*$CH_{3(mesityl)}$), 132.4 ($C_{ipso(mesityl)}$), 131.7 (*p*-*C*$CH_{3(p\text{-tolyl})}$), 129.4 (*m*-*C*$H_{(mesityl)}$), 124.1 (*o*-*C*$H_{(p\text{-tolyl})}$), 116.1 (N*CC*N), 67.6 (*2*-allyl), 59.2 (*1*-allyl), 48.7 (*3*-allyl), 20.8 (*p*-C*C*$H_{3(mesityl)}$) + *p*-C*C*$H_{3(p\text{-}}$

$_{tolyl)}$), 18.5 (*o*-C*C*H$_{3(mesityl)}$), 18.4 (*o*-C*C*H$_{3(mesityl)}$) ppm. **Anal. Calcd. for $C_{32}H_{36}N_4SPd$ (%):** C, 62.48; H, 5.90; N, 9.11; **Found (%):** C, 62.75; H, 5.72; N, 8.86.

Bis(1-(1,3-dimesityl-1H-imidazol-2(3H)-ylidene)-3-*p*-tolylthioureato)) Nickel (II) (9)

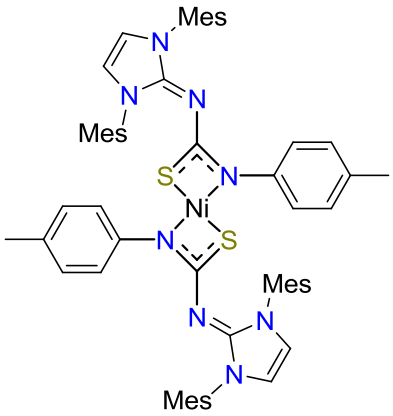

1c (51.0 mg, 0.106 mmol) and NaHMDS (40.0 mg, 0.213 mmol) were added to a Schlenk tube and dissolved in THF. The resulting solution was stirred for 1 h. To a separate Schlenk tube, bis(cyclooctadiene)nickel(0) (29.2 mg, 0.106 mmol) was added and dissolved in THF. This solution was cooled to -78 °C and an excess of chlorobenzene (119.0 mg, 1.06 mmol) was added to the solution. After 10 min the former solution was added to the latter, warmed to room temperature and stirred for 18 h. The mixture was filtered and the volatiles removed in vacuo. The product was further purified by recrystallization from THF and diethyl ether to give a spectroscopically-pure green solid (64 mg, 0.065 mmol, 61% yield). **^{1}H NMR (400 MHz, C_6D_6, 25 °C):** δ 6.93 (d, $^3J_{HH}$ = 8.32 Hz, 2H, *o*-CH$_{(p\text{-tolyl})}$), 6.75 (d, $^3J_{HH}$ = 8.12 Hz, 2H, , *m*-CH$_{(p\text{-tolyl})}$), 6.72 (s, 4H, , *m*-CH$_{(mesityl)}$), 5.63 (s, 2H, NCHCHN), 2.14 (s, 6H, *p*-CH$_{3(mesityl)}$), 2.04 (s, 15H, *o*-CH$_{3(mesityl)}$ / *p*-CH$_{3(p\text{-tolyl})}$) ppm. **^{13}C{^{1}H} NMR (100 MHz, C_6D_6, 25 °C):** δ 173.3 (*C*=*S*), 145.0 ($C_{ipso(p\text{-tolyl})}$), 143.6 (N*C*N), 138.5 (*p*-*C*CH$_{3(mesityl)}$), 135.7 (*o*-*C*CH$_{3(mesityl)}$), 132.3 ($C_{ipso(mesityl)}$), 129.9 (*p*-*C*CH$_{3(p\text{-tolyl})}$), 129.2 (*m*-*C*H$_{(mesityl)}$), 124.7 (*o*-*C*H$_{(p\text{-tolyl})}$), 115.6 (N*C*CN), 20.9 (*p*-C*C*H$_{3(mesityl)}$), 20.6 (*p*-C*C*H$_{3(p\text{-}}$

$_{tolyl)}$), 18.1 ppm (*o*-C*C*H$_{3(mesityl)}$) ppm. **Anal. Calcd. for $C_{58}H_{64}N_8S_2Ni$ (%):** 69.94 C, 6.48 H, 11.25 N. **Found (%):** 70.18 C, 6.63 H, 10.98 N.

2-Imino-1,3-dimesityl-2,3-dihydro-1H-naphtho[2,3-d]imidazole-4,9-dione (13)

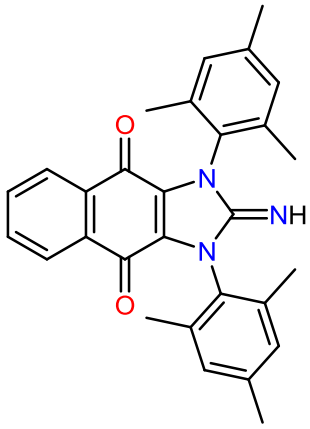

To an oven dried Schlenk tube was added **3** (1.40 g, 3.22 mmol) and 10 mL of toluene. TMS-azide (600 µL, 4.51 mmol) was added, and the solution stirred for 72 h at 120 °C under reflux conditions. The reaction mixture was then filtered through a cannula and the filtrate was dried in vacuo. The resulting purple solid was dissolved in methanol, stirred for 1 h, and dried. A spectroscopically pure dark purple solid was obtained (1.10 g, 2.45 mmol, 62%). **^{1}H NMR (300 MHz, C_6D_6, 25 °C):** δ 7.84 (m, $^3J_{HH}$ = 2.98 Hz, 2H, 5,8-CH$_{(dione)}$), 6.92 (m, $^3J_{HH}$ = 2.99 Hz, 2H, 6,7-CH$_{(dione)}$), 6.79 (s, 4H, *m*-CH$_{(mesityl)}$), 6.72 (s, 1H, C=N*H*), 2.15 (s, 12 H, *o*-CH$_{3(mesityl)}$), 2.11 (s, 6H, *p*-CH$_{3(mesityl)}$) ppm. **^{13}C{^{1}H} NMR (75 MHz, C_6D_6, 25 °C):** δ 173.8 (*C*=O), 151.4 (*C*=N), 138.6 ($C_{ipso(mesityl)}$), 136.4 (*o*-*C*CH$_{3(mesityl)}$), 132.9 (6,7-*C*H$_{(dione)}$), 132.1 (4,9-$C_{(dione)}$), 131.1 (*p*-*C*CH$_{3(mesityl)}$), 129.5 (*m*-*C*CH$_{3(mesityl)}$), 129.1 (1,2-$C_{(dione)}$), 125.6 (5,8-*C*H$_{(dione)}$), 21.2 (*p*-*C*H$_{3(mesityl)}$), 18.0 (*o*-*C*H$_{3(mesityl)}$) ppm. **FTIR (C_6D_6-Cast) $\nu_{C=O}$:** 1653 cm^{-1}. **Anal. Calcd. for $C_{29}H_{27}N_3O_2$ (%):** C, 77.48; H, 6.05; N, 9.35; **Found (%):** C, 77.69; H, 6.04; N, 9.36.

1-(1,3-Dimesityl-4,9-dioxo-1H-naphtho[2,3-d]imidazol-2(3H,4H,9H)-ylidene)-3-*p*-tolylurea (14a)

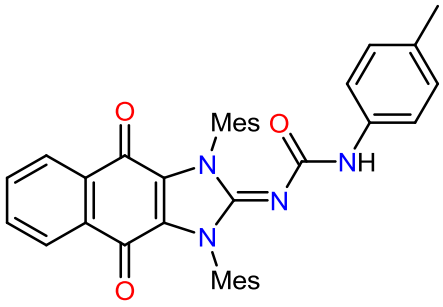

To a 2 mL toluene solution of **13** (300 mg, 0.670 mmol) was added a 5% excess of *p*-tolyl isocyanate (93 μL, 0.701 mmol) as a toluene solution and the reaction mixture was stirred at room temperature for 24 h. The solvent was dried in vacuo and the crystalline red solid was washed with cold pentane. A spectroscopically pure red solid was obtained (351 mg, 0.603 mmol , 90%). **NMR (300 MHz, C_6D_6, 25 °C):** δ 7.81 (m, $^3J_{HH}$ = 3.21 Hz, 2H, 5,8-$CH_{(dione)}$), 6.90 (m, $^3J_{HH}$ = 3.21 Hz, 2H, 6,7-$CH_{(dione)}$), 6.81 (s, 4H, *m*-$CH_{(mesityl)}$), 6.76 (s, 4H, *o/p*-$CH_{(p\text{-tolyl})}$), 6.23 (s, 1H, N*H*) 2.31 (s, 12H, *o*-$CH_{3(mesityl)}$), 2.09 (s, 6H, *p*-$CH_{3(mesityl)}$), 1.97 (s, 3H, *p*-$CH_{3(p\text{-tolyl})}$) ppm. **$^{13}C\{^1H\}$ NMR (75 MHz, C_6D_6, 25 °C):** 173.7 (*C*=$O_{(dione)}$), 156.1 (*C*=O), 147.9 (*C*=N), 138.8 ($C_{ipso(mesityl)}$), 137.4 ($C_{ipso(p\text{-tolyl})}$), 135.9 (*o*-*C*$CH_{3(mesityl)}$), 133.3 (6,7-*C*$H_{(dione)}$), 131.9 (4,9-$C_{(dione)}$), 131.3 (*p*-*C*$CH_{3(mesityl)}$), 130.8 (*p*-*C*$CH_{3(p\text{-tolyl})}$), 129.4 (*m*-*C*$CH_{3(mesityl)}$), 128.8 (1,2-$C_{(dione)}$), 126.0 (5,8-*C*$H_{(dione)}$), 118.9 (*o/p*-*C*$H_{(p\text{-tolyl})}$), 20.8 (*p*-C*C*$H_{3(mesityl)}$)), 20.4 (*p*-*C*$H_{3(p\text{-tolyl})}$), 18.0 (*o*-C*C*$H_{3(mesityl)}$) ppm. **FTIR (C_6D_6-Cast) $\nu_{C=O}$:** 1663, 1591 cm^{-1}. **Anal. Calcd. for $C_{37}H_{34}N_4O_3$ (%):** C, 76.27; H, 5.88; N, 9.62; **Found (%):** C, 75.94; H, 5.79; N, 9.43.

(1-(1,3-Dimesityl-4,9-dioxo-1H-naphtho[2,3-d]imidazol-2(3H,4H,9H)-ylidene)-3-*p*-tolylureato)cyclopentadienyl Titanium (IV) dichloride (15)

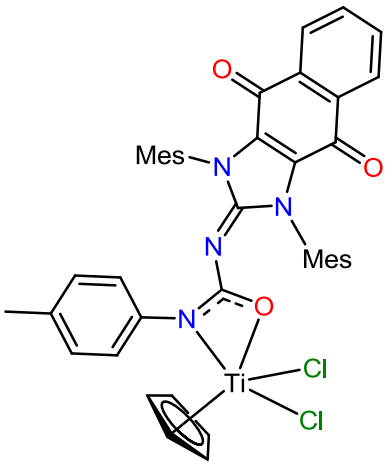

Compound **14a** (50.0 mg, 0.0844 mmol) dissolved in 2 mL of toluene was added to a solution of NaHMDS (17.3 mg, 0.0946 mmol) in 2 mL of toluene. The reaction mixture was stirred for 1 h at room temperature and then cooled to -40 °C. The solution was then added to a cooled toluene solution of $CpTiCl_3$ (19.7 mg, 0.0844 mmol). The resulting solution was stirred for 12 h, filtered and dried under reduced pressure. The recovered brown solid was dissolved in benzene and precipitated by slow diffusion of *n*-pentane, giving a spectroscopically-pure brown solid (55 mg, 0.071 mmol, 83%). **^{1}H NMR (400 MHz, C_6D_6, 25 °C):** δ 7.76 (m, $^3J_{HH}$ = 3.08 Hz, 2H, 5,8-$CH_{(dione)}$), 7.30 (d, $^3J_{HH}$ = 8.04 Hz, 2H, *o*-$CH_{(p\text{-tolyl})}$), 7.11 (d, $^3J_{HH}$ = 7.28 Hz, 2H, *m*-$CH_{(p\text{-tolyl})}$), 6.88 (m, $^3J_{HH}$ = 3.04 Hz, 2H, 6,7-$CH_{(dione)}$), 6.87 (s, 4H, *o/p*-$CH_{(p\text{-tolyl})}$), 6.13 (s, 5H, Cp), 2.15 (s, 12H, *o*-$CH_{3(mesityl)}$), 2.13 (s, 3H, *p*-$CH_{3(p\text{-tolyl})}$), 2.10 (s, 6H, *p*-$CH_{3(mesityl)}$) ppm. **^{13}C{^{1}H} NMR (100 MHz, C_6D_6, 25 °C):** 173.7 (*C*=$O_{(dione)}$), 162.7 (*C*=O), 147.8 (*C*=N), 144.3 ($C_{ipso(mesityl)}$), 140.3 ($C_{ipso(p\text{-tolyl})}$), 135.9 (*o*-*C*$CH_{3(mesityl)}$), 133.3 (6,7-*C*$H_{(dione)}$), 131.9 (4,9-$C_{(dione)}$), 130.1 (*p*-*C*$CH_{3(mesityl)}$), 130.0 (*p*-*C*$CH_{3(p\text{-tolyl})}$), 129.3 (*m*-*C*$CH_{3(mesityl)}$), 128.8 (1,2-$C_{(dione)}$), 126.4 (5,8-*C*$H_{(dione)}$), 120.7 (Cp), 119.4 (*o/p*-*C*$H_{(p\text{-tolyl})}$), 21.4 (*p*-C*C*$H_{3(mesityl)}$)), 21.0 (*p*-*C*$H_{3(p\text{-tolyl})}$), 18.1 (*o*-C*C*$H_{3(mesityl)}$) ppm **FTIR (toluene-Cast) $\nu_{C=O}$:** 1604, 1495 cm^{-1}. **Anal. Calcd. for**

$C_{42}H_{38}Cl_2N_4O_3Ti$ (%): C, 65.89; H, 5.00; N, 7.32; **Found (%):** C, 65.67; H, 4.78; N, 7.19.

Sodium (1,3-dimesityl-4,9-dioxo-1H-naphtho[2,3-d]imidazol-2(3H,4H,9H)-ylidene)amide (18)

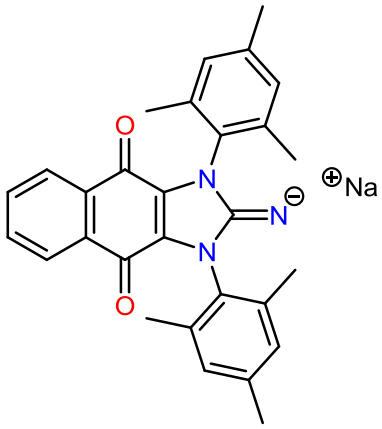

To a toluene solution (10 mL) of **13** (1.00 g, 2.22 mmol) was added a solution of NaHDMS (0.489 mg, 2.64 mmol) in 10 mL of toluene. The reaction mixture was allowed to stir for 24 h, filtered and dried under reduced pressure. A spectroscopically pure dark purple solid was obtained (0.889 g, 1.89 mmol, 85%). **^{1}H NMR (300 MHz, $CDCl_3$, 25 °C):** δ 7.87 (m, 2H), 7.59 (m, 2H), 7.05 (s, 2H), 7.00 (s, 2H), 2.36 (s, 3H), 2.31 (s, 3H), 2.16 (s, 6H), 2.13 (s, 6H) ppm. **^{13}C{^{1}H} NMR (75 MHz, C_6D_6, 25 °C):** δ 174.5 (*C*=O), 174.0 (*C=O)*, 151.6 (*C*=N), 139.8 ($C_{ipso(mesityl)}$), 139.0 ($C_{ipso(mesityl)}$), 136.6 (*o*-$CCH_{3(mesityl)}$), 135.5 (*o*-$CCH_{3(mesityl)}$), 133.5 (6,7-$CH_{(dione)}$), 131.7 (4,9-$C_{(dione)}$), 131.6 (*p*-$CCH_{3(mesityl)}$), 129.8 (*m*-$CCH_{3(mesityl)}$), 129.5 (*m*-$CCH_{3(mesityl)}$), 129.2 (1,2-$C_{(dione)}$), 126.5 (5,8-$CH_{(dione)}$), 21.4 (*p*-$CH_{3(mesityl)}$), 18.0 (*o*-$CH_{3(mesityl)}$), 17.8 (*o*-$CH_{3(mesityl)}$) ppm. **FTIR (C_6D_6-Cast) $\nu_{C=O}$:** 1653 cm^{-1}.

Chapter 5: References

5.0 References

1. Crabtree, R. H., *The Organometallic Chemistry of the Transition Metals*. 5 ed.; Wiley: Hoboken, New Jersey, 2009.
2. Nicolas Marion, Rubén S Ramón, Steven P. Nolan, [(NHC)AuI]-Catalyzed Acid-Free Alkyne Hydration at Part-per-Million Catalyst Loadings. *Journal of the American Chemical Society* **2009,** *131* (2), 448.
3. Michael Ulman, Robert H. Grubbs, Relative Reaction Rates of Olefin Substrates with Ruthenium(II) Carbene Metathesis Initiators. *Organometallics* **1998,** *17* (12), 2484.
4. Heck, Richard F., Palladium-catalyzed reactions of organic halides with olefins. *Accounts of Chemical Research* **1979,** *12* (4), 146.
5. All Nobel Prizes In Chemisry. http://www.nobelprize.org/nobel_prizes/chemistry/laureates/ (accessed November 2nd).
6. Eugene You-Xian Chen, Tobin J. Marks, Cocatalysts for Metal-Catalyzed Olefin Polymerization: Activators, Activation Processes, and Structure−Activity Relationships. *Chemical Reviews* **2000,** *100* (4), 1391.
7. Otto G. Piringer, A. L. Baner, *Plastic Packaging: Interactions with Food and Pharmaceuticals, 2nd, Completely Revised Edition*. Wiley-VCH: Weinheim, 2008.
8. Cossee, P, Ziegler-Natta catalysis I. Mechanism of polymerization of α-olefins with Ziegler-Natta catalysts. *Journal of Catalysis* **1964,** *3* (1), 80.
9. Hans H. Brintzinger, David Fischer, Rolf Miilhaupt, Bernhard Rieger, Robert M. Waymouth Stereospecific Olefin Polymerization with Chiral Metallocene Catalyst. *Angewandte Chemie International Edition* **1995,** (34), 1143.
10. Ashley L. Black Ramirez, Zachary S. Kean, Joshua A. Orlicki, Mangesh Champhekar, Sarah M. Elsakr, Wendy E. Krause, Stephen L. Craig, Mechanochemical strengthening of a synthetic polymer in response to typically destructive shear forces. *Nature Chemistry* **2013,** *5*, 757.
11. Hansjörg Sinn, Walter Kaminsky, Hans-Jürgen Vollmer, Rüdiger Woldt, "Living Polymers" on Polymerization with Extremely Productive Ziegler Catalysts. *Angewandte Chemie International Edition* **1980,** *19* (5), 390.
12. George J. P. Britovsek, Vernon C. Gibson, Duncan F. Wass, The Search for New-Generation Olefin Polymerization Catalysts: Life beyond Metallocenes. *Angewandte Chemie International Edition* **1999,** *38* (4), 428.
13. Jae Seung Oh, Bun Yeoul Lee, Tai Ho Park, Recycling of methylaluminoxane (MAO) cocatalyst in ethylene polymerization with supported metallocene catalyst. *Korean Journal of Chemical Engineering* **2004,** *21* (1), 110.
14. Irina V. Vasilenko, Sergei V. Kostjuk, Fyodor N. Kaputsky, Polina M. Nedorezova, Alexander M. Aladyshev, Effect of Different Aluminum Alkyls on the Metallocene/Methylaluminoxane Catalyzed Polymerization of Higher α-Olefins and Styrene. *Macromolecular Chemistry and Physics* **2008,** *209* (12), 1255.
15. Steven D. Ittel, Lynda K. Johnson, Late-Metal Catalysts for Ethylene Homo- and Copolymerization. *Chemical Reviews* **2000,** *100* (4), 1169.

16. Lynda K. Johnson, Christopher M. Killian, Maurice Brookhart, New Pd(II)- and Ni(II)-Based Catalysts for Polymerization of Ethylene and α-Olefins. *Journal of the American Chemical Society* **1995,** *117* (23), 6414.
17. Liqun Deng, Tom K. Woo, Luigi Cavallo, Peter M. Margl, Tom Ziegler, The Role of Bulky Substituents in Brookhart-Type Ni(II) Diimine Catalyzed Olefin Polymerization: A Combined Density Functional Theory and Molecular Mechanics Study. *Journal of the American Chemical Society* **1997,** *119* (26), 6177.
18. Terunori Fujita, Haruyuki Makio, Shigekazu Matsui, Makoto Mitani, Masatoshi Nitabaru, Junji Saito, Kiyoaki Sugi, Yasushi Tohi, Toshiyuki Tsutsui Olefin polymerization catalysts, transition metal compounds, processes for olefin polymerization, and Alpha-olefin/conjugated diene copolymers. 1997. **EP0874005.**
19. Alison Margaret Anne Bennett, Edward Bryan Coughlin, Jerald Feldman, Elisabeth Hauptman, Steven Dale Ittel, Lynda Kaye Johnson, Anju Parthasarathy, Robert D Simpson, Lin Wang Polymerization of olefins. 1997. **WO 1998030609.**
20. D. A. Bansleben, S. K. Friedriich, T. D. Younkin, R. H. Grubbs, C. Wang, R. T. Li 1998. **WO 9842664.**
21. Shigekazu Matsui, Terunori Fujita, FI Catalysts: super active new ethylene polymerization catalysts. *Catalysis Today* **2000,** *66* (1), 63.
22. Lisa S. Boffa, Bruce M. Novak, Copolymerization of Polar Monomers with Olefins Using Transition-Metal Complexes. *Chemical Reviews* **2000,** *100* (4), 1479.
23. B. Scott Williams, Mark D. Leatherman, Peter S. White, Maurice Brookhart, Reactions of Vinyl Acetate and Vinyl Trifluoroacetate with Cationic Diimine Pd(II) and Ni(II) Alkyl Complexes: Identification of Problems Connected with Copolymerizations of These Monomers with Ethylene. *Journal of the American Chemical Society* **2005,** *127* (14), 5132.
24. Haruyuki Makio, Norio Kashiwa, Terunori Fujita, FI Catalysts: A New Family of High Performance Catalysts for Olefin Polymerization. *Advanced Synthesis and Catalysis* **2002,** *344* (5), 477.
25. Naoto Matsukawa, Shigekazu Matsui, Makoto Mitani, Junji Saito, Kazutaka Tsuru, Norio Kashiwa, Terunori Fujita, Ethylene polymerization activity under practical conditions displayed by zirconium complexes having two phenoxy-imine chelate ligands. *Journal of Molecular Catalysis A: Chemical* **2001,** *169,* 99.
26. Anthony J. Arduengo III, Richard L. Harlow, Michael Kline, A stable crystalline carbene. *Journal of the American Chemical Society* **1991,** *113* (1), 361.
27. George C. Fortman, Steven P. Nolan N-Heterocyclic carbene (NHC) ligands and palladium in homogeneous cross-coupling catalysis: a perfect union. *Chemical Society Reviews* **2011,** *40* (10), 5151.
28. B. A. Bhanu Prasad, Scott R. Gilbertson, One-Pot Synthesis of Unsymmetrical N-Heterocyclic Carbene Ligands from N-(2-Iodoethyl)arylamine Salts. *Organic Letters* **2009,** *11* (16), 3710.
29. Kühl, Olaf, *Functionalised N-Heterocyclic Carbene Complexes*. Wiley: 2010; p 353.

30. Herve Clavier, Steven P. Nolan, N-Heterocyclic carbenes: advances in transition metal-mediated transformations and organocatalysis. *Annual Reports Section "B" (Organic Chemistry)* **2007,** *103*, 193.
31. Niloufar Hadei, Eric Assen B. Kantchev, Christopher J. O'Brien, Michael G. Organ Electronic Nature of N-Heterocyclic Carbene Ligands: Effect on the Suzuki Reaction. *Organic Letters* **2005,** *7* (10), 1991.
32. Thay Ung, Andrew Hejl, Robert H. Grubbs, Yann Schrodi, Latent Ruthenium Olefin Metathesis Catalysts That Contain an N-Heterocyclic Carbene Ligand. *Organometallics* **2004,** *23* (23), 5399.
33. Sébastien Kuhl, Raphaël Schneider, Yves Fort, Transfer Hydrogenation of Imines Catalyzed by a Nickel(0)/NHC Complex. *Organometallics* **2003,** *22* (21), 4184.
34. David S. McGuinness, Nadja Saendig, Brian F. Yates, Kingsley J. Cavell, Kinetic and Density Functional Studies on Alkyl-Carbene Elimination from PdII Heterocylic Carbene Complexes: A New Type of Reductive Elimination with Clear Implications for Catalysis. *Journal of the American Chemical Society* **2001,** *123* (17), 4029.
35. David S. McGuinness, Vernon C. Gibson, Jonathan W. Steed, Bis(carbene)pyridine Complexes of the Early to Middle Transition Metals: Survey of Ethylene Oligomerization and Polymerization Capability. *Organometallics* **2004,** *23* (26), 6288.
36. Craig A. Wheaton, John-Paul J. Bow, Mark Stradiotto, New Phosphine-Functionalized NHC Ligands: Discovery of an Effective Catalyst for the Room-Temperature Amination of Aryl Chlorides with Primary and Secondary Amines. *Organometallics* **2013,** *32* (21), 6148.
37. Gereon Altenhoff, Richard Goddard, Christian W. Lehmann, Frank Glorius, Sterically Demanding, Bioxazoline-Derived N-Heterocyclic Carbene Ligands with Restricted Flexibility for Catalysis. *Journal of the American Chemical Society* **2004,** *126* (46), 15195.
38. Sarim Dastgir, Gino G. Lavoie, Coordination study of a new class of imine imidazol-2-imine ligands to titanium(IV) and palladium(II). *Dalton Transactions* **2010,** *39*, 6493.
39. Stephan, Douglas W., The Road to Early-Transition-Metal Phosphinimide Olefin Polymerization Catalysts. *Organometallics* **2004,** *24* (11), 2548.
40. Haruyuki Makio, Hiroshi Terao, Akihiko Iwashita, Terunori Fujita, FI Catalysts for Olefin Polymerization—A Comprehensive Treatment. *Chemical Reviews* **2011,** *11*, 2363.
41. Sarim Dastgir, Gino G. Lavoie, Titanium(IV) imido complexes of imine imidazol-2-imine ligands. *Dalton Transactions* **2012,** *41*, 9651.
42. Skrela, Barbara C. Synthesis and Coordination Chemistry of New Multidentate Ligands for Applications in Olefin Polymerization and Dinitrogen Activation. York University, Toronto, 2012.
43. Tarun K. Panda, Alexandra G. Trambitas, Thomas Bannenberg, Cristian G. Hrib, So.ren Randoll, Peter G. Jones, Matthias Tamm, Imidazolin-2-iminato Complexes of Rare Earth Metals with Very Short Metal-Nitrogen Bonds: Experimental and Theoretical Studies. *Inorganic Chemistry* **2009,** *48*, 5462.

44. Lavoie Group, Tim Larocque and Anna Badaj (Ph. D. candidate), York University, personal communication.
45. Gusev, Dmitry G., Electronic and Steric Parameters of 76 N-Heterocyclic Carbenes in Ni(CO)3(NHC). *Organometallics* **2009,** *28,* 6458.
46. Lavoie Group, Edwin Alvarado (M. Sc. candidate), York University, personal communication.
47. Lavoie Group, Louie Fan, York University, CHEM 4000 Thesis.
48. Haiping Wang, Hung-Wing Li, Zuowei Xie, Multiple Insertion of Unsaturated Molecules into the Zr−N Bonds of [η5:σ-Me2A(C9H6)(C2B10H10)]Zr(NMe2)2 (A = C, Si). *Organometallics* **2003,** *22* (22), 4522.
49. Yamaguchi, R. B. Penland, S. Mizushima, T. J. Lane, Columba Curran, J. V. Quagliano, Infrared Absorption Spectra of Inorganic Coordination Complexes. XIV. Infrared Studies of Some Metal Thiourea Complexes. *Journal of the American Chemical Society* **1958,** *80* (3), 527.
50. Michael B. Harkness, Edwin Alvarado, Anna C. Badaj, Barbara C. Skrela, Louie Fan, Gino G. Lavoie, Coordination and Reactivity Study of Group 4 and 10 Transition Metal Complexes of N-Imidazol-2-ylidene-N′-p-tolylureate and Thioureate Ligands. *Organometallics* **2013,** *32,* 3309.
51. Weijun Liu, Jon M. Malinoski, Maurice Brookhart, Ethylene Polymerization and Ethylene/Methyl 10-Undecenoate Copolymerization Using Nickel(II) and Palladium(II) Complexes Derived from a Bulky P,O Chelating Ligand. *Organometallics* **2002,** *21* (14), 2836.
52. Shusuke Noda, Takuya Kochi, Kyoko Nozaki, Synthesis of Allylnickel Complexes with Phosphine Sulfonate Ligands and Their Application for Olefin Polymerization without Activators. *Organometallics* **2009,** *28* (2), 656.
53. Shengsheng Liu, Sachin Borkar, David Newsham, Hemant Yennawar, Ayusman Sen, Synthesis of Palladium Complexes with an Anionic PO Chelate and Their Use in Copolymerization of Ethene with Functionalized Norbornene Derivatives: Unusual Functionality Tolerance. *Organometallics* **2007,** *26* (1), 210.
54. Ulrich Klabunde, Steven D. Itten, Nickel catalysis for ethylene homo- and co-polymerization. *Journal of Molecular Catalysis* **1987,** *41,* 123.
55. Peter Margl, Tom Ziegler, A Nonlocal Density Functional Study of the Pd(II)-Assisted Copolymerization of Ethylene and CO. *Journal of the American Chemical Society* **1996,** *118* (31), 7337.
56. Dong-Po Song, Xin-Cui Shi, Yong-Xia Wang, Ji-Xing Yang, Yue-Sheng Li, Ligand Steric and Electronic Effects on β-Ketiminato Neutral Nickel(II) Olefin Polymerization Catalysts. *Organometallics* **2012,** *31* (3), 966.
57. Wen-Hua Sun, Wen Zhang, Tielong Gao, Xiubo Tang, Liyi Chen, Yan Li, Xianglin Jin, Synthesis and characterization of N-(2-pyridyl)benzamide-based nickel complexes and their activity for ethylene oligomerization. *Journal of Organometallic Chemistry* **2004,** (689), 917.

58. Benjamin E. Ketz, Xavier G. Ottenwaeldera, Robert M. Waymouth, Synthesis, structure, and olefin polymerization with nickel(II) N-heterocyclic carbene enolates. *Chemical Communications* **2005,** (45), 5693.
59. Frank H. Allen, Olga Kennard, David G. Watson, Tables of Bond Lengths determined by X-Ray and Neutron Diffraction. Part I. Bond Lengths in Organic Compounds *Journal of the Chemical Society, Perkin Transactions II* **1987**.
60. Vernon C. Gibson, Carl Redshaw, William Clegg, Mark R. J. Elsegood Isocyanate versus isothiocyanate insertion into alkoxo and imido ligands. *Journal of the Chemical Society, Chemical Communications* **1994,** (22), 2635.
61. Herbert Mayr, Martin Breugst, Armin R. Ofial, Farewell to the HSAB Treatment of Ambident Reactiviy. *Angewandte Chemie International Edition* **2011,** *50* (29), 6470.
62. Matthias Tamm, Sören Randoll, Eberhardt Herdtweck, Nina Kleigrewe, Gerald Kehr, Gerhard Erkerc, Bernhard Riegerd Imidazolin-2-iminato titanium complexes: synthesis, structure and use in ethylene polymerization catalysis. *Dalton Transactions* **2006**, 8.
63. Anthony J. Arduengo III, Frederic Davidson, H. V. R. Dias, Jens R. Goerlich, Dilip Khasnis, William J. Marshall, T. K. Prakasha, An Air Stable Carbene and Mixed Carbene "Dimers". *Journal of the American Chemical Society* **1997,** *119* (52), 12742.
64. J. Matthew Hopkins, Michael Bowdridge, Katherine N. Robertson, T. Stanley Cameron, Hilary A. Jenkins, Jason A. C. Clyburne, Generation of Azines by the Reaction of a Nucleophilic Carbene with Diazoalkanes: A Synthetic and Crystallographic Study. *Journal of Organic Chemistry* **2001,** *66*, 5713.
65. Anthony J. Arduengo III, H. V. Rasika Dias, Richard L. Harlow, Michael Kline, Electronic stabilization of nucleophilic carbenes. *Journal of the American Chemical Society* **1992,** *114* (14), 5530.
66. Julia V. Dickschat, Slawomir Urban, Tania Pape, Frank Glorius, F. Ekkehardt Hahn, Sterically demanding and chiral N,N'-disubstituted N-heterocyclic germylenes and stannylenes. *Dalton Transactions* **2010,** *39*, 11519.
67. Wen Huang, Jianping Guo, Yuanjing Xiao, Miaofen Zhu, Gang Zou, Jie Tang, Palladium–benzimidazolium salt catalyst systems for Suzuki coupling: development of a practical and highly active palladium catalyst system for coupling of aromatic halides with arylboronic acids. *Tetrahedron* **2005,** (62), 9783.
68. Yannick Borguet, Guillermo Zaragoza, Albert Demonceaua, Lionel Delaude, Assessing the ligand properties of 1,3-dimesitylbenzimidazol-2-ylidene in ruthenium-catalyzed olefin metathesis. *Dalton Transactions* **2013,** *42*, 7287.
69. Patrick R Bazinet, Darrin S Richeson Carbene Ligands and their Use. 2005.
70. Patrick Bazinet, Tiow-Gan Ong, Julie S. O'Brien, Nathalie Lavoie, Eleanor Bell, Glenn P. A. Yap, Ilia Korobkov, Darrin S. Richeson, Design of Sterically Demanding, Electron-Rich Carbene Ligands with the Perimidine Scaffold. *Organometallics* **2007,** (26), 2285.
71. Jiachang Gong, Shana J. Sturla, A Synthetic Nucleoside Probe that Discerns a DNA Adduct from Unmodified DNA. *Journal of the American Chemical Society* **2007,** *129* (16), 4882.

72. John M. Herbert, Paul D. Woodgate, William A. Denny, Potential Antitumor Agents. 53. Synthesis, DNA Binding Properties, and Biological Activity of Perimidines Designed as "Minimal" DNA-Intercalating Agents. *Journal of Medicinal Chemistry* **1987,** *30,* 2081.
73. Robert J. Ono, Yasuo Suzuki, Dimitri M. Khramov, Mitsuru Ueda, Jonathan L. Sessler, Christopher W. Bielawski, Synthesis and Study of Redox-Active Acyclic Triazenes: Toward Electrochromic Applications. *Journal of Organic Chemistry* **2011,** *76* (9), 3239.
74. Matthew D. Sanderson, Justin W. Kamplain, Christopher W. Bielawski, Quinone-Annulated N-Heterocyclic Carbene-Transition-Metal Complexes: Observation of pi-Backbonding Using FT-IR Spectroscopy and Cyclic Voltammetry. *Journal of the American Chemical Society* **2006,** (128), 16514.
75. Matthias Tamm, Dejan Petrovic, Sören Randoll, Stephan Beer, Thomas Bannenberg, Peter G. Jonesa, Jörg Grunenbergb Structural and theoretical investigation of 2-iminoimidazolines – carbene analogues of iminophosphoranes. *Organic & Biomolecular Chemistry* **2007,** *5*, 523.
76. Timothy G. Larocque, Gino G. Lavoie, Coordination and reactivity study of titanium phenoxo complexes containing a bulky bidentate imino-N-heterocyclic carbene ligand. *Journal of Organometallic Chemistry* **2012,** (26), 715.
77. Sei-ichi Ishii, Junji Saito, Makoto Mitani, Jun-ichi Mohri, Naoto Matsukawa,; Yasushi Tohi, Shigekazu Matsui, Norio Kashiwa, Terunori Fujita, Highly active ethylene polymerization catalysts based on titanium complexes having two phenoxy-imine chelate ligands. *Journal of Molecular Catalysis A: Chemical* **2002,** *179*, 11.
78. Eugene Chong, Sadaf Qayyum, Laurel L. Schafer, Rhett Kempe, 2-Aminopyridinate Titanium Complexes for the Catalytic Hydroamination of Primary Aminoalkenes. *Organometallics* **2013,** *23* (6), 1858.
79. David C. Leitch, Philippa R. Payne, Christine R. Dunbar, Laurel L. Schafer, Broadening the Scope of Group 4 Hydroamination Catalysis Using a Tethered Ureate Ligand. *Journal of the American Chemical Society* **2009,** (131), 18246.
80. Mark C. Wood, David C. Leitch, Charles S. Yeung, Jennifer A. Kozak, Laurel L. Schafer, Chiral Neutral Zirconium Amidate Complexes for the Asymmetric Hydroamination of Alkenes. *Angewandte Chemie International Edition* **2007,** *46*, 354.
81. Olivier Back, Martin Henry-Ellinger, Caleb D. Martin, David Martin, Guy Bertrand, 31P NMR Chemical Shifts of Carbene–Phosphinidene Adducts as an Indicator of the π-Accepting Properties of Carbenes. *Angewandte Chemie International Edition* **2013,** *52* (10), 2939.
82. Annika Liske, Kathrin Verlinden, Hannes Buhl, Klaus Schaper, Christian Ganter, Determining the π-Acceptor Properties of N‑Heterocyclic Carbenes by Measuring the 77Se NMR Chemical Shifts of Their Selenium Adducts. *Organometallics* **2013,** *32* (19), 5269.
83. Dimitri M. Khramov, Vincent M. Lynch, Christopher W. Bielawski, N-Heterocyclic Carbene−Transition Metal Complexes: Spectroscopic and Crystallographic Analyses of π-Back-bonding Interactions. *Organometallics* **2007,** *26* (24), 6042.

84. Anna Kausamo, Heikki M. Tuononen, Kelly E. Krahulic, Roland Roesler, N-Heterocyclic Carbenes with Inorganic Backbones: Electronic Structures and Ligand Properties. *Inorganic Chemistry* **2008,** *47* (3), 1145.
85. Tolman, Chadwick A., Steric effects of phosphorus ligands in organometallic chemistry and homogeneous catalysis. *Chemical Reviews* **1977,** *77* (3), 313.
86. Maryanoff, Bruce E., Multiple bonds and low coordination in phosphorus chemistry. *Heteroatom Chemistry* **1993,** *4* (1), 105.
87. Rolf Appel, Fritz Knoll, Ingo Ruppert, Phospha-alkenes and Phospha-alkynes, Genesis and Properties of the (p-p)π-Multiple Bond. *Angewandte Chemie International Edition* **1981,** *20* (9), 731.
88. Manuel Alcarazo, Timon Stork, Anakuthil Anoop, Walter Thiel, Alois Fürstner, Steering the Surprisingly Modular π-Acceptor Properties of N-Heterocyclic Carbenes: Implications for Gold Catalysis. *Angewandte Chemie International Edition* **2010,** *49* (14), 2542.
89. Christina Chai , W.L.F. Armarego, *Purification of Laboratory Chemicals*. 5 ed.; ButterworthHeinemann: 2003.
90. Andrew G. Tennyson, Vincent M. Lynch, Christopher W. Bielawski, Arrested Catalysis: Controlling Kumada Coupling Activity via a Redox-Active N-Heterocyclic Carbene. *Journal of the American Chemical Society* **2010,** *132* (27), 9240.
91. Gideon Fraenkel, Mark Henrichs, James M. Hewitt, Biing Ming Su, Michael J. Geckle, Dynamic behavior and aggregation of propyllithium from carbon-13 and lithium-6 NMR at high field. *Journal of the American Chemical Society* **1980,** *102* (10), 3345.
92. Anthony J. Arduengo III, H. V. Rasika Dias, Joseph C. Calabrese, A Carbene•Phosphinidene Adduct: "Phosphaalkene". *Chemistry Letters* **1997,** *26* (2), 144.
93. Anthony J. Arduengo III, Joseph C. Calabrese, Alan H. Cowley, H. V. Rasika Dias, Jens R. Goerlich, William J. Marshall, Bernhard Riegel, Carbene−Pnictinidene Adducts. *Inorganic Chemistry* **1997,** *36* (10), 2151.
94. Timothy G. Larocque, Sarim Dastgir, Gino G. Lavoie Coordination and Reactivity Study of Titanium and Zirconium Complexes of the First Imidazol-2-imine Ethenolate Ligand. *Organometallics* **2013,** *32* (15), 4314.
95. Andrew G. Tennyson, Eric J. Moorhead, Brian L. Madison, Joyce A. V. Er, Vincent M. Lynch, Christopher W. Bielawski, Methylation of Ylidene-Triazenes: Insight and Guidance for 1,3-Dipolar Cycloaddition Reactions. *European Journal of Organic Chemistry* **2010,** *2010* (32), 6277.

Chapter 6: Appendix

6.0 Appendix

6.1 NMR Spectra

^{1}H NMR Spectrum of 7 in C_6D_6 400 MHz

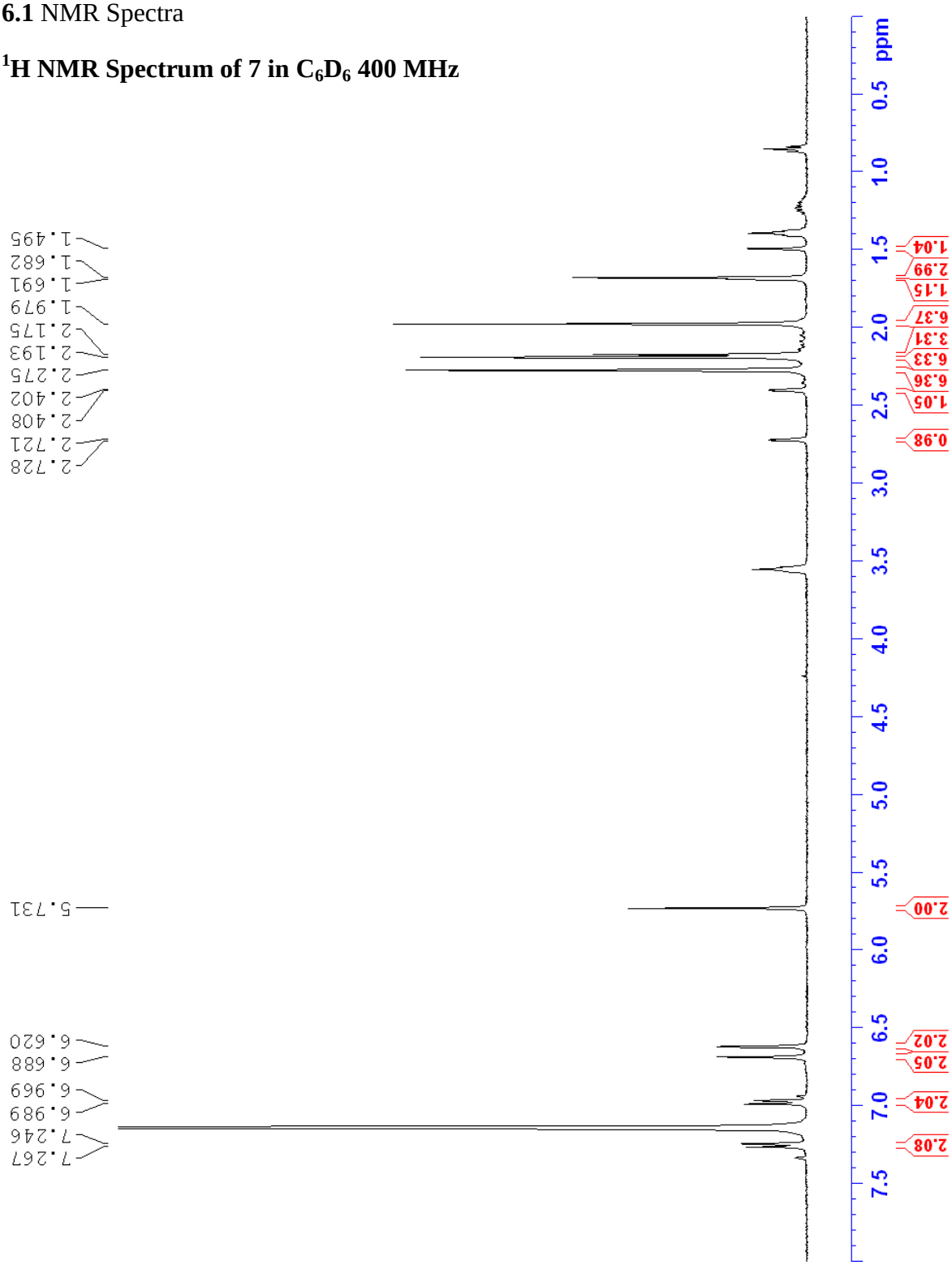

^{13}C NMR Spectrum of 7 in C_6D_6 400 MHz

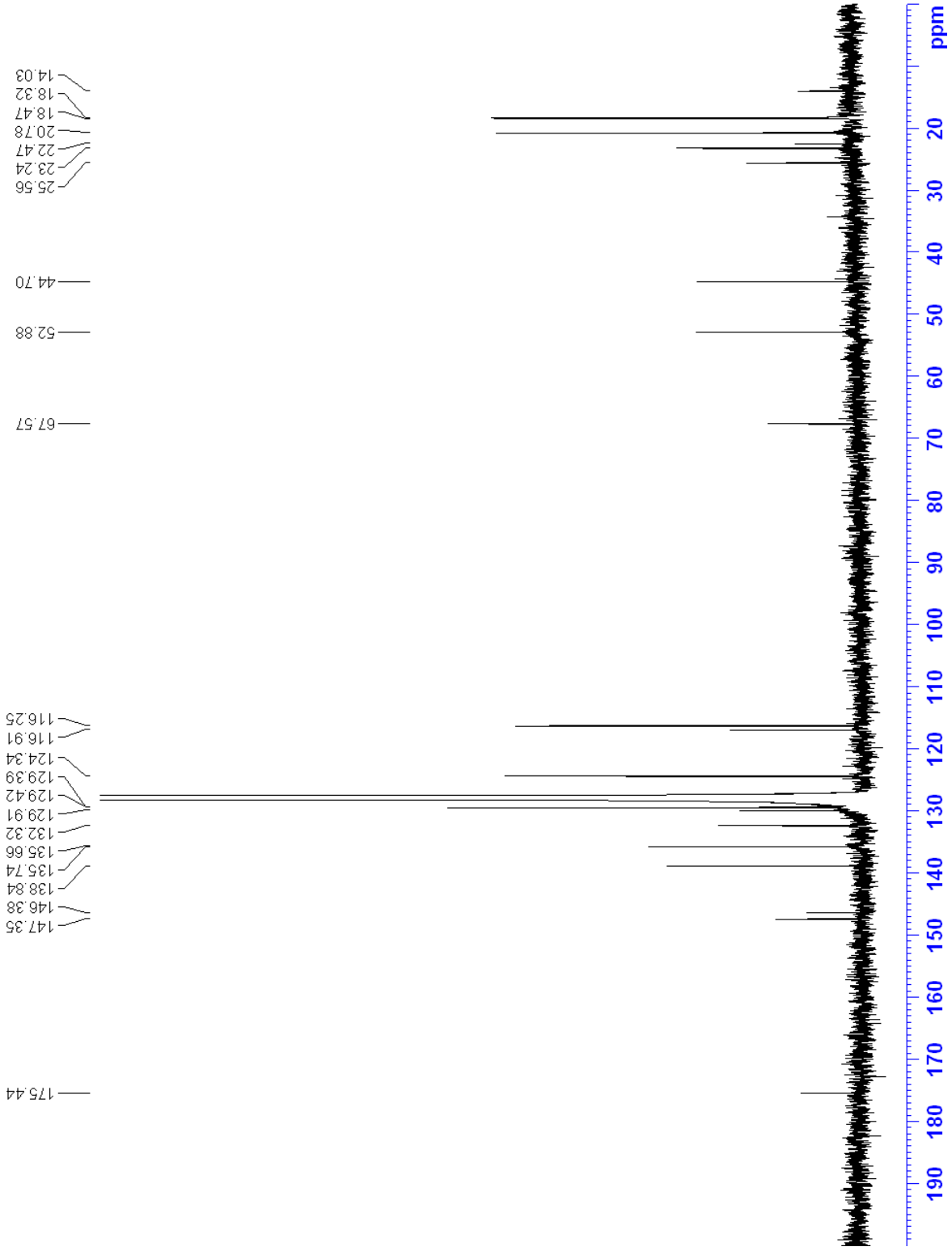

^{1}H NMR Spectrum of 8 in C_6D_6 400 MHz

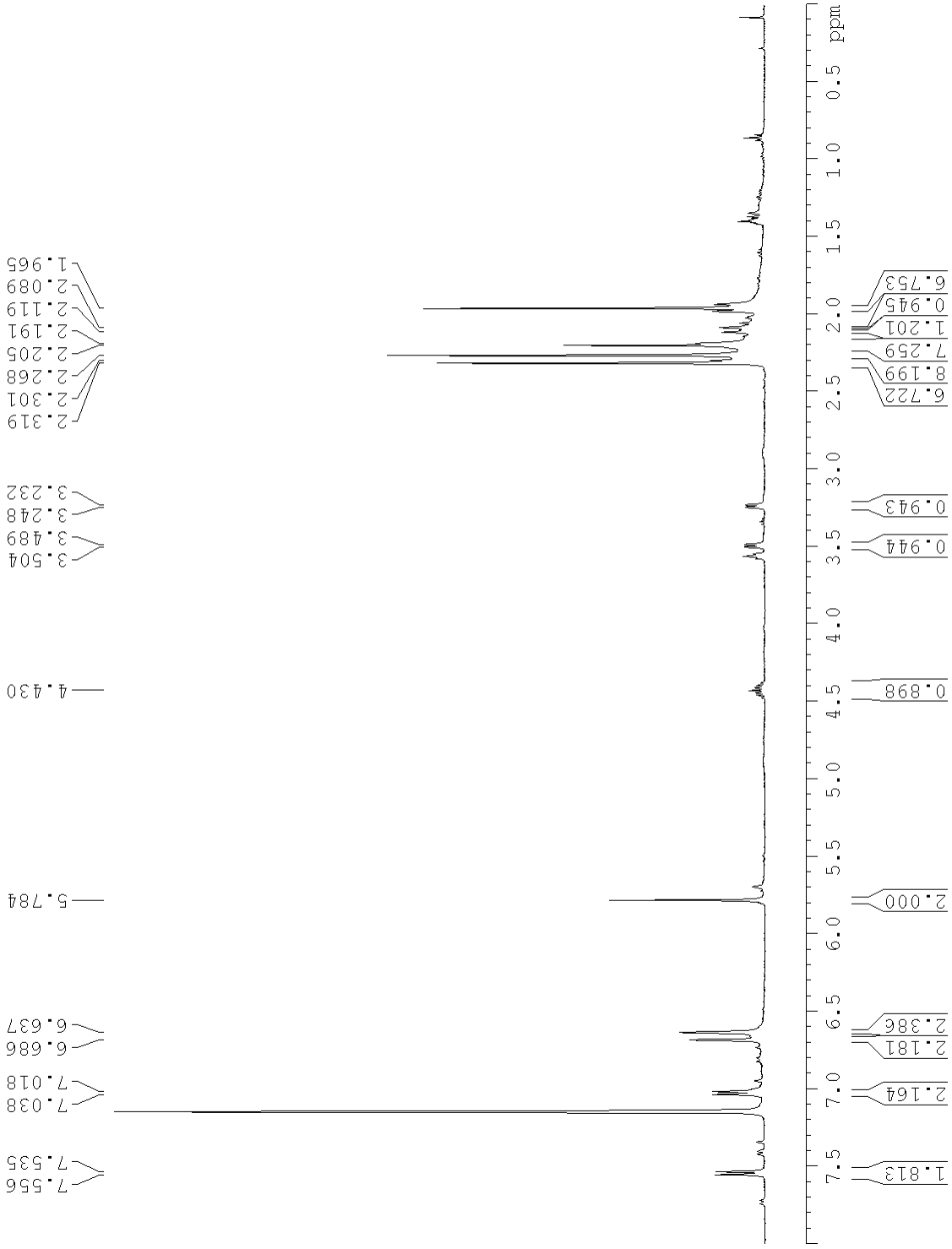

^{13}C NMR Spectrum of 8 in C_6D_6 400 MHz

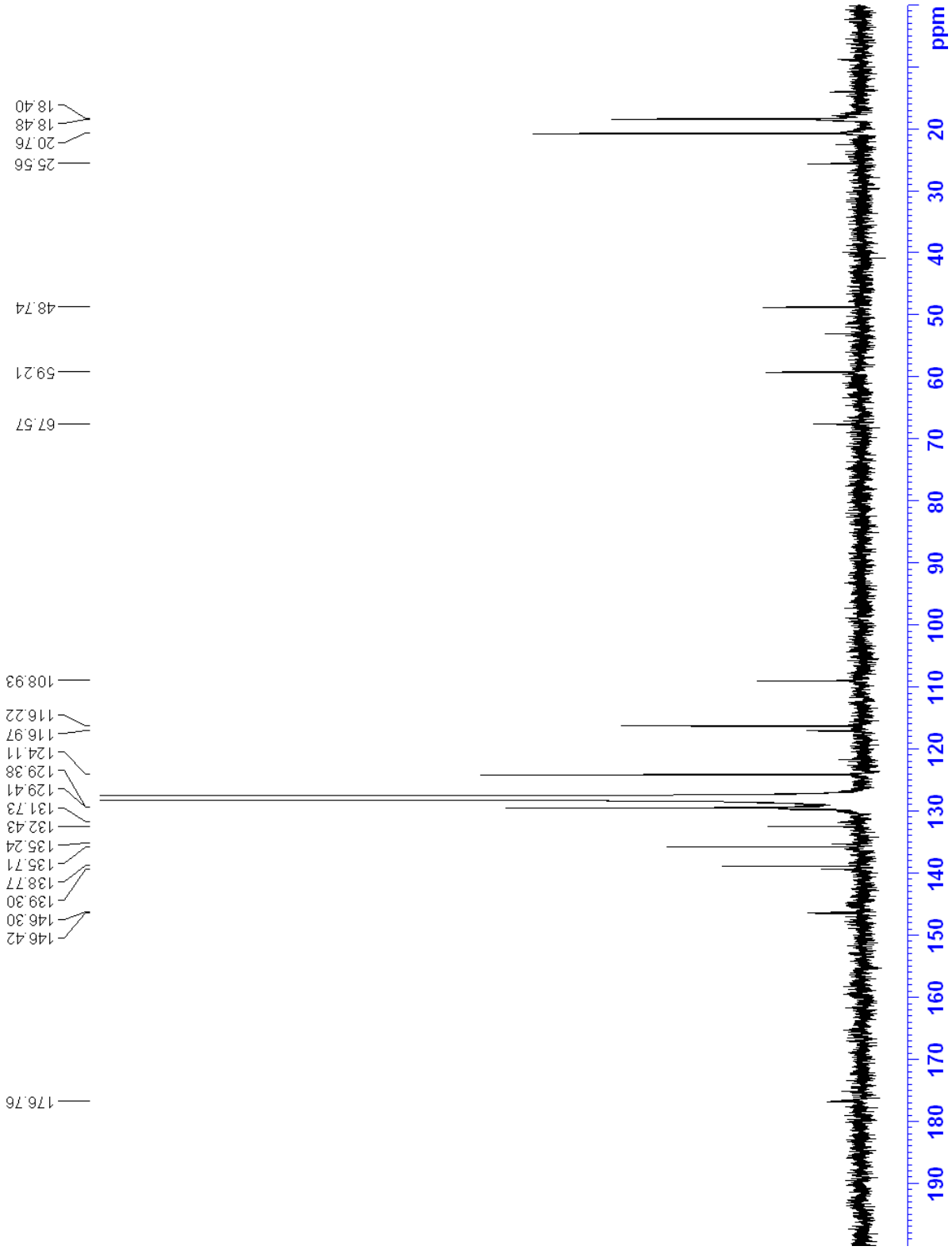

^{1}H NMR Spectrum of 9 in C_6D_6 400 MHz

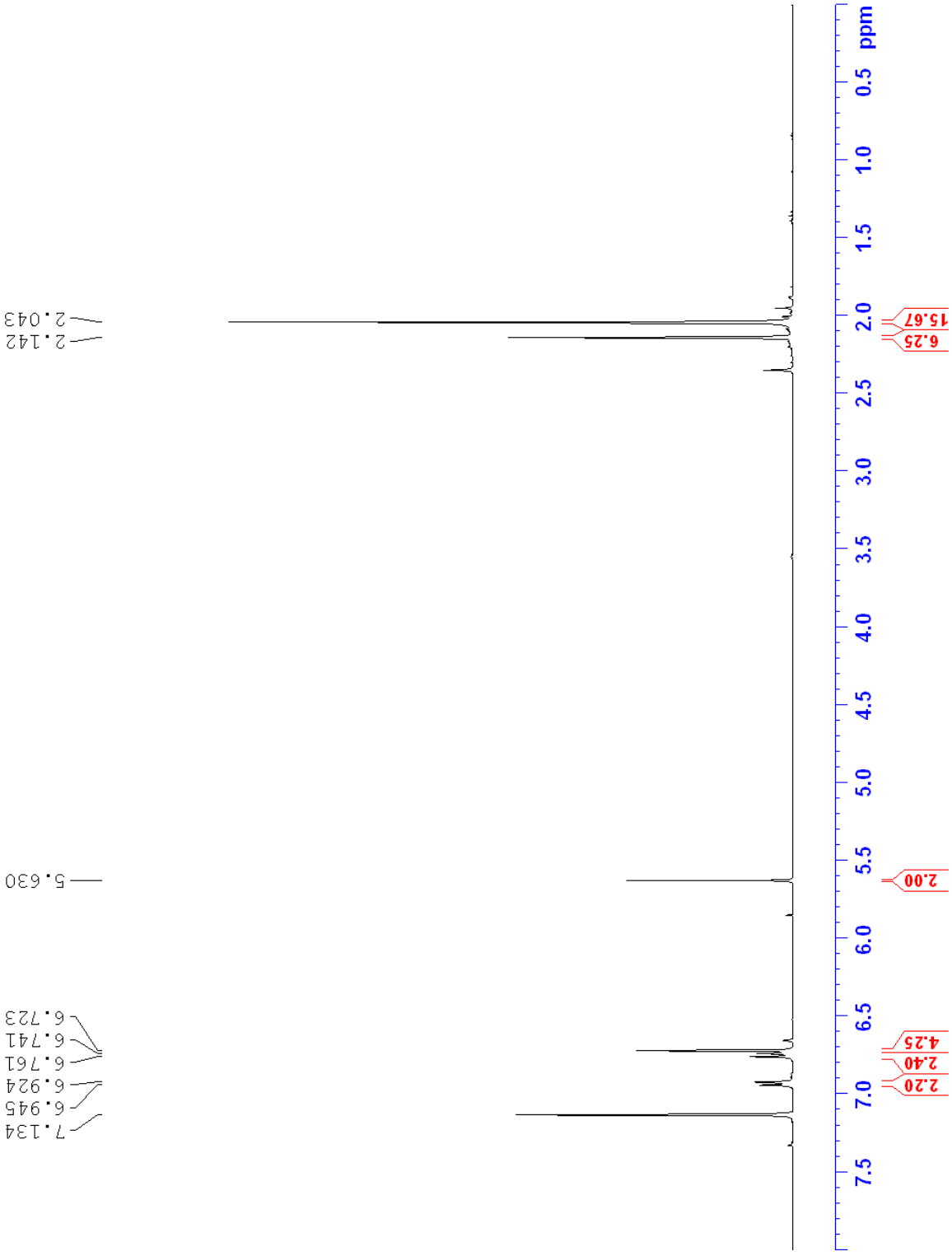

^{13}C NMR Spectrum of 9 in C_6D_6 400 MHz

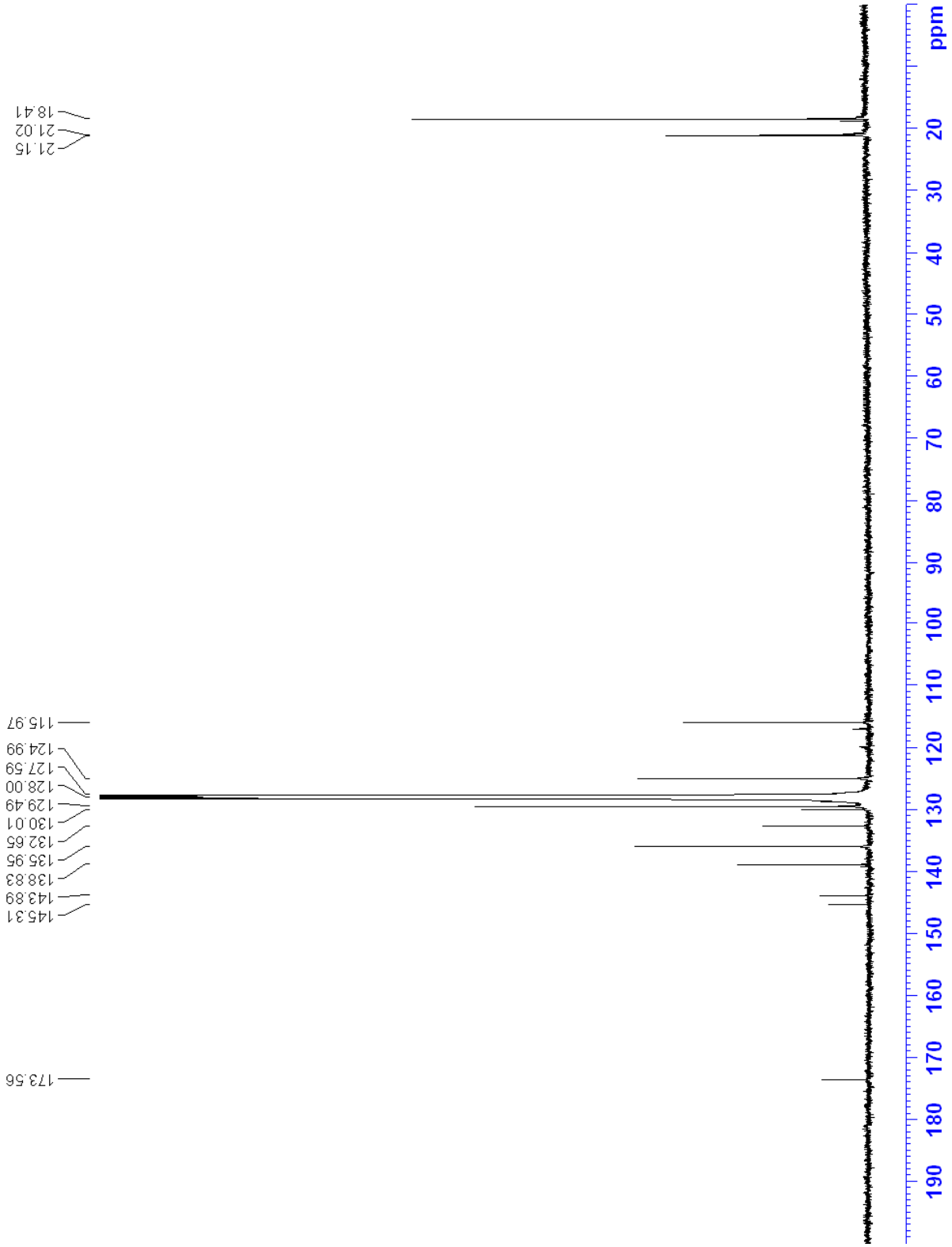

^{1}H NMR Spectrum of 13 in C_6D_6 300 MHz

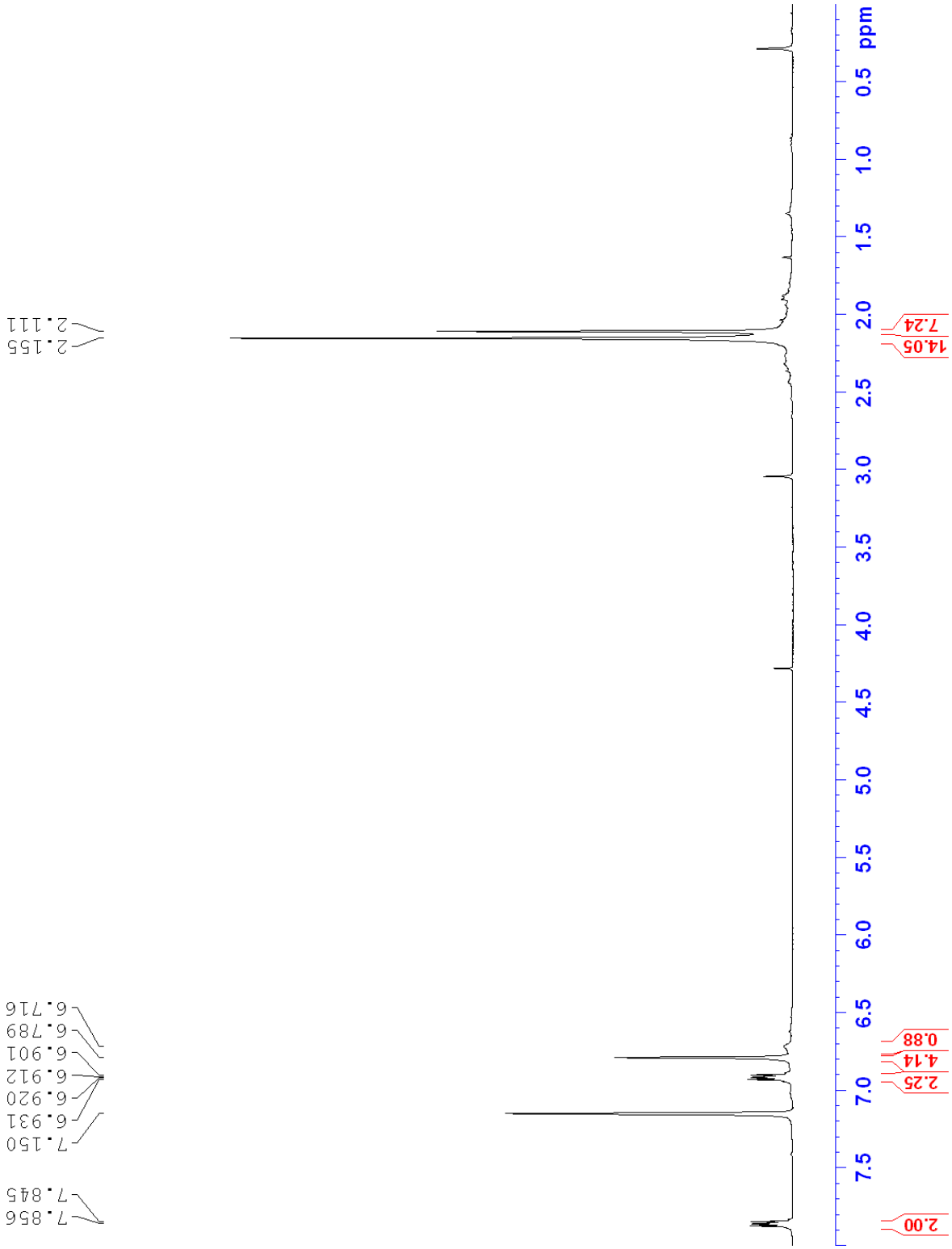

^{13}C NMR Spectrum of 13 in C_6D_6 300 MHz

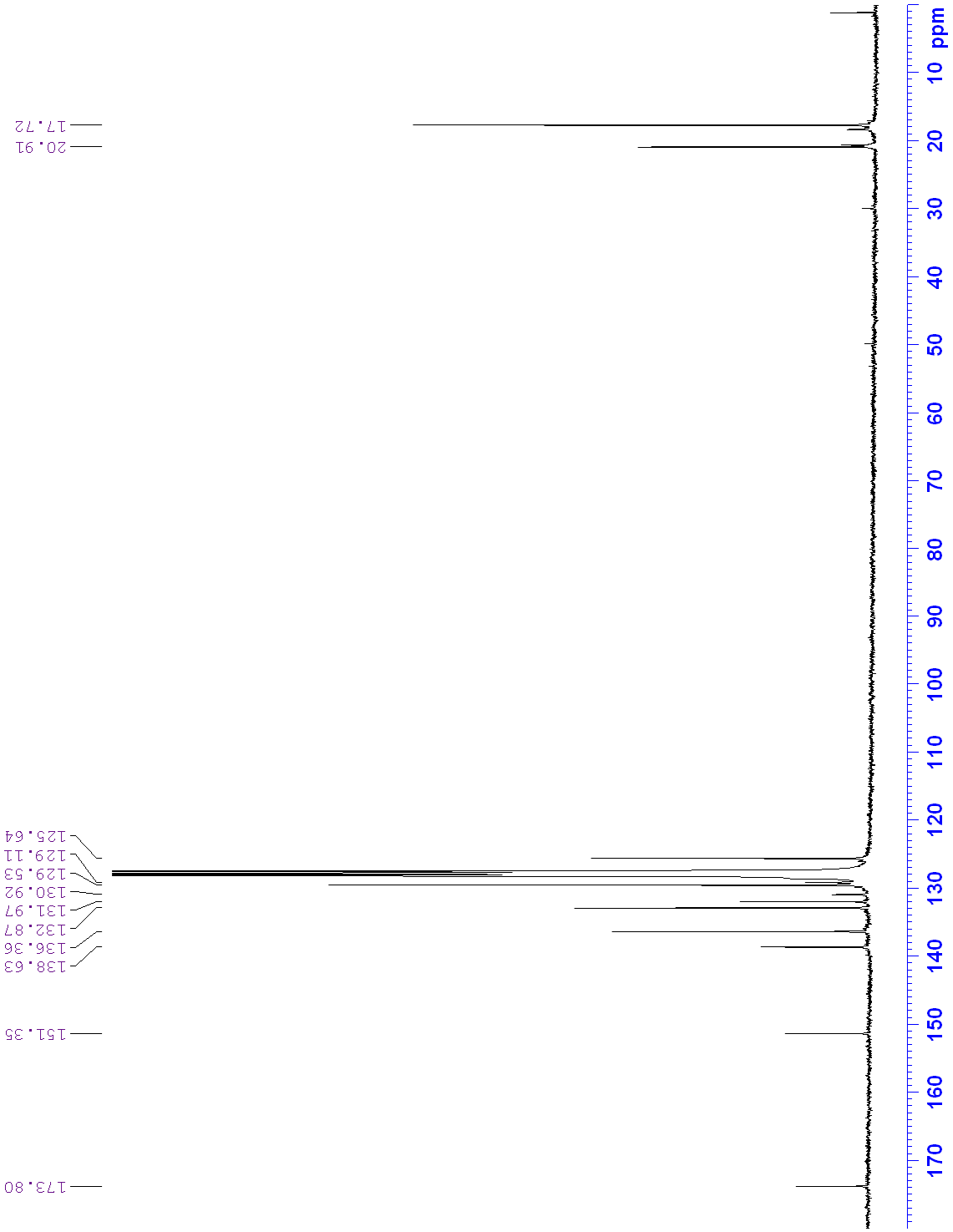

^{1}H NMR Spectrum of 14a in C_6D_6 300 MHz

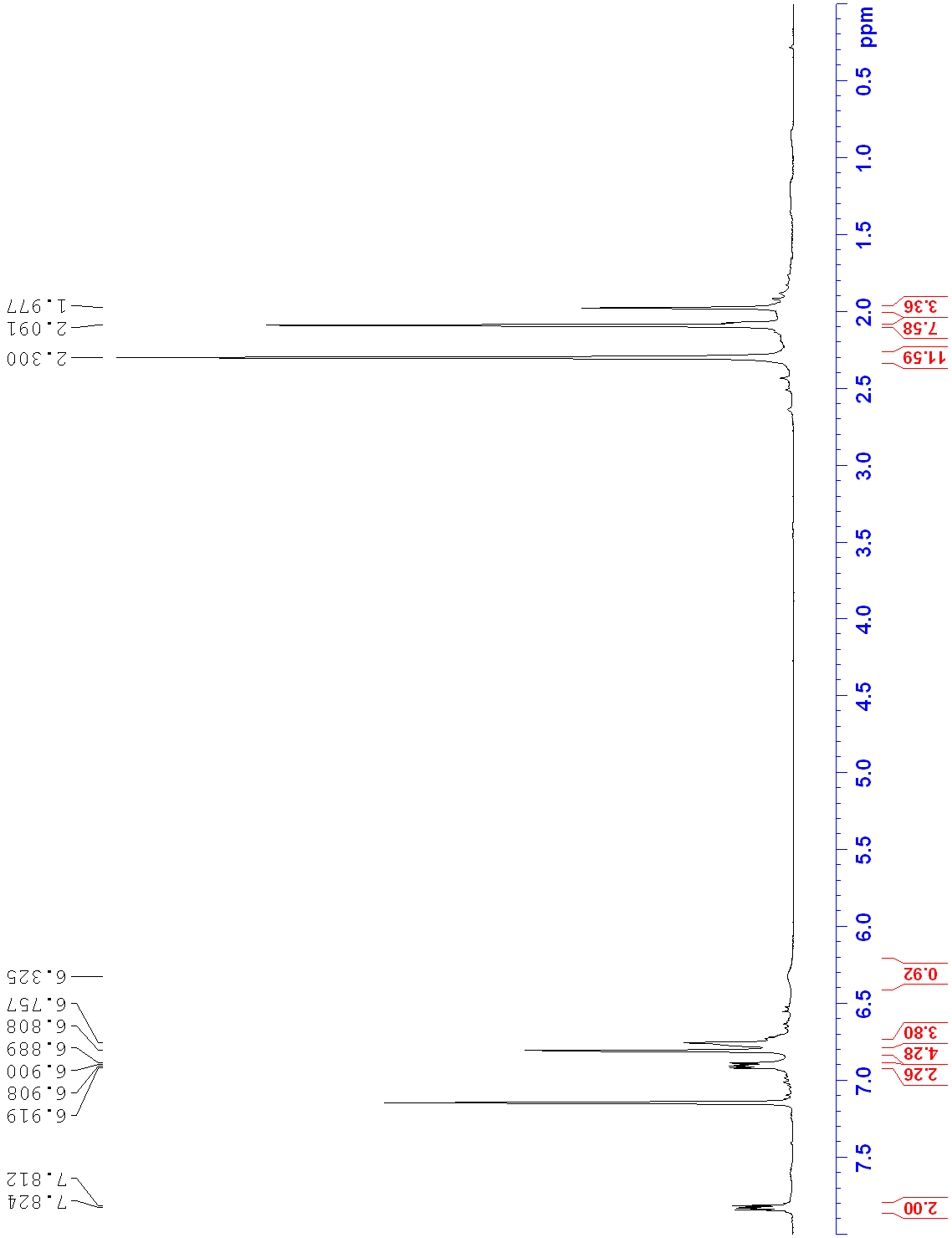

^{13}C NMR Spectrum of 14a in C_6D_6 300 MHz

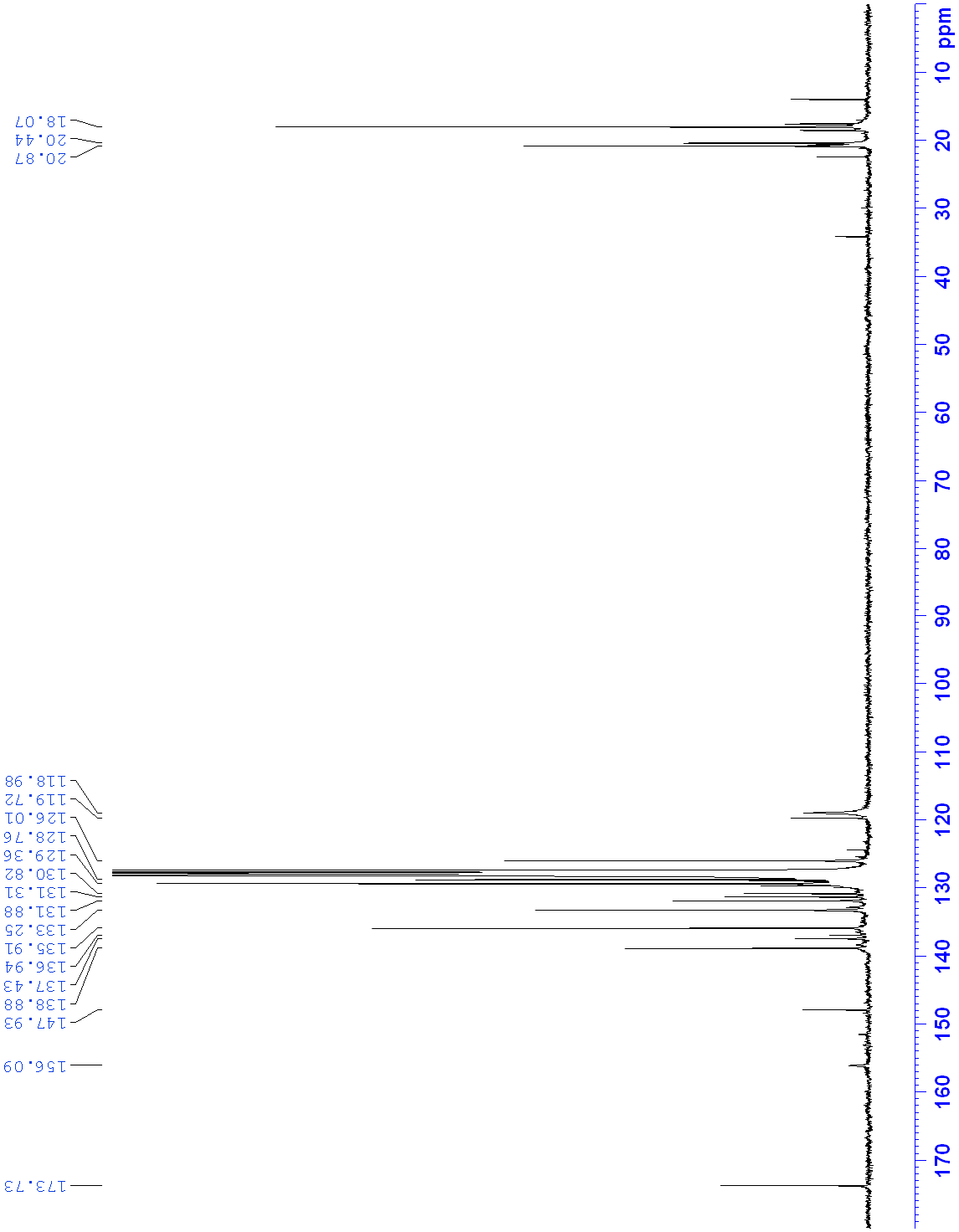

^{1}H NMR Spectrum of 15 in C_6D_6 300 MHz

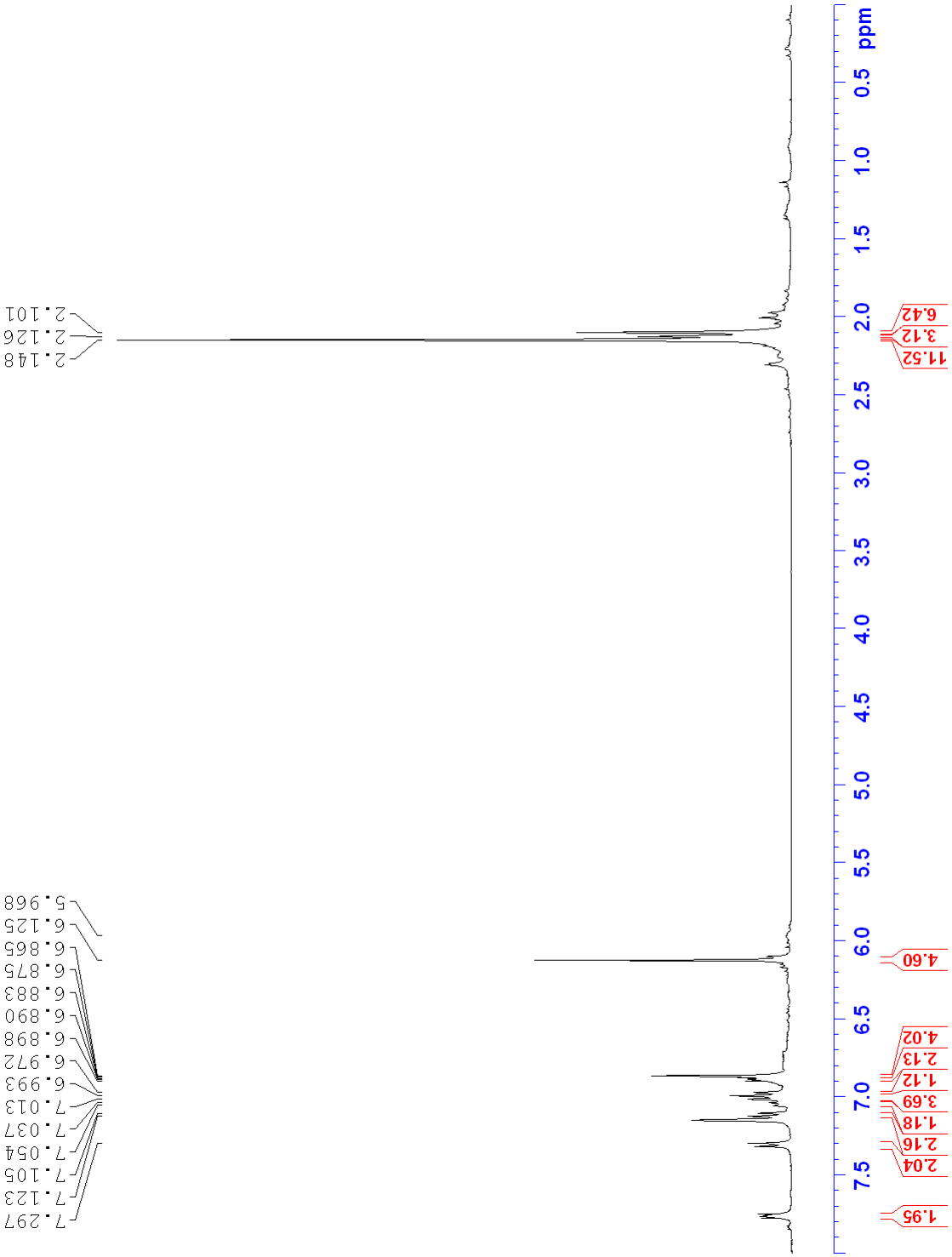

^{13}C NMR Spectrum of 15 in C_6D_6 300 MHz

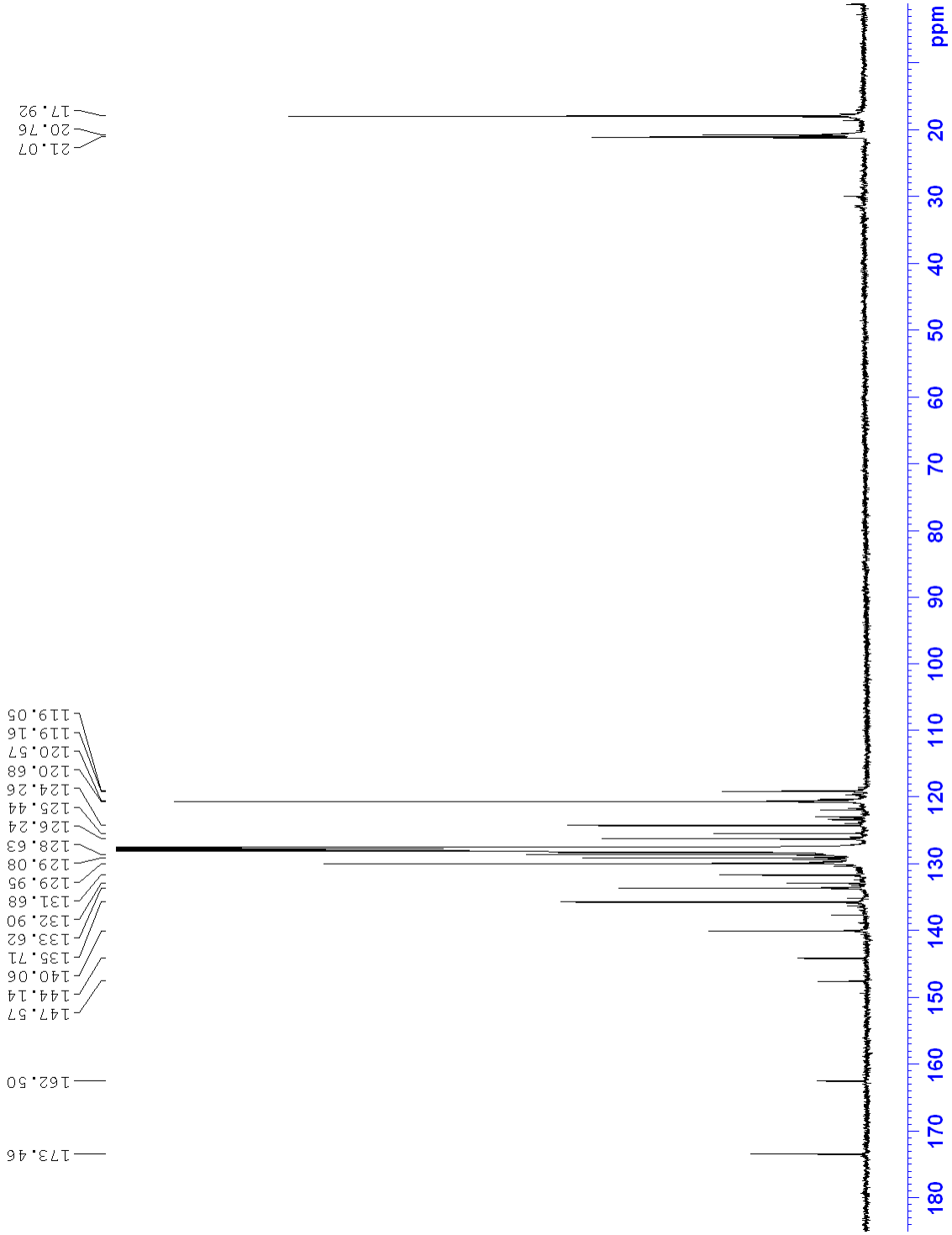

^{1}H NMR Spectrum of 18 in $CDCl_3$ 300 MHz

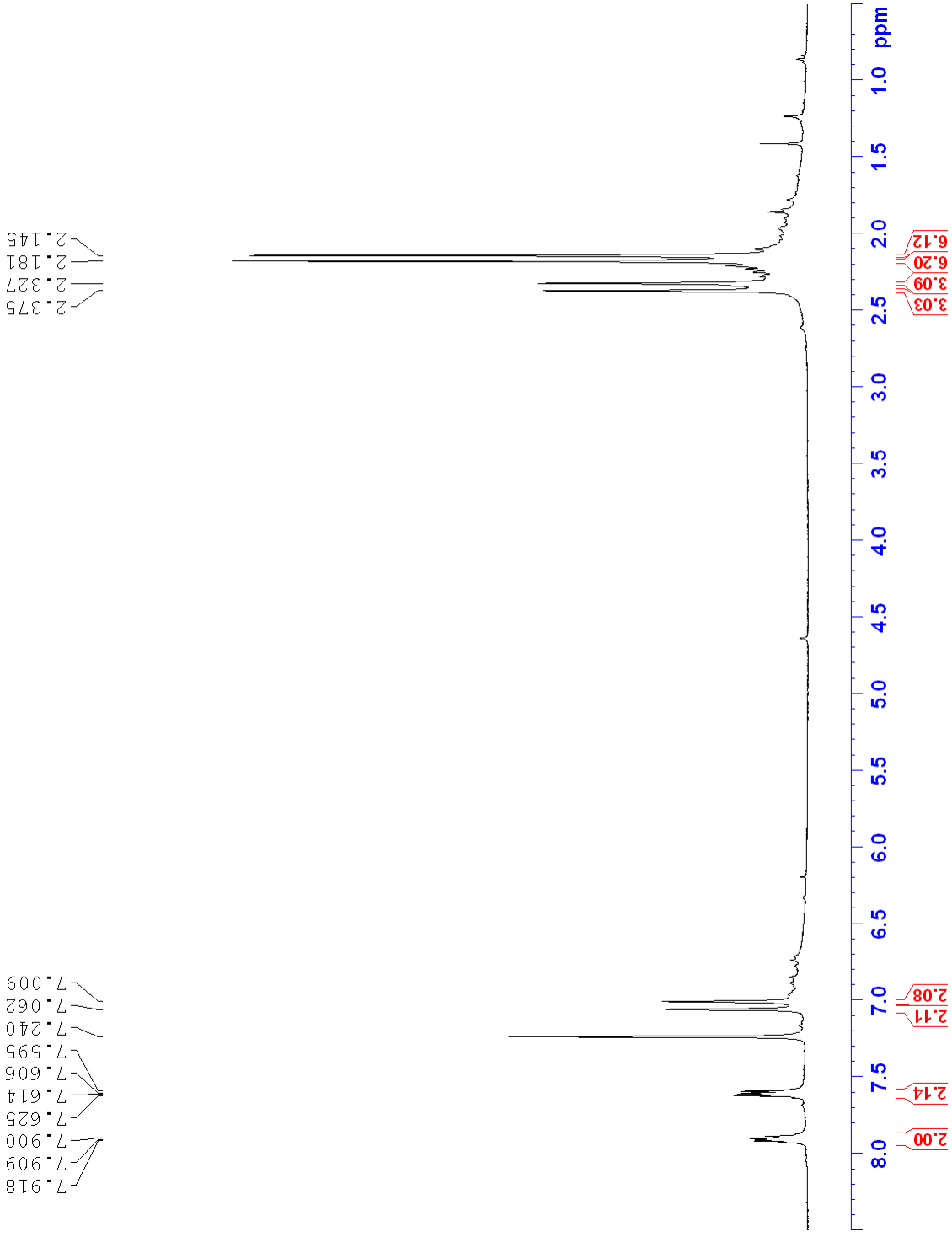

^{13}C NMR Spectrum of 18 in $CDCl_3$ 300 MHz

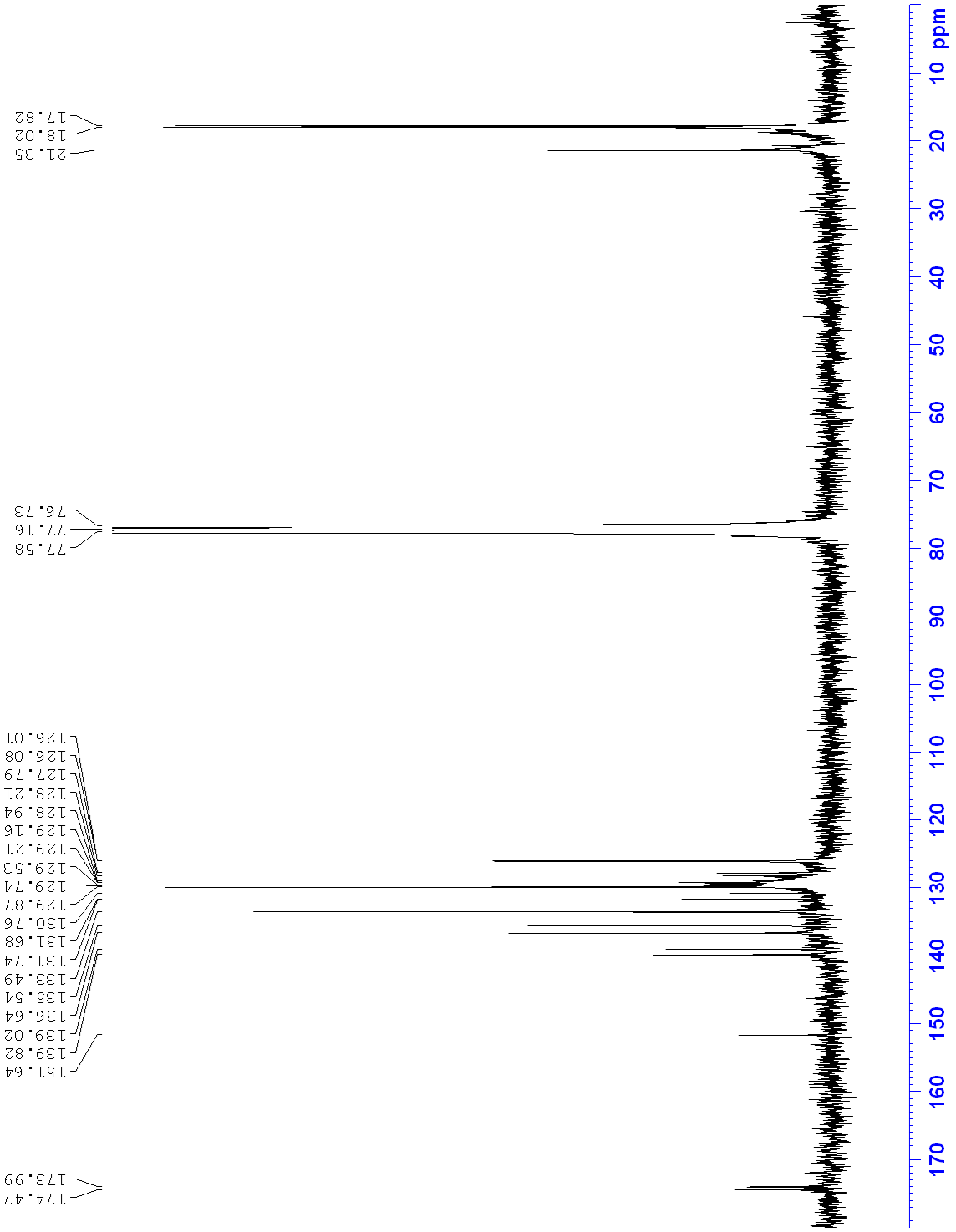

6.2 Miscellaneous Experimental Procedures

Sodium (1,3-dimesityl-1H-imidazol-2(3H)-ylidenecarbamothioyl)(p-tolyl)amide

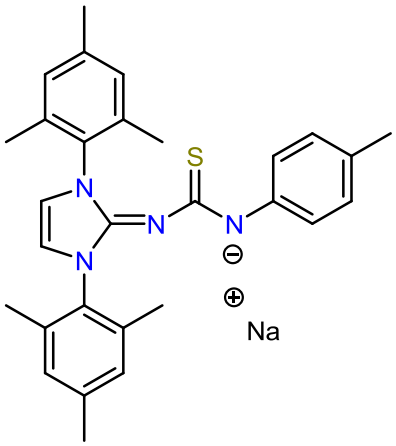

1c (50.0 mg, 0.106 mmol) in 2 mL of THF was added to a solution of NaHDMS (21.0 mg, 0.114 mmol) in 2 mL of THF. The reaction mixture was allowed to stir for 1 h, filtered and dried under reduced pressure. A spectroscopically pure dark yellow solid was obtained in 89% yield (43.1 mg, 0.087 mmol). **^{1}H NMR (400 MHz, C_6D_6, 25 °C):** δ 7.30 (d, $^{3}J_{HH}$ = 8.12 Hz, 2H, *o*-$CH_{(p\text{-tolyl})}$), 6.85 (d, $^{3}J_{HH}$ = 8.20 Hz, 2H, *m*-$CH_{(p\text{-tolyl})}$), 6.70 (s, 4H, *m*-$CH_{(mesityl)}$), 5.67 (s, 2H, NCHCHN), 2.11 (s, 15H, , *o*-$CH_{3(mesityl)}$ + *p*-$CH_{3(p\text{-tolyl})}$), 2.09 (s, 6H, *p*-$CH_{3(mesityl)}$) ppm. **^{13}C{^{1}H} NMR (100 MHz, C_6D_6, 25 °C):** δ 175.6 (*C*=*S*), 144.6 (N*C*N), 144.4 ($C_{ipso(p\text{-tolyl})}$), 138.6 (*p*-*C*$CH_{3(mesityl)}$), 135.6 (*o*-*C*$CH_{3(mesityl)}$), 132.3 ($C_{ipso(mesityl)}$), 129.9 (*p*-*C*$CH_{3(p\text{-tolyl})}$), 129.2 (*m*-*C*$H_{(mesityl)}$), 124.2 (*o*-*C*$CH_{3(p\text{-tolyl})}$), 115.6 (N*C*C*N*), 20.8 (*o*-C*C*$H_{3(mesityl)}$), 20.7 (*p*-C*C*$H_{3(p\text{-tolyl})}$), 18.0 (*p*-C*C*$H_{3(mesityl)}$) ppm

1,3-Dimesityl-2-(phenylphosphinylidene)-2,3-dihydro-1H-naphtho[2,3-d]imidazole-4,9-dione (17)

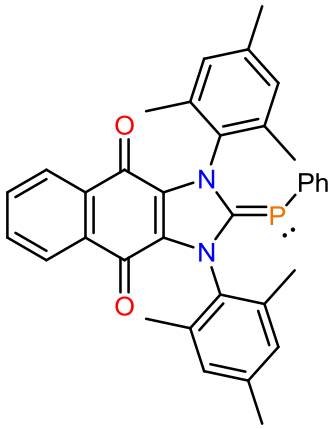

3 (500.0 mg, 1.15 mmol) in 2 mL of THF was added to a solution of $(PPh)_5$ (124.3 mg, 0.23 mmol) in 2 mL of THF. The reaction mixture was allowed to stir for 24 h, filtered and dried under reduced pressure. A dark green solid was obtained in 70% yield (436.0 mg, 0.81 mmol). **^{31}P NMR (300 MHz, C_6D_6, 25 °C):** δ – 3.6 ppm.

6.3 X-Ray Data

Table 1. Crystal data and structure refinement for **9**.

Identification code	d1337	
Empirical formula	C62 H72 N8 Ni O S2	
Formula weight	1068.11	
Temperature	150(2) K	
Wavelength	0.71073 Å	
Crystal system	Triclinic	
Space group	P -1	
Unit cell dimensions	a = 11.5188(14) Å	α= 96.840(3)°.
	b = 15.159(2) Å	β= 93.540(3)°.
	c = 17.772(2) Å	γ = 110.670(3)°.
Volume	2864.7(6) $Å^3$	
Z	2	
Density (calculated)	1.238 Mg/m^3	
Absorption coefficient	0.459 mm^{-1}	
F(000)	1136	
Crystal size	0.220 x 0.200 x 0.130 mm^3	
Theta range for data collection	1.45 to 27.55°.	
Index ranges	-14<=h<=14, -19<=k<=19, -23<=l<=23	
Reflections collected	49175	
Independent reflections	13097 [R(int) = 0.0403]	
Completeness to theta = 27.55°	99.1 %	
Absorption correction	Semi-empirical from equivalents	
Max. and min. transmission	0.7455 and 0.6683	
Refinement method	Full-matrix least-squares on F^2	
Data / restraints / parameters	13097 / 0 / 686	
Goodness-of-fit on F^2	1.030	
Final R indices [I>2sigma(I)]	R1 = 0.0476, wR2 = 0.1217	
R indices (all data)	R1 = 0.0695, wR2 = 0.1337	
Largest diff. peak and hole	1.041 and -0.916 $e.Å^{-3}$	

Table 2. Atomic coordinates (x 10^4) and equivalent isotropic displacement parameters ($Å^2$x 10^3) for **9**. U(eq) is defined as one third of the trace of the orthogonalized U^{ij} tensor.

	x	y	z	U(eq)
Ni(1A)	5000	0	0	25(1)
Ni(1B)	0	5000	5000	30(1)
S(1A)	3635(1)	-766(1)	726(1)	28(1)
S(1B)	1055(1)	4978(1)	3993(1)	36(1)
N(4A)	3779(2)	-1497(1)	2456(1)	32(1)
N(2B)	-133(2)	3061(1)	3384(1)	35(1)
N(1B)	-510(2)	3708(1)	4567(1)	33(1)
N(3A)	3397(2)	-2954(1)	1924(1)	32(1)
N(1A)	5739(2)	-780(1)	470(1)	23(1)
N(3B)	1767(2)	3099(2)	2856(1)	46(1)
N(2A)	4885(2)	-1779(1)	1376(1)	25(1)
N(4B)	219(2)	3105(2)	2084(1)	45(1)
C(2B)	-1241(2)	2824(2)	4768(1)	29(1)
C(1A)	4869(2)	-1155(1)	917(1)	23(1)
C(3A)	7368(2)	-935(2)	-261(1)	28(1)
C(2A)	6850(2)	-966(1)	426(1)	23(1)
C(12A)	3322(2)	-3750(2)	1370(1)	32(1)
C(5B)	-2676(3)	1061(2)	5187(1)	37(1)
C(22A)	5545(2)	-29(2)	2940(1)	32(1)
C(23B)	-3096(3)	2170(2)	1323(2)	57(1)
C(8B)	-3443(3)	110(2)	5398(2)	52(1)
C(7A)	7480(2)	-1155(2)	1043(1)	30(1)
C(13A)	2379(2)	-4049(2)	762(1)	39(1)
C(10B)	2117(3)	3071(2)	2119(2)	61(1)
C(24B)	-3301(3)	2990(2)	1218(2)	59(1)
C(20B)	868(3)	1314(2)	3416(2)	68(1)
C(14A)	2280(3)	-4862(2)	265(2)	49(1)
C(17B)	1983(3)	2141(2)	3826(2)	54(1)
C(25B)	-2317(3)	3863(2)	1427(2)	55(1)

C(23A)	6020(3)	964(2)	3110(1)	38(1)
C(9A)	4052(2)	-2032(2)	1867(1)	27(1)
C(4B)	-3137(2)	1787(2)	5165(2)	40(1)
C(11B)	1186(3)	3072(2)	1655(2)	62(1)
C(1B)	80(2)	3770(2)	3948(1)	31(1)
C(18B)	3997(3)	4650(2)	3509(2)	58(1)
C(3B)	-2432(2)	2661(2)	4963(1)	35(1)
C(5A)	9101(2)	-1286(2)	280(1)	30(1)
C(12B)	2431(3)	3001(2)	3525(2)	47(1)
C(8A)	10296(2)	-1473(2)	209(2)	43(1)
C(26A)	3504(2)	33(2)	2558(1)	39(1)
C(21A)	4293(2)	-474(2)	2650(1)	31(1)
C(25A)	4029(3)	1020(2)	2739(2)	45(1)
C(4A)	8476(2)	-1091(2)	-329(1)	32(1)
C(22B)	-1950(3)	2183(2)	1616(2)	49(1)
C(27B)	-1754(3)	1285(2)	1744(2)	64(1)
C(15B)	3659(3)	2832(2)	4863(2)	59(1)
C(6A)	8586(2)	-1312(2)	962(1)	34(1)
C(19A)	2953(4)	-6226(2)	-195(2)	79(1)
C(9B)	595(2)	3129(2)	2825(1)	38(1)
C(11A)	2953(2)	-2110(2)	2875(2)	42(1)
C(10A)	2722(2)	-3002(2)	2551(1)	42(1)
C(27A)	6363(3)	-582(2)	3092(1)	38(1)
C(13B)	3512(3)	3752(2)	3860(2)	49(1)
C(7B)	-760(3)	2107(2)	4808(2)	41(1)
C(17A)	4187(3)	-4187(2)	1462(2)	40(1)
C(6B)	-1476(3)	1243(2)	5010(2)	42(1)
C(29A)	2139(3)	-451(2)	2295(2)	53(1)
C(19B)	4277(4)	2760(3)	5611(2)	71(1)
C(21B)	-985(3)	3071(2)	1797(1)	44(1)
C(15A)	3094(3)	-5342(2)	349(2)	52(1)
C(26B)	-1157(3)	3918(2)	1712(1)	48(1)
C(16B)	2603(3)	2088(2)	4495(2)	59(1)
C(29B)	-99(3)	4865(2)	1926(2)	59(1)

C(28B)	-4538(4)	2962(3)	888(3)	89(1)
C(18A)	1553(3)	-3503(2)	633(2)	52(1)
C(14B)	4111(3)	3642(2)	4521(2)	54(1)
C(24A)	5285(3)	1500(2)	3000(2)	43(1)
C(16A)	4046(3)	-4984(2)	938(2)	52(1)
C(20A)	5258(3)	-3779(2)	2083(2)	55(1)
C(28A)	5832(3)	2569(2)	3164(2)	59(1)
O(1S)	1819(3)	3347(4)	6703(4)	204(3)
C(1S)	1575(5)	3945(3)	6404(4)	114(2)
C(2S)	2408(4)	4843(4)	6305(4)	125(2)
C(3S)	909(6)	2555(5)	6942(5)	169(4)
C(4S)	1281(5)	1754(5)	6858(4)	134(2)

Table 3. Bond lengths [Å] and angles [°] for **9**.

Ni(1A)-N(1A)	1.9177(17)
Ni(1A)-N(1A)#1	1.9177(17)
Ni(1A)-S(1A)	2.1915(5)
Ni(1A)-S(1A)#1	2.1915(5)
Ni(1A)-C(1A)	2.503(2)
Ni(1A)-C(1A)#1	2.503(2)
Ni(1B)-N(1B)#2	1.8827(18)
Ni(1B)-N(1B)	1.8827(18)
Ni(1B)-S(1B)	2.2274(6)
Ni(1B)-S(1B)#2	2.2274(6)
Ni(1B)-C(1B)	2.508(2)
Ni(1B)-C(1B)#2	2.508(2)
S(1A)-C(1A)	1.750(2)
S(1B)-C(1B)	1.767(2)
N(4A)-C(9A)	1.369(3)
N(4A)-C(11A)	1.397(3)
N(4A)-C(21A)	1.440(3)
N(2B)-C(1B)	1.322(3)
N(2B)-C(9B)	1.328(3)
N(1B)-C(1B)	1.323(3)
N(1B)-C(2B)	1.410(3)
N(3A)-C(9A)	1.354(3)
N(3A)-C(10A)	1.392(3)
N(3A)-C(12A)	1.437(3)
N(1A)-C(1A)	1.327(3)
N(1A)-C(2A)	1.409(3)
N(3B)-C(9B)	1.365(4)
N(3B)-C(10B)	1.396(3)
N(3B)-C(12B)	1.425(4)
N(2A)-C(9A)	1.323(3)
N(2A)-C(1A)	1.326(3)
N(4B)-C(9B)	1.353(4)

N(4B)-C(11B)	1.400(3)
N(4B)-C(21B)	1.430(4)
C(2B)-C(3B)	1.379(3)
C(2B)-C(7B)	1.390(3)
C(3A)-C(4A)	1.387(3)
C(3A)-C(2A)	1.390(3)
C(2A)-C(7A)	1.392(3)
C(12A)-C(17A)	1.390(4)
C(12A)-C(13A)	1.393(4)
C(5B)-C(6B)	1.375(4)
C(5B)-C(4B)	1.384(4)
C(5B)-C(8B)	1.507(3)
C(22A)-C(21A)	1.393(3)
C(22A)-C(23A)	1.395(3)
C(22A)-C(27A)	1.497(3)
C(23B)-C(24B)	1.376(5)
C(23B)-C(22B)	1.381(5)
C(7A)-C(6A)	1.388(3)
C(13A)-C(14A)	1.394(4)
C(13A)-C(18A)	1.489(4)
C(10B)-C(11B)	1.312(5)
C(24B)-C(25B)	1.395(4)
C(24B)-C(28B)	1.492(5)
C(20B)-C(17B)	1.511(5)
C(14A)-C(15A)	1.386(5)
C(17B)-C(16B)	1.375(5)
C(17B)-C(12B)	1.406(4)
C(25B)-C(26B)	1.370(5)
C(23A)-C(24A)	1.385(4)
C(4B)-C(3B)	1.390(3)
C(18B)-C(13B)	1.505(4)
C(5A)-C(6A)	1.380(3)
C(5A)-C(4A)	1.381(3)
C(5A)-C(8A)	1.509(3)

C(12B)-C(13B)	1.395(4)
C(26A)-C(25A)	1.389(4)
C(26A)-C(21A)	1.395(3)
C(26A)-C(29A)	1.497(4)
C(25A)-C(24A)	1.389(4)
C(22B)-C(21B)	1.395(4)
C(22B)-C(27B)	1.497(4)
C(15B)-C(14B)	1.384(4)
C(15B)-C(16B)	1.391(5)
C(15B)-C(19B)	1.503(5)
C(19A)-C(15A)	1.509(4)
C(11A)-C(10A)	1.331(4)
C(13B)-C(14B)	1.382(5)
C(7B)-C(6B)	1.382(3)
C(17A)-C(16A)	1.389(4)
C(17A)-C(20A)	1.501(4)
C(21B)-C(26B)	1.390(4)
C(15A)-C(16A)	1.377(5)
C(26B)-C(29B)	1.507(4)
C(24A)-C(28A)	1.501(4)
O(1S)-C(1S)	1.207(5)
O(1S)-C(3S)	1.417(7)
C(1S)-C(2S)	1.401(6)
C(3S)-C(4S)	1.419(8)

N(1A)-Ni(1A)-N(1A)#1	180.00(13)
N(1A)-Ni(1A)-S(1A)	74.62(5)
N(1A)#1-Ni(1A)-S(1A)	105.38(5)
N(1A)-Ni(1A)-S(1A)#1	105.38(5)
N(1A)#1-Ni(1A)-S(1A)#1	74.62(5)
S(1A)-Ni(1A)-S(1A)#1	180.00(4)
N(1A)-Ni(1A)-C(1A)	31.54(7)
N(1A)#1-Ni(1A)-C(1A)	148.46(7)
S(1A)-Ni(1A)-C(1A)	43.15(5)

S(1A)#1-Ni(1A)-C(1A)	136.85(5)
N(1A)-Ni(1A)-C(1A)#1	148.46(7)
N(1A)#1-Ni(1A)-C(1A)#1	31.54(7)
S(1A)-Ni(1A)-C(1A)#1	136.85(5)
S(1A)#1-Ni(1A)-C(1A)#1	43.15(5)
C(1A)-Ni(1A)-C(1A)#1	180.00(12)
N(1B)#2-Ni(1B)-N(1B)	180.000(1)
N(1B)#2-Ni(1B)-S(1B)	105.70(5)
N(1B)-Ni(1B)-S(1B)	74.30(5)
N(1B)#2-Ni(1B)-S(1B)#2	74.30(5)
N(1B)-Ni(1B)-S(1B)#2	105.70(5)
S(1B)-Ni(1B)-S(1B)#2	180.0
N(1B)#2-Ni(1B)-C(1B)	148.88(7)
N(1B)-Ni(1B)-C(1B)	31.12(7)
S(1B)-Ni(1B)-C(1B)	43.31(5)
S(1B)#2-Ni(1B)-C(1B)	136.69(5)
N(1B)#2-Ni(1B)-C(1B)#2	31.12(7)
N(1B)-Ni(1B)-C(1B)#2	148.88(7)
S(1B)-Ni(1B)-C(1B)#2	136.69(5)
S(1B)#2-Ni(1B)-C(1B)#2	43.31(5)
C(1B)-Ni(1B)-C(1B)#2	180.000(1)
C(1A)-S(1A)-Ni(1A)	77.94(7)
C(1B)-S(1B)-Ni(1B)	76.83(7)
C(9A)-N(4A)-C(11A)	108.71(19)
C(9A)-N(4A)-C(21A)	126.65(18)
C(11A)-N(4A)-C(21A)	124.57(19)
C(1B)-N(2B)-C(9B)	122.0(2)
C(1B)-N(1B)-C(2B)	122.15(18)
C(1B)-N(1B)-Ni(1B)	101.52(14)
C(2B)-N(1B)-Ni(1B)	136.26(14)
C(9A)-N(3A)-C(10A)	109.88(19)
C(9A)-N(3A)-C(12A)	124.21(18)
C(10A)-N(3A)-C(12A)	125.62(19)
C(1A)-N(1A)-C(2A)	125.07(18)

C(1A)-N(1A)-Ni(1A)	99.34(13)
C(2A)-N(1A)-Ni(1A)	135.59(14)
C(9B)-N(3B)-C(10B)	108.4(3)
C(9B)-N(3B)-C(12B)	124.3(2)
C(10B)-N(3B)-C(12B)	127.0(3)
C(9A)-N(2A)-C(1A)	121.65(18)
C(9B)-N(4B)-C(11B)	108.2(3)
C(9B)-N(4B)-C(21B)	125.1(2)
C(11B)-N(4B)-C(21B)	126.6(3)
C(3B)-C(2B)-C(7B)	118.1(2)
C(3B)-C(2B)-N(1B)	121.0(2)
C(7B)-C(2B)-N(1B)	120.8(2)
N(2A)-C(1A)-N(1A)	125.85(19)
N(2A)-C(1A)-S(1A)	126.00(15)
N(1A)-C(1A)-S(1A)	107.90(15)
N(2A)-C(1A)-Ni(1A)	174.89(15)
N(1A)-C(1A)-Ni(1A)	49.12(10)
S(1A)-C(1A)-Ni(1A)	58.91(6)
C(4A)-C(3A)-C(2A)	121.0(2)
C(3A)-C(2A)-C(7A)	117.85(19)
C(3A)-C(2A)-N(1A)	118.85(19)
C(7A)-C(2A)-N(1A)	123.27(18)
C(17A)-C(12A)-C(13A)	122.9(2)
C(17A)-C(12A)-N(3A)	118.8(2)
C(13A)-C(12A)-N(3A)	118.3(2)
C(6B)-C(5B)-C(4B)	117.2(2)
C(6B)-C(5B)-C(8B)	120.9(2)
C(4B)-C(5B)-C(8B)	122.0(2)
C(21A)-C(22A)-C(23A)	117.7(2)
C(21A)-C(22A)-C(27A)	122.2(2)
C(23A)-C(22A)-C(27A)	120.2(2)
C(24B)-C(23B)-C(22B)	122.3(3)
C(6A)-C(7A)-C(2A)	120.2(2)
C(12A)-C(13A)-C(14A)	116.8(3)

C(12A)-C(13A)-C(18A)	121.6(2)
C(14A)-C(13A)-C(18A)	121.6(3)
C(11B)-C(10B)-N(3B)	107.9(3)
C(23B)-C(24B)-C(25B)	118.5(3)
C(23B)-C(24B)-C(28B)	121.6(3)
C(25B)-C(24B)-C(28B)	119.9(3)
C(15A)-C(14A)-C(13A)	122.3(3)
C(16B)-C(17B)-C(12B)	117.4(3)
C(16B)-C(17B)-C(20B)	122.1(3)
C(12B)-C(17B)-C(20B)	120.4(3)
C(26B)-C(25B)-C(24B)	121.8(3)
C(24A)-C(23A)-C(22A)	121.9(3)
N(2A)-C(9A)-N(3A)	122.7(2)
N(2A)-C(9A)-N(4A)	130.7(2)
N(3A)-C(9A)-N(4A)	106.11(18)
C(5B)-C(4B)-C(3B)	121.9(2)
C(10B)-C(11B)-N(4B)	108.5(3)
N(2B)-C(1B)-N(1B)	124.8(2)
N(2B)-C(1B)-S(1B)	127.97(17)
N(1B)-C(1B)-S(1B)	106.96(16)
N(2B)-C(1B)-Ni(1B)	168.15(18)
N(1B)-C(1B)-Ni(1B)	47.35(11)
S(1B)-C(1B)-Ni(1B)	59.86(6)
C(2B)-C(3B)-C(4B)	120.3(2)
C(6A)-C(5A)-C(4A)	117.4(2)
C(6A)-C(5A)-C(8A)	120.8(2)
C(4A)-C(5A)-C(8A)	121.8(2)
C(13B)-C(12B)-C(17B)	121.7(3)
C(13B)-C(12B)-N(3B)	119.5(3)
C(17B)-C(12B)-N(3B)	118.8(3)
C(25A)-C(26A)-C(21A)	117.2(2)
C(25A)-C(26A)-C(29A)	120.3(3)
C(21A)-C(26A)-C(29A)	122.4(2)
C(22A)-C(21A)-C(26A)	122.4(2)

C(22A)-C(21A)-N(4A)	119.1(2)
C(26A)-C(21A)-N(4A)	118.5(2)
C(26A)-C(25A)-C(24A)	122.5(2)
C(5A)-C(4A)-C(3A)	121.4(2)
C(23B)-C(22B)-C(21B)	117.2(3)
C(23B)-C(22B)-C(27B)	121.4(3)
C(21B)-C(22B)-C(27B)	121.4(3)
C(14B)-C(15B)-C(16B)	117.8(3)
C(14B)-C(15B)-C(19B)	121.3(3)
C(16B)-C(15B)-C(19B)	121.0(3)
C(5A)-C(6A)-C(7A)	122.2(2)
N(2B)-C(9B)-N(4B)	124.6(3)
N(2B)-C(9B)-N(3B)	127.8(3)
N(4B)-C(9B)-N(3B)	107.0(2)
C(10A)-C(11A)-N(4A)	108.0(2)
C(11A)-C(10A)-N(3A)	107.2(2)
C(14B)-C(13B)-C(12B)	117.9(3)
C(14B)-C(13B)-C(18B)	121.6(3)
C(12B)-C(13B)-C(18B)	120.5(3)
C(6B)-C(7B)-C(2B)	120.7(2)
C(16A)-C(17A)-C(12A)	117.1(3)
C(16A)-C(17A)-C(20A)	122.0(3)
C(12A)-C(17A)-C(20A)	120.8(2)
C(5B)-C(6B)-C(7B)	121.8(2)
C(26B)-C(21B)-C(22B)	122.4(3)
C(26B)-C(21B)-N(4B)	119.2(2)
C(22B)-C(21B)-N(4B)	118.4(3)
C(16A)-C(15A)-C(14A)	118.2(3)
C(16A)-C(15A)-C(19A)	120.7(3)
C(14A)-C(15A)-C(19A)	121.0(3)
C(25B)-C(26B)-C(21B)	117.9(3)
C(25B)-C(26B)-C(29B)	121.2(3)
C(21B)-C(26B)-C(29B)	120.9(3)
C(17B)-C(16B)-C(15B)	122.7(3)

C(13B)-C(14B)-C(15B)	122.4(3)
C(23A)-C(24A)-C(25A)	118.2(2)
C(23A)-C(24A)-C(28A)	120.7(3)
C(25A)-C(24A)-C(28A)	121.1(3)
C(15A)-C(16A)-C(17A)	122.5(3)
C(1S)-O(1S)-C(3S)	123.8(5)
O(1S)-C(1S)-C(2S)	127.0(5)
C(4S)-C(3S)-O(1S)	110.3(6)

Symmetry transformations used to generate equivalent atoms:

#1 -x+1,-y,-z #2 -x,-y+1,-z+1

Table 4. Anisotropic displacement parameters ($Å^2 x\ 10^3$)for **9**. The anisotropic displacement factor exponent takes the form: $-2\pi^2[\ h^2 a^{*2} U^{11} + ... + 2\ h\ k\ a^*\ b^*\ U^{12}\ ]$

	U^{11}	U^{22}	U^{33}	U^{23}	U^{13}	U^{12}
Ni(1A)	22(1)	26(1)	29(1)	9(1)	10(1)	10(1)
Ni(1B)	42(1)	22(1)	30(1)	4(1)	20(1)	12(1)
S(1A)	23(1)	33(1)	36(1)	15(1)	14(1)	13(1)
S(1B)	48(1)	23(1)	34(1)	3(1)	25(1)	8(1)
N(4A)	34(1)	31(1)	30(1)	5(1)	17(1)	7(1)
N(2B)	41(1)	25(1)	34(1)	0(1)	21(1)	5(1)
N(1B)	44(1)	22(1)	32(1)	3(1)	22(1)	10(1)
N(3A)	35(1)	28(1)	27(1)	6(1)	13(1)	2(1)
N(1A)	22(1)	23(1)	27(1)	8(1)	9(1)	8(1)
N(3B)	46(1)	42(1)	46(1)	-2(1)	28(1)	10(1)
N(2A)	24(1)	26(1)	27(1)	9(1)	11(1)	10(1)
N(4B)	50(1)	42(1)	32(1)	-4(1)	23(1)	1(1)
C(2B)	41(1)	23(1)	24(1)	1(1)	13(1)	10(1)
C(1A)	23(1)	21(1)	25(1)	3(1)	7(1)	7(1)
C(3A)	27(1)	29(1)	30(1)	6(1)	10(1)	11(1)
C(2A)	20(1)	18(1)	29(1)	2(1)	7(1)	5(1)
C(12A)	37(1)	24(1)	27(1)	6(1)	14(1)	-1(1)
C(5B)	52(2)	27(1)	27(1)	3(1)	16(1)	8(1)
C(22A)	40(1)	31(1)	27(1)	4(1)	14(1)	13(1)
C(23B)	58(2)	39(2)	49(2)	-12(1)	14(2)	-7(1)
C(8B)	69(2)	31(1)	50(2)	9(1)	26(2)	8(1)
C(7A)	27(1)	36(1)	27(1)	4(1)	6(1)	11(1)
C(13A)	40(1)	34(1)	34(1)	9(1)	12(1)	-1(1)
C(10B)	52(2)	72(2)	49(2)	-6(2)	34(2)	11(2)
C(24B)	58(2)	55(2)	46(2)	-8(1)	1(1)	2(2)
C(20B)	77(2)	36(2)	95(3)	3(2)	36(2)	23(2)
C(14A)	54(2)	38(1)	32(1)	1(1)	11(1)	-9(1)
C(17B)	61(2)	39(2)	72(2)	4(1)	36(2)	27(1)
C(25B)	70(2)	42(2)	38(2)	2(1)	0(1)	3(1)

C(23A)	43(1)	33(1)	33(1)	1(1)	13(1)	9(1)
C(9A)	27(1)	28(1)	26(1)	7(1)	8(1)	8(1)
C(4B)	40(1)	33(1)	47(2)	5(1)	21(1)	8(1)
C(11B)	62(2)	69(2)	40(2)	-6(1)	35(2)	7(2)
C(1B)	37(1)	23(1)	33(1)	3(1)	16(1)	10(1)
C(18B)	50(2)	59(2)	60(2)	14(2)	18(2)	9(2)
C(3B)	40(1)	29(1)	39(1)	5(1)	17(1)	14(1)
C(5A)	19(1)	26(1)	43(1)	-2(1)	5(1)	6(1)
C(12B)	50(2)	47(2)	52(2)	4(1)	27(1)	23(1)
C(8A)	26(1)	47(2)	58(2)	-1(1)	7(1)	17(1)
C(26A)	42(1)	46(2)	35(1)	2(1)	18(1)	21(1)
C(21A)	35(1)	30(1)	29(1)	3(1)	15(1)	11(1)
C(25A)	59(2)	46(2)	44(2)	7(1)	22(1)	34(1)
C(4A)	30(1)	30(1)	36(1)	5(1)	16(1)	12(1)
C(22B)	57(2)	37(1)	37(1)	-7(1)	22(1)	0(1)
C(27B)	69(2)	34(2)	76(2)	-8(1)	34(2)	3(1)
C(15B)	68(2)	56(2)	71(2)	16(2)	31(2)	39(2)
C(6A)	28(1)	39(1)	35(1)	4(1)	-1(1)	13(1)
C(19A)	102(3)	33(2)	78(2)	-11(2)	43(2)	-4(2)
C(9B)	46(2)	23(1)	38(1)	-2(1)	23(1)	4(1)
C(11A)	43(1)	43(1)	33(1)	5(1)	23(1)	3(1)
C(10A)	44(2)	38(1)	32(1)	6(1)	20(1)	-2(1)
C(27A)	45(2)	36(1)	32(1)	1(1)	4(1)	15(1)
C(13B)	49(2)	49(2)	55(2)	10(1)	28(1)	18(1)
C(7B)	42(1)	33(1)	52(2)	11(1)	21(1)	16(1)
C(17A)	45(2)	29(1)	42(1)	12(1)	13(1)	6(1)
C(6B)	56(2)	29(1)	48(2)	10(1)	19(1)	20(1)
C(29A)	42(2)	68(2)	53(2)	-2(2)	16(1)	26(1)
C(19B)	86(3)	71(2)	79(2)	26(2)	22(2)	49(2)
C(21B)	50(2)	39(1)	26(1)	-1(1)	16(1)	-3(1)
C(15A)	66(2)	27(1)	48(2)	1(1)	30(2)	-4(1)
C(26B)	60(2)	37(1)	27(1)	4(1)	8(1)	-6(1)
C(16B)	69(2)	44(2)	83(2)	18(2)	34(2)	36(2)
C(29B)	66(2)	38(2)	50(2)	10(1)	2(2)	-9(1)

C(28B)	72(3)	75(3)	95(3)	-16(2)	-23(2)	13(2)
C(18A)	41(2)	52(2)	52(2)	10(1)	-2(1)	3(1)
C(14B)	50(2)	55(2)	63(2)	10(2)	21(2)	24(1)
C(24A)	63(2)	33(1)	38(1)	4(1)	22(1)	20(1)
C(16A)	63(2)	32(1)	63(2)	11(1)	26(2)	13(1)
C(20A)	57(2)	50(2)	60(2)	16(1)	1(2)	20(2)
C(28A)	90(2)	34(2)	55(2)	3(1)	22(2)	25(2)
O(1S)	70(2)	205(5)	366(8)	205(6)	-2(3)	36(3)
C(1S)	85(3)	65(3)	185(6)	12(3)	-34(4)	30(3)
C(2S)	57(3)	111(4)	207(6)	73(4)	-7(3)	20(3)
C(3S)	84(4)	123(5)	315(11)	112(6)	14(5)	33(4)
C(4S)	90(4)	158(6)	148(5)	56(5)	21(4)	27(4)

Table 5. Hydrogen coordinates (x 10^4) and isotropic displacement parameters ($Å^2$x 10^3) for **9**.

	x	y	z	U(eq)
H(3A)	6966	-808	-682	33
H(23B)	-3751	1586	1193	68
H(8B1)	-3741	-355	4946	78
H(8B2)	-4141	165	5642	78
H(8B3)	-2936	-86	5741	78
H(7A)	7161	-1176	1511	36
H(10B)	2875	3055	1980	73
H(20A)	808	746	3626	102
H(20B)	964	1222	2883	102
H(20C)	122	1448	3480	102
H(14A)	1645	-5090	-138	59
H(25B)	-2453	4422	1372	66
H(23A)	6854	1275	3304	45
H(4B)	-3943	1687	5288	49
H(11B)	1171	3055	1129	74
H(18A)	4744	5087	3810	87
H(18B)	3377	4938	3491	87
H(18C)	4180	4498	3000	87
H(3B)	-2765	3138	4960	42
H(8A1)	10866	-1166	660	65
H(8A2)	10664	-1224	-227	65
H(8A3)	10116	-2147	150	65
H(25A)	3521	1372	2683	54
H(4A)	8805	-1064	-794	38
H(27A)	-1069	1237	1483	96
H(27B)	-2497	746	1551	96
H(27C)	-1571	1296	2280	96
H(6A)	8993	-1439	1380	41

H(19A)	3746	-6169	-368	119
H(19B)	2362	-6299	-624	119
H(19C)	2663	-6774	61	119
H(11A)	2622	-1928	3304	51
H(10A)	2205	-3554	2713	50
H(27D)	5928	-1100	3353	57
H(27E)	7115	-170	3402	57
H(27F)	6568	-830	2617	57
H(7B)	52	2210	4697	49
H(6B)	-1137	771	5026	50
H(29A)	2001	-1037	1966	79
H(29B)	1858	-41	2021	79
H(29C)	1685	-584	2729	79
H(19D)	5155	3125	5651	107
H(19E)	4151	2104	5638	107
H(19F)	3918	3004	6022	107
H(16B)	2304	1532	4711	71
H(29D)	-359	5362	1780	89
H(29E)	605	4856	1667	89
H(29F)	133	4982	2467	89
H(28A)	-5035	2323	654	133
H(28B)	-4418	3381	511	133
H(28C)	-4958	3164	1286	133
H(18D)	1166	-3423	1087	79
H(18E)	919	-3847	218	79
H(18F)	2039	-2889	512	79
H(14B)	4845	4130	4743	64
H(16A)	4615	-5288	986	63
H(20D)	5822	-3181	1976	83
H(20E)	5691	-4214	2108	83
H(20F)	4947	-3681	2562	83
H(28D)	5586	2829	2742	88
H(28E)	6726	2777	3239	88
H(28F)	5534	2784	3616	88

H(1S1)	932	4067	6679	137
H(1S2)	1175	3631	5897	137
H(2S1)	2961	5134	6766	187
H(2S2)	1949	5238	6188	187
H(2S3)	2887	4772	5894	187
H(3S1)	803	2715	7472	203
H(3S2)	114	2401	6639	203
H(4S1)	1333	1572	6328	200
H(4S2)	679	1233	7045	200
H(4S3)	2083	1916	7142	200

Table 6. Crystal data and structure refinement for d13109 (decomposition product).

Identification code	d13109 (decomposition product)	
Empirical formula	C50 H50 Cl N5 O3	
Formula weight	804.40	
Temperature	293(2) K	
Wavelength	0.71073 Å	
Crystal system	Triclinic	
Space group	P -1	
Unit cell dimensions	a = 10.2309(5) Å	α= 104.081(2)°.
	b = 14.1761(6) Å	β= 101.678(3)°.
	c = 17.395(7) Å	γ = 108.248(3)°.
Volume	2215.2(9) $Å^3$	
Z	2	
Density (calculated)	1.206 Mg/m^3	
Absorption coefficient	0.134 mm^{-1}	
F(000)	852	
Crystal size	0.05x 0.05 x 0.26 mm^3	
Theta range for data collection	2.58 to 25.04°.	
Index ranges	-12<=h<=7, -16<=k<=16, -20<=l<=20	
Reflections collected	25053	
Independent reflections	7426 [R(int) = 0.0401]	
Completeness to theta = 25.04°	94.8 %	
Refinement method	Full-matrix least-squares on F^2	
Data / restraints / parameters	7426 / 0 / 556	
Goodness-of-fit on F^2	1.067	
Final R indices [I>2sigma(I)]	R1 = 0.0410, wR2 = 0.1063	
R indices (all data)	R1 = 0.0543, wR2 = 0.1196	
Largest diff. peak and hole	0.281 and -0.264 $e.Å^{-3}$	

Table 7. Atomic coordinates (x 10^4) and equivalent isotropic displacement parameters ($Å^2$x 10^3) for d13109 (decomposition product). U(eq) is defined as one third of the trace of the orthogonalized U^{ij} tensor.

	x	y	z	U(eq)
Cl(1)	5117(1)	1294(1)	1156(1)	31(1)
O(1)	7891(1)	6446(1)	1361(1)	38(1)
O(2)	9149(2)	10008(1)	3888(1)	44(1)
O(3)	1212(2)	9282(1)	2164(1)	47(1)
N(1)	6349(2)	9545(1)	792(1)	34(1)
N(3)	7603(2)	9677(1)	2145(1)	30(1)
N(2)	7081(2)	8222(1)	1112(1)	29(1)
N(4)	2676(2)	9245(1)	1323(1)	41(1)
N(5)	3173(2)	10753(1)	2354(1)	42(1)
C(21)	7771(2)	10744(1)	2575(1)	30(1)
C(19)	4786(3)	5285(2)	-2186(1)	57(1)
C(2S)	3830(3)	8487(2)	4296(2)	78(1)
C(13)	7288(2)	7638(1)	-280(1)	32(1)
C(12)	6508(2)	7473(1)	276(1)	29(1)
C(22)	6891(2)	10877(1)	3074(1)	34(1)
C(17)	5197(2)	6639(1)	73(1)	33(1)
C(18)	8645(2)	8589(2)	-64(1)	41(1)
C(6)	9248(2)	8306(1)	3468(1)	33(1)
C(31)	1911(2)	8247(2)	714(1)	37(1)
C(15)	5416(2)	6053(1)	-1310(1)	39(1)
C(33)	60(3)	6515(2)	128(1)	51(1)
C(20)	4370(2)	6494(2)	690(1)	42(1)
C(34)	432(3)	6333(2)	-602(1)	50(1)
C(25)	8916(2)	12581(1)	2894(1)	44(1)
C(8)	9950(2)	8408(2)	4272(1)	40(1)
C(7)	8909(2)	7379(1)	2815(1)	33(1)
C(30)	2253(2)	9722(2)	1963(1)	38(1)
C(23)	7069(2)	11903(2)	3480(1)	41(1)

C(11)	9986(2)	6686(2)	3786(1)	46(1)
C(32)	790(2)	7449(2)	785(1)	46(1)
C(9)	9283(2)	6573(1)	2982(1)	40(1)
C(26)	8791(2)	11571(1)	2468(1)	35(1)
C(14)	6716(2)	6897(1)	-1074(1)	37(1)
C(24)	8068(2)	12756(2)	3399(1)	46(1)
C(10)	10315(2)	7598(2)	4428(1)	45(1)
C(5)	8163(2)	7234(1)	1940(1)	30(1)
C(42)	3713(3)	13354(2)	3709(1)	53(1)
C(40)	2098(3)	12089(2)	4089(1)	56(1)
C(3)	7778(2)	8114(1)	1839(1)	29(1)
C(43)	3826(2)	12560(2)	3112(1)	45(1)
C(4)	8863(2)	9193(1)	3331(1)	32(1)
C(29)	9698(2)	11399(2)	1909(1)	45(1)
C(2)	8096(2)	9005(1)	2471(1)	29(1)
C(36)	2314(2)	8060(2)	-11(1)	40(1)
C(37)	-419(3)	5321(2)	-1323(2)	75(1)
C(38)	3047(2)	11511(2)	2992(1)	40(1)
C(27)	5805(2)	9964(2)	3176(1)	46(1)
C(35)	1593(2)	7114(2)	-652(1)	45(1)
C(39)	2196(2)	11279(2)	3502(1)	48(1)
C(16)	4665(2)	5937(1)	-732(1)	38(1)
C(41)	2839(3)	13137(2)	4202(1)	55(1)
C(1S)	3046(3)	8217(2)	3479(2)	74(1)
C(44)	2671(3)	14007(2)	4828(2)	80(1)
C(6S)	3196(4)	7497(3)	2874(2)	98(1)
C(3S)	4752(5)	8019(4)	4485(2)	129(2)
C(5S)	4163(8)	7068(4)	3058(3)	166(3)
C(4S)	4929(9)	7310(6)	3859(3)	199(4)
C(1)	6969(2)	9176(1)	1311(1)	29(1)
C(28)	8218(3)	13856(2)	3852(2)	72(1)

Table 8. Bond lengths [Å] and angles [°] for d13109 (decomposition product).

O(1)-C(5)	1.219(2)
O(2)-C(4)	1.220(2)
O(3)-C(30)	1.219(2)
N(1)-C(1)	1.303(2)
N(3)-C(1)	1.363(2)
N(3)-C(2)	1.392(2)
N(3)-C(21)	1.453(2)
N(2)-C(1)	1.359(2)
N(2)-C(3)	1.390(2)
N(2)-C(12)	1.448(2)
N(4)-C(30)	1.378(3)
N(4)-C(31)	1.407(3)
N(5)-C(30)	1.371(3)
N(5)-C(38)	1.403(3)
C(21)-C(26)	1.384(3)
C(21)-C(22)	1.394(3)
C(19)-C(15)	1.510(3)
C(2S)-C(3S)	1.346(5)
C(2S)-C(1S)	1.374(4)
C(13)-C(12)	1.391(3)
C(13)-C(14)	1.391(2)
C(13)-C(18)	1.502(3)
C(12)-C(17)	1.390(3)
C(22)-C(23)	1.388(3)
C(22)-C(27)	1.494(3)
C(17)-C(16)	1.386(3)
C(17)-C(20)	1.509(3)
C(6)-C(8)	1.386(3)
C(6)-C(7)	1.403(2)
C(6)-C(4)	1.487(2)
C(31)-C(32)	1.386(3)
C(31)-C(36)	1.394(3)

C(15)-C(14)	1.383(3)
C(15)-C(16)	1.393(3)
C(33)-C(32)	1.384(3)
C(33)-C(34)	1.386(3)
C(34)-C(35)	1.382(3)
C(34)-C(37)	1.513(3)
C(25)-C(24)	1.388(3)
C(25)-C(26)	1.394(3)
C(8)-C(10)	1.382(3)
C(7)-C(9)	1.387(3)
C(7)-C(5)	1.491(3)
C(23)-C(24)	1.375(3)
C(11)-C(10)	1.381(3)
C(11)-C(9)	1.383(3)
C(26)-C(29)	1.504(3)
C(24)-C(28)	1.510(3)
C(5)-C(3)	1.459(2)
C(42)-C(41)	1.377(3)
C(42)-C(43)	1.386(3)
C(40)-C(41)	1.383(3)
C(40)-C(39)	1.383(3)
C(3)-C(2)	1.353(2)
C(43)-C(38)	1.389(3)
C(4)-C(2)	1.457(2)
C(36)-C(35)	1.380(3)
C(38)-C(39)	1.389(3)
C(41)-C(44)	1.514(3)
C(1S)-C(6S)	1.347(5)
C(6S)-C(5S)	1.339(7)
C(3S)-C(4S)	1.375(6)
C(5S)-C(4S)	1.353(7)

C(1)-N(3)-C(2)	107.47(13)
C(1)-N(3)-C(21)	124.27(14)

C(2)-N(3)-C(21)	128.19(14)
C(1)-N(2)-C(3)	107.90(13)
C(1)-N(2)-C(12)	123.53(14)
C(3)-N(2)-C(12)	128.54(13)
C(30)-N(4)-C(31)	127.60(18)
C(30)-N(5)-C(38)	127.86(18)
C(26)-C(21)-C(22)	123.56(16)
C(26)-C(21)-N(3)	118.52(16)
C(22)-C(21)-N(3)	117.92(15)
C(3S)-C(2S)-C(1S)	119.0(3)
C(12)-C(13)-C(14)	116.75(17)
C(12)-C(13)-C(18)	122.63(16)
C(14)-C(13)-C(18)	120.56(16)
C(13)-C(12)-C(17)	123.74(15)
C(13)-C(12)-N(2)	118.21(15)
C(17)-C(12)-N(2)	118.04(15)
C(23)-C(22)-C(21)	117.04(17)
C(23)-C(22)-C(27)	120.93(18)
C(21)-C(22)-C(27)	122.03(16)
C(16)-C(17)-C(12)	116.98(17)
C(16)-C(17)-C(20)	120.71(17)
C(12)-C(17)-C(20)	122.31(16)
C(8)-C(6)-C(7)	119.79(17)
C(8)-C(6)-C(4)	118.18(16)
C(7)-C(6)-C(4)	122.03(16)
C(32)-C(31)-C(36)	118.42(18)
C(32)-C(31)-N(4)	124.55(18)
C(36)-C(31)-N(4)	117.02(17)
C(14)-C(15)-C(16)	118.97(16)
C(14)-C(15)-C(19)	120.95(18)
C(16)-C(15)-C(19)	120.05(19)
C(32)-C(33)-C(34)	122.2(2)
C(35)-C(34)-C(33)	117.7(2)
C(35)-C(34)-C(37)	121.2(2)

C(33)-C(34)-C(37)	121.1(2)
C(24)-C(25)-C(26)	122.15(18)
C(10)-C(8)-C(6)	120.05(18)
C(9)-C(7)-C(6)	119.47(17)
C(9)-C(7)-C(5)	118.73(16)
C(6)-C(7)-C(5)	121.79(16)
O(3)-C(30)-N(5)	124.50(18)
O(3)-C(30)-N(4)	124.53(18)
N(5)-C(30)-N(4)	110.96(17)
C(24)-C(23)-C(22)	121.98(19)
C(10)-C(11)-C(9)	120.22(18)
C(33)-C(32)-C(31)	119.72(19)
C(11)-C(9)-C(7)	120.19(18)
C(21)-C(26)-C(25)	116.52(18)
C(21)-C(26)-C(29)	122.20(16)
C(25)-C(26)-C(29)	121.26(17)
C(15)-C(14)-C(13)	121.90(17)
C(23)-C(24)-C(25)	118.74(17)
C(23)-C(24)-C(28)	120.0(2)
C(25)-C(24)-C(28)	121.2(2)
C(11)-C(10)-C(8)	120.29(18)
O(1)-C(5)-C(3)	123.04(16)
O(1)-C(5)-C(7)	122.83(16)
C(3)-C(5)-C(7)	114.13(14)
C(41)-C(42)-C(43)	121.7(2)
C(41)-C(40)-C(39)	122.5(2)
C(2)-C(3)-N(2)	107.79(14)
C(2)-C(3)-C(5)	123.94(15)
N(2)-C(3)-C(5)	128.25(15)
C(42)-C(43)-C(38)	120.4(2)
O(2)-C(4)-C(2)	122.51(16)
O(2)-C(4)-C(6)	123.19(16)
C(2)-C(4)-C(6)	114.30(14)
C(3)-C(2)-N(3)	108.17(14)

C(3)-C(2)-C(4)	123.76(15)
N(3)-C(2)-C(4)	128.05(15)
C(35)-C(36)-C(31)	120.94(19)
C(43)-C(38)-C(39)	118.61(18)
C(43)-C(38)-N(5)	117.13(18)
C(39)-C(38)-N(5)	124.26(19)
C(36)-C(35)-C(34)	120.99(19)
C(40)-C(39)-C(38)	119.6(2)
C(17)-C(16)-C(15)	121.63(17)
C(42)-C(41)-C(40)	117.1(2)
C(42)-C(41)-C(44)	121.4(2)
C(40)-C(41)-C(44)	121.4(2)
C(6S)-C(1S)-C(2S)	120.9(3)
C(5S)-C(6S)-C(1S)	120.1(3)
C(2S)-C(3S)-C(4S)	119.7(4)
C(6S)-C(5S)-C(4S)	120.0(4)
C(5S)-C(4S)-C(3S)	120.3(5)
N(1)-C(1)-N(2)	125.59(15)
N(1)-C(1)-N(3)	125.76(15)
N(2)-C(1)-N(3)	108.66(14)

Symmetry transformations used to generate equivalent atoms:

Table 9. Anisotropic displacement parameters ($Å^2 x\ 10^3$)for d13109 (decomposition product). The anisotropic

displacement factor exponent takes the form: $-2\pi^2[\ h^2 a^{*2} U^{11} + ... + 2\ h\ k\ a^*\ b^*\ U^{12}\ ]$

	U^{11}	U^{22}	U^{33}	U^{23}	U^{13}	U^{12}
Cl(1)	34(1)	32(1)	27(1)	7(1)	9(1)	14(1)
O(1)	46(1)	26(1)	35(1)	5(1)	10(1)	12(1)
O(2)	58(1)	35(1)	29(1)	3(1)	2(1)	17(1)
O(3)	43(1)	48(1)	49(1)	14(1)	23(1)	11(1)
N(1)	42(1)	30(1)	25(1)	4(1)	3(1)	17(1)
N(3)	35(1)	25(1)	25(1)	5(1)	5(1)	11(1)
N(2)	33(1)	25(1)	25(1)	5(1)	6(1)	10(1)
N(4)	39(1)	40(1)	43(1)	10(1)	19(1)	9(1)
N(5)	38(1)	44(1)	41(1)	10(1)	19(1)	11(1)
C(21)	34(1)	26(1)	24(1)	4(1)	1(1)	11(1)
C(19)	77(2)	37(1)	35(1)	0(1)	8(1)	10(1)
C(2S)	62(2)	85(2)	71(2)	17(2)	25(2)	12(2)
C(13)	33(1)	32(1)	31(1)	9(1)	8(1)	15(1)
C(12)	34(1)	24(1)	26(1)	5(1)	4(1)	12(1)
C(22)	36(1)	36(1)	26(1)	7(1)	4(1)	15(1)
C(17)	36(1)	26(1)	33(1)	9(1)	7(1)	11(1)
C(18)	37(1)	43(1)	40(1)	12(1)	13(1)	10(1)
C(6)	33(1)	33(1)	32(1)	12(1)	9(1)	10(1)
C(31)	35(1)	39(1)	41(1)	15(1)	12(1)	17(1)
C(15)	52(1)	28(1)	31(1)	5(1)	5(1)	15(1)
C(33)	54(1)	37(1)	61(1)	16(1)	23(1)	12(1)
C(20)	39(1)	40(1)	42(1)	14(1)	12(1)	8(1)
C(34)	58(1)	39(1)	50(1)	11(1)	13(1)	19(1)
C(25)	42(1)	28(1)	48(1)	13(1)	-2(1)	4(1)
C(8)	44(1)	41(1)	31(1)	12(1)	9(1)	13(1)
C(7)	33(1)	29(1)	34(1)	12(1)	9(1)	8(1)
C(30)	37(1)	42(1)	37(1)	14(1)	12(1)	15(1)
C(23)	48(1)	42(1)	31(1)	4(1)	6(1)	24(1)

C(11)	50(1)	43(1)	51(1)	25(1)	12(1)	19(1)
C(32)	51(1)	41(1)	49(1)	16(1)	24(1)	16(1)
C(9)	43(1)	31(1)	43(1)	15(1)	11(1)	12(1)
C(26)	35(1)	32(1)	31(1)	11(1)	2(1)	9(1)
C(14)	46(1)	37(1)	29(1)	9(1)	13(1)	19(1)
C(24)	51(1)	34(1)	39(1)	2(1)	-3(1)	18(1)
C(10)	48(1)	50(1)	38(1)	22(1)	7(1)	16(1)
C(5)	30(1)	24(1)	33(1)	9(1)	10(1)	6(1)
C(42)	51(1)	46(1)	51(1)	6(1)	13(1)	14(1)
C(40)	50(1)	64(2)	47(1)	7(1)	23(1)	14(1)
C(3)	30(1)	27(1)	27(1)	9(1)	7(1)	7(1)
C(43)	40(1)	51(1)	41(1)	11(1)	12(1)	15(1)
C(4)	34(1)	28(1)	29(1)	7(1)	7(1)	7(1)
C(29)	38(1)	50(1)	47(1)	22(1)	12(1)	11(1)
C(2)	30(1)	26(1)	28(1)	9(1)	7(1)	7(1)
C(36)	39(1)	42(1)	43(1)	18(1)	15(1)	16(1)
C(37)	93(2)	47(1)	64(2)	4(1)	23(2)	11(1)
C(38)	33(1)	48(1)	35(1)	9(1)	8(1)	16(1)
C(27)	45(1)	50(1)	46(1)	18(1)	19(1)	18(1)
C(35)	53(1)	47(1)	42(1)	16(1)	18(1)	23(1)
C(39)	46(1)	49(1)	43(1)	9(1)	18(1)	12(1)
C(16)	41(1)	25(1)	38(1)	7(1)	5(1)	5(1)
C(41)	48(1)	57(1)	49(1)	2(1)	14(1)	17(1)
C(1S)	48(2)	80(2)	91(2)	44(2)	21(1)	9(1)
C(44)	78(2)	66(2)	78(2)	-4(1)	36(2)	20(1)
C(6S)	122(3)	74(2)	64(2)	21(2)	6(2)	7(2)
C(3S)	136(4)	208(5)	67(2)	53(3)	19(2)	98(4)
C(5S)	327(9)	127(4)	90(3)	38(3)	56(4)	150(5)
C(4S)	349(10)	264(7)	115(4)	94(4)	83(5)	253(8)
C(1)	30(1)	27(1)	26(1)	6(1)	7(1)	9(1)
C(28)	86(2)	36(1)	75(2)	-3(1)	5(1)	27(1)

Table 10. Hydrogen coordinates (x 10^4) and isotropic displacement parameters ($Å^2$x 10^3) for d13109 (decomposition product).

	x	y	z	U(eq)
H(19A)	4159	5513	-2519	85
H(19B)	4246	4600	-2178	85
H(19C)	5552	5253	-2419	85
H(2S)	3725	8987	4711	93
H(18A)	8402	9146	-192	62
H(18B)	9254	8415	-380	62
H(18C)	9145	8813	519	62
H(33)	-704	5992	179	62
H(20A)	3434	5943	410	63
H(20B)	4262	7138	938	63
H(20C)	4888	6308	1116	63
H(25)	9591	13156	2837	53
H(8)	10175	9022	4706	48
H(23)	6495	12016	3816	49
H(11)	10239	6145	3895	55
H(32)	530	7541	1272	55
H(9)	9061	5956	2552	48
H(14)	7222	6972	-1458	44
H(10)	10783	7668	4968	54
H(42)	4241	14051	3779	63
H(40)	1513	11922	4420	68
H(43)	4428	12730	2789	54
H(29A)	9965	10819	1956	68
H(29B)	10554	12023	2069	68
H(29C)	9156	11246	1343	68
H(36)	3079	8580	-63	48
H(37A)	94	4858	-1331	113
H(37B)	-544	5475	-1835	113

H(37C)	-1348	4989	-1261	113
H(27A)	6293	9665	3519	69
H(27B)	5258	9443	2640	69
H(27C)	5166	10199	3434	69
H(35)	1893	7000	-1124	55
H(39)	1694	10583	3449	58
H(16)	3786	5375	-890	46
H(1S)	2404	8534	3343	89
H(44A)	1676	13925	4695	120
H(44B)	3249	14676	4810	120
H(44C)	2982	13971	5375	120
H(6S)	2628	7298	2327	118
H(3S)	5266	8174	5036	155
H(5S)	4307	6604	2635	200
H(4S)	5579	6995	3987	239
H(28A)	7670	13831	4239	108
H(28B)	7863	14156	3457	108
H(28C)	9216	14281	4146	108
H(99)	3780(30)	11009(17)	2123(14)	46(6)
H(98)	3310(20)	9676(17)	1200(13)	39(6)
H(101)	6210(20)	10124(18)	988(13)	44(6)
H(100)	6000(20)	9147(17)	267(14)	42(6)